5-1-2017

Analysis of Suspended Particulate Matter Concentrations in Weeks Bay, Alabama Using Landsat Imagery

Devon Lee Flickinger

Analysis of suspended particulate matter concentrations in Weeks Bay, Alabama using Landsat imagery

By

Devon Lee Flickinger

A Thesis
Submitted to the Faculty of
Mississippi State University
in Partial Fulfillment of the Requirements
for the Degree of Master of Science
in Geospatial Science
in the Department of Geosciences

Mississippi State, Mississippi

May 2017

Analysis of suspended particulate matter concentrations

in Weeks Bay, Alabama using Landsat imagery

By

Devon Lee Flickinger

Approved:

_____

John C. Rodgers, III
(Major Professor)

_____

Padmanava Dash
(Committee Member)

_____

Adam Skarke
(Committee Member)

_____

Renee M. Clary
(Graduate Coordinator)

_____

Rick Travis
Interim Dean
College of Arts & Sciences

Name: Devon Lee Flickinger

Date of Degree: May 1, 2017

Institution: Mississippi State University

Major Field: Geospatial Science

Select Appropriate Title: Dr. John C. Rodgers, III

Title of Study: Analysis of suspended particulate matter concentrations in Weeks Bay, Alabama using Landsat imagery

Pages in Study: 128

Candidate for Degree of Master of Science

Estuaries are valuable ecosystems that are easily affected by human activities within the watershed. One determinant of water quality for in an estuary is the presence of suspended sediments. The use of satellite sensors to remotely sense visible and near-infrared reflectance allows for suspended particulate matter (SPM) and suspended particulate inorganic matter (SPIM) concentrations to be monitored on a repetitive synoptic scale. Previously presented algorithms for relating remote sensing reflectance (Rrs) and SPM/SPIM concentrations were evaluated for the Weeks Bay estuary in Alabama. Additionally, numerous potential SPM/SPIM concentration retrieval algorithms using the Landsat-8 satellite were determined through regression analysis, as well as through the consideration of the inherent optical properties of the water body. The most robust empirical algorithm produced an RMSE of 12.50% and utilized the band combination of Ln(Band4)/Ln(Band3), while the most robust semi-analytical algorithm produced an RMSE of 16.34% and utilized the band combination of Band4/Band3.

DEDICATION

This work is dedicated to my close friends and family who have supported me throughout this entire process including my parents, grandparents, and Chris Elcik. A special dedication to my father, Barry Flickinger, who made multiple trips to Mississippi in order to help with field collection and lab processing.

ACKNOWLEDGEMENTS

I would like to express my thanks for my thesis advisor, Dr. John Rodgers, and to my committee members, Dr. Padmanava Dash and Dr. Adam Skarke. Dr. Padmanava Dash introduced me to the world of remote sensing and taught me everything I know.

I would like to thank Dr. Scott Phipps and the Weeks Bay National Estuarine Research Reserve for providing lodging, as well as ferrying us around Weeks Bay. Dr. Scott Phipps graciously tolerated the constant rescheduling due to weather that would not cooperate, as well as the busy schedules of those involved with field collection. This project would not have been possible without your hospitality.

Additionally, I would like to thank Sankar Sasidharan and Rusch Ragland who sacrificed their time to take multiple trips to Weeks Bay to collect field samples. An additional thanks for all of those who came in late to help with the lab work that followed each sampling trip.

I would like to thank the Mississippi State University Geosciences Department for funding my graduate education by providing me with a teaching assistantship. Lastly, I would like to thank my friends and family for always supporting me.

TABLE OF CONTENTS

LIST OF TABLES

LIST OF FIGURES

CHAPTER I

INTRODUCTION

1.1 Introduction

Estuaries are partially enclosed bodies of brackish water that are critical habitats for a significant variety of wildlife. They are one of the most productive types of ecosystems and serve not only as valuable ecological habitats, but also possess significant economic and cultural value (Potter, n.d.). Estuaries are used for transport, commercial industry, recreation, and research resulting in many of the watersheds surrounding estuaries to have widely differing land use types, including a large percentage of land used for urban and agricultural purposes. An understanding of suspended particulate concentration and transport in coastal waters is vital when studying carbon and nitrogen biochemistry (Kumar et al., 2011; Bhavya et al., 2016), as well the transport of various toxic metals and pollutants such as polycyclic aromatic hydrocarbons (Booth et al., 2000; Gregg et al., 2015; Ma et al., 2015). Furthermore, an understanding of seasonal suspended particulate concentrations is important for determining sediment budgets (Chalov et al., 2014). Suspended sediments may be used as a determinant of estuarine health (EPA, 2000). Although there are no quantitative criteria for acceptable levels for SSCs, the National Academy of Sciences recommends that the concentration of total suspended solids should not be allowed to reduce light penetration by more than 10%

(Kentucky Water Watch, n.d.). There is still much to be understood concerning the transport of suspended sediments, thus warranting a method of constant SSC monitoring

1.2 Weeks Bay Overview

Modeling suspended particulate matter in a small estuary could help with our understanding sediment transport by providing a more controlled environment. The Weeks Bay estuary on the eastern shore of Mobile Bay in Alabama is an ideal setting to investigate this. Weeks Bay has been established as an active research environment, and possess a watershed that is completely within the confines of a single county.

In 1986, Weeks Bay became the 16th site of the NERRS and was renamed as the Weeks Bay National Estuarine Research Reserve. Weeks Bay is located in Baldwin County, Alabama, approximately 30 miles southeast of the city of Mobile. Baldwin County is one of the fastest growing counties in Alabama due an increase in the suburbanization of Mobile ('State by State'). Weeks Bay is fed by the Fish and Magnolia Rivers, such that its 200 square mile watershed completely lies within the boundaries of Baldwin County. From 1990 to 2000, the Weeks Bay watershed experienced an increase in urban/built-up land cover by 92.47% (Cartwright, 2002). Changes in land use/land cover (LULC) within the watershed can have significant effects on the runoff of sediment, nutrients, and freshwater volume that enters the estuary (Estes et al., 2015). A higher percentage of urban land cover, and therefore impervious surfaces, increases surface runoff and allows for accumulated sediment and pollutants to be directed into surface water sources (Basnyat et al., 1999). It is therefore important to monitor changes in water quality and sediment concentrations in order to assess the impact this urbanization is having on the bay. Weeks Bay provides the necessary habitat for an

abundant variety of wildlife including plankton, nekton, amphibian, reptile, mammal, and bird species (Miller-Way et al., 1996). The health of these species depends largely on the water quality of the bay and tributary rivers.

1.3 Suspended Particulate Matter (SPM)

A primary concern in the Weeks Bay estuary is the threat of increased sediment transport within the watershed due to a rapid increase in development. Suspended particulate matter (SPM) includes all material transported through suspension in flowing water. This includes both the organic (SPOM) and inorganic (SPIM) components. This study will focus on the optically active constituents (OACs) present in the water body including inorganic suspended sediments (non-algal particulates, or NAP), chlorophyll a (Chl a), color dissolved organic matter (CDOM), and phycocyanin (PC) that will affect the optical properties of the water. For the purpose of this study, SPM will be defined as the organic and inorganic filterable quantity of the OACs, including phytoplankton (Chl a and PC) and mineral particulates (NAP) (Gohin, 2011; Merrit, 2016). SPIM will be defined as only the inorganic filterable quantity of the OACs present in the water body, and may also be referred to as the suspended sediment concentration (SSC). These materials, as well as non-optically active constituents, will be transported with runoff from the watershed into the water body during precipitation events. Furthermore, in addition to being transported through runoff, SPM may be transported into the estuary through variations in currents and tidal influences from the mouth of the bay. Moreover, currents and wind-induced waves may suspend bottom sediment in shallow coastal environments (Booth et al., 2000).

1.4 Remote Sensing of SPM

Previously, to determine the SPM concentrations within a body of water, it was necessary to collect *in situ* water samples to be filtered for suspended particulates. Repetitive sampling was required to establish a time series of SPM concentrations. *In situ* data collection is not only time consuming and expensive, but is also limited in spatial and temporal scales. For studies of features that vary substantially temporally and spatially such as those on material transport, *in situ* measurements are limited in the functionality and understanding they may provide (Booth et al., 2000). With the advance in remote sensing technology, it is possible to study suspended particles remotely, and on a wider scale. Many studies have demonstrated the effectiveness of using combinations of various band reflectance data to observe suspended sediment (Chen et al., 2011; Han et al., 2006; Kaba et al., 2014; Miller et al., 2004; Zhao et al., 2011). Several sensors such as the Moderate Resolution Imagery Spectroradiometer (MODIS) and Sea-viewing Wide Field-of-view Sensor (SeaWiFS) were designed specifically for ocean color studies, but with relatively coarse spatial resolutions (250 m to 1 km), they are unsuitable for small inland and coastal water studies. The Landsat satellites, while designed for land surface studies, have often been selected to study suspended sediment in smaller bodies of water due to the superior spatial resolution of 30 meters for bands 1-5 and 7 (Jenson, 2006). In order to accurately assess SPM and SPIM concentrations using remotely sensed imagery, site specific algorithms must be developed and applied to atmospherically corrected satellite imagery. With its high spatial resolution, Landsat may be used to develop an algorithm in order to assess SPM concentrations in Weeks Bay.

1.5 Hypothesis and Objectives

While numerous studies have developed predictive models for the remote sensing of SPM/SPIM concentrations in estuaries in the Gulf of Mexico and around the world, none have been attempted for the Weeks Bay Estuary in Alabama. Because the Landsat satellites have the potential to quantify SPM/SPIM, and Weeks Bay is a sensitive estuary undergoing rapid development of its watershed, the primary objective of this study was to develop a site-specific algorithm correlating *in situ* observations of SPM and SPIM with observations of reflectance from the Landsat-8 satellite sensor. Additionally, a semi-analytical simulation was implemented to confirm the influence of the various OACs present in the water body. This research will help us to better understand SPM/SPIM and to provide a low cost methodology for quantifying SPM and SPIM concentrations. This will improve our overall understanding of SPM/SPIM in Weeks Bay and by extension, all similar estuarine environments. It is hypothesized that a relationship exists between *in situ* observed SPM concentrations of Weeks Bay and corresponding radiometer data simulated to represent the Rrs values observed by the Landsat-8 satellite. The specific objectives of this study are as follows:

1) To model *in situ* observed SPM and SPIM concentrations within Weeks Bay with corresponding radiometer data simulated to represent the Rrs values observed by the Landsat-8 satellite. The creation of an algorithm for the retrieval of SPM and SPIM concentrations will provide a low cost methodology for future SPM and SPIM research.
2) To examine the individual spectral contributions of OACs including NAP, Chl a, CDOM, and PC. This assessment will allow an improved understanding of

the OACs that comprise both SPM and SPIM and their contribution to total Rrs.

1.6 Significance

Estuaries are important ecosystems that provide environmental, commercial, recreational, and cultural benefits (NOAA, 2005). Estuaries are vital habitats for a variety of wildlife, serving as buffers to protect inland regions from storms and flooding, and regulating water quality (Needles et al., 2015). Not only are estuaries important environmentally, they are also vital to the economy. Weeks Bay in particular is home to numerous species with a commercial importance to the region. The estuary serves as a nursery for all three southeastern species of commercial shrimps (Miller-Way et al., 1996). Weeks Bay is also home to blue crabs, as well as numerous species of finfish including sheepshead, white trout, mullet, speckled trout, redfish, and flounder (Miller-Way et al., 1996). Between 2001 and 2006, 46% by weight and 68% by economic value of the commercially harvested fish and shellfish in the United States were species that rely on estuaries during some stage of their life cycle. These percentages increase to 97% by weight and 93% by economic value when specifically evaluating the Gulf of Mexico region (Lellis-Dibble et al., 2008). Many estuaries are located in close proximity to growing urban populations (Hu et al., 2004). The Weeks Bay National Estuarine Research Research (NERR) is located in proximity to the growing suburbs of Mobile, Alabama. The growth of these suburbs have altered the nature of the Weeks Bay watershed.

The model derived from this study can be used as a tool for future studies used to monitor the health of the Weeks Bay ecosystem. As a NERR location, Weeks Bay is a

common study area for research. With the use of this model, it will be possible for researchers to investigate the influence of human activities such as agriculture and new development on SPM concentrations. The model may be applied to historical images over a longer time frame in order to assess changes in water quality.

CHAPTER II

BACKGROUND

2.1 Water Quality Parameters

The U.S. Environmental Protection Agency (EPA) has identified certain parameters that may directly relate to and impair the health of an ecosystem, and refers to them as "stressors" (EPA, 2000; Hu et al., 2004). Common stressors for estuarine ecosystems include increased nutrient concentrations, low dissolved oxygen, sustained algal blooms, and sediment contamination (EPA, 2000). Suspended sediments are the most common contaminant in both weight and volume for freshwater systems (Ritchie & Cooper, 2001). A single liter of water from a turbid estuary may contain several million particles that are large enough to be caught on a filter (47 mm pore size), but too small for the un-aided eye to see (Bowers & Binding, 2006). Excess nutrients and sediment have been found to be the most common stressor for seagrass, a sentinel species for the overall health of an ecosystem (Orth et al., 2006). Submerged aquatic vegetation is indirectly affected by suspended sediment concentrations due to the obstruction of sunlight essential to photosynthesis. The majority of seagrass loss is the result of human activities within the watershed that lead to an increase in the amount of sediment and nutrient runoff (Orth et al., 2006). Seagrass provides a vital habitat and food source for various aquatic organisms (Coll et al., 2011).

Not only do suspended sediments block sunlight from reaching underwater vegetation, they also serve as a proxy for other contaminants that may bind to sediment particles such as phosphorus, insecticides, and metals (Ritchie & Cooper, 2001). SPM has been associated with quantities of nutrients, toxins, harmful algae, pathogens, and bacteria, making SPM concentrations an important aspect of water quality of monitor (Merritt, 2016). Lastly, suspended sediments may clog the gills of fish and other aquatic organisms (Hill, 1997). Significant increases in the concentrations of total suspended solids may result in a significant decrease the population of macroinvertebrates (Kentucky Water Watch, n.d.). Weeks Bay receives high concentrations of suspended sediment during major runoff events from the Fish River, as well as from tidal inputs from Mobile Bay and resuspension of sediment during periods of strong winds, which together result in a relatively turbid water column (Miller-Way et al., 1996).

2.2 Optically Active Constituents (OACs)

Because the objective of this study is to develop a method of remotely sensing SPM, it will focus on the optically active constituents (OACs) present in the water that contribute to the bio-optical properties of the water. Water bodies vary in the type and concentrations of OACs present within them. Morel and Prieur (1977) identified two extreme types of waters that they separated into “Case-1” and “Case-2” waters. Case-1 waters contain a high concentration of phytoplankton compared to the other OACs, whereas inorganic particles are dominant in Case-2 waters (Morel and Prieur, 1977). Although ideal Case-1 (pure phytoplankton) and Case-2 waters (pure nonliving material) do not exist in nature, we still use these classifications to describe the difference between clear open ocean water and more complex coastal and inland waters.

Satellite data may be used to determine chlorophyll concentrations in clear Case-1 waters, however Case-2 waters contain a more complex signal due to the presence of terrestrial substances in addition to phytoplankton (Doxaran et al., 2002). These natural coastal waters are heterogeneous, with highly variable concentrations of dissolved and particulate matter (Mobley, 2010). Some degree of correlation between sediments, chl-a, and CDOM is often observed (Tassan, 1994). Processes that effect one component will affect the other components as well (Merritt, 2016). In this study, SPM will be defined as the filterable quantity of OACs including both inorganic and organic matter. SPIM will be defined as the inorganic filterable quantity of OACs, and may also be referred to as the suspended sediment concentration (SSC). SPIM inhibits primary production in coastal waters (Doxaran et al., 2002). Chl-a is an algal pigment found in all phytoplankton and may be an indicator of biomass and therefore used to predict total algal concentrations (Hu et al., 2004; Dash et al., 2011). Chl-a concentration and absorption are key variables for determining primary production (Nieke et al., 1997). Terrestrial dissolved organic matter (DOM) serves as a carbon source for bacteria (Kutser et al., 2005). In Case-2 waters, humic and fulvic acids account for 70% of the DOM and contribute significantly to light absorption and fluorescence, particularly in the short-wavelength region of solar radiation (Nieke et al., 1997; Kutser et el., 2005). The portion of DOM that absorbs light is referred to as CDOM and effects the light available for primary producers (Nieke et al., 1997; Kutser et al., 2005). CDOM is derived from the decay of phytoplankton, as well as from terrestrial sources of plant decay (Nieke et al., 1997; Merritt, 2016).

2.3 Apparent and Inherent Optical Properties

The remote sensing of water presents different challenges than terrestrial remote sensing due to the different OACs present within the water body, as well as the increased sensitivity to atmospheric noise. When light interacts with a medium, it may be absorbed, scattered, or emitted. The optical properties of water may be divided into apparent and inherent optical property (AOP and IOP, respectively) measurements (Doxaran et al., 2006). IOPs are properties of the medium itself, and do not depend on the incident light (Mobley, 2010). This includes the absorption and backscattering properties of the water and other optically active components. Absorption, as expressed by the absorption coefficient, is the distance into a material that light of a certain wavelength may permeate before being absorbed and having its energy converted into a nonradiant form (Mobley, 2010). Backscattering, as expressed by the backscattering coefficient, is the quantitative measure of the energy returned to the sensor from the terrain, or in this study, water body (Jenson, 2006).

IOPs vary by orders of magnitude depending on the composition, morphology, and concentration of particulate and dissolved material in the water (Mobley, 2010). Absorption (a) and backscattering (b_b) coefficients may be determined for all OACs including water, CDOM, Chl-a, and SPIM (Dash et al., 2011). AOPs describe the bulk optical properties of water that depend on both the medium and on the direction of the radiance distribution (Mobley, 2010). AOPs include the upwelling (E_u) and down welling (E_d) irradiances. E_u and E_d are the amount of radiant flux incident upon a surface per unit area that is emitted upwards and downwards, respectively (Jenson, 2006).

Historically, it was easier to measure radiometric variables, and therefore the AOPs than it was to determine the IOPs (Mobley, 2010). IOPs may now be determined easily in either the field or lab through the use of spectrophotometry, therefore, the absorption and backscattering coefficients will be used in this study. By using a spectrophotometer, it is possible to determine the absorption coefficient at each wavelength for SPM, as well as for the SPIM and SPOM components by removing organic material from the filtered sample using methanol and once again using a spectrophotometer.

Through AOPs, remote sensing reflectance (Rrs) may be determined by the following equation:

$$Rrs = \frac{radiance}{irradiance} \tag{2.1}$$

Similarly, through IOPs, Rrs may be determined by the following equation:

$$Rrs = \frac{f}{Q}\frac{b_b}{a+b_b} \tag{2.2}$$

Where f is the coefficient of anisotropy of the light field, and often takes a value of 0.33 for the sun at its zenith over a level sea surface; Q is the conversion factor between radiance and Rrs; b_b is the backscattering coefficient, such that all OACs of the water are accounted for, and a is the absorption coefficient such that all OACs of the water are accounted for.

For ocean color radiometry, it is important to atmospherically correct the reflectance values to Rrs measurements due to the fact that the water-leaving reflectance is only a small portion of the total reflectance reflected by Earth and received by the satellite sensors. Only approximately 10% of the radiation recorded by the satellite

sensors is contributed by the water surface, with the additional 90% being contributed by air molecules and aerosols within the atmosphere (Franz et al, 2015).

2.4 Landsat

One of the most common satellites used in study of bio-optical properties in small inland and coastal waterbodies is Landsat. On July 23, 1972, the first civilian Earth observation satellite was launched. Initially known as the Earth Resources Technology Satellite (ERTS-1), this satellite was later renamed as Landsat-1 (USGS, 2015a). The Landsat mission has since launched Landsat-2, Landsat-3, Landsat-4, Landsat-5, Landsat-7, and Landsat-8 in 1975, 1978, 1982, 1984, 1999, and 2013 respectively and is the longest continuous collection of space-based moderate-resolution remotely sensed imagery (USGS, 2015a).

The Landsat satellites prior to Landsat-8 were all of a whisk broom design, meaning a mirror moved back and forth to reflect light from various points in the swath view to a single sensor. Landsat-8 is the first Landsat satellite to incorporate a push broom design so that a line of sensors perpendicular to the flight measure the entire swath width simultaneously. All of the Landsat satellites rely on sensors to measure reflectance in various sectors of the electromagnetic spectrum (EMS). Electromagnetic radiation (EMR) that is emitted from the sun travels through space and the atmosphere to reach the surface of the earth where it is reflected back into the atmosphere and then recorded by the sensors aboard the satellite. Different surface types reflect various portions of the EMS differently, which results in varying reflectance values. These values, known as brightness values (BV), are digitally recorded and may be displayed as images using

various band combinations, opposed to photographic images that only records information in the visible portion of the spectrum (Jenson, 2006).

Due to advancing technology, the sensors aboard each Landsat satellite have improved overtime. Landsat-1, Landsat-2, and Landsat-3 contained the Multispectral Scanner (MSS) as the primary sensor and had a repeat cycle of 18 days. The MSS has a spatial resolution of 79 meters and collects information in four spectral bands that include both visible and NIR reflectance (Jenson, 2006). Landsat-4 and Landsat-5 carried the Thematic Mapper (TM) sensor as well as the MSS sensor and had a repeat cycle of 16 days. The addition of the TM sensor provided spectral bands in the shortwave infrared (SWIR) and thermal regions as well as an improved spatial resolution of 30 meters for the visible and infrared bands (USGS, 2015a). Landsat 7 carries the Enhanced Thematic Mapper Plus (ETM+) sensor which provides the addition of a 15 meter resolution panchromatic band and improves the spatial resolution of the thermal band (Jenson, 2006). Landsat 8, the satellite utilized for this study, contains the Operational Land Imager (OLI) and the Thermal Infrared Sensor (TIRS) that provide the addition of a deep blue band for coastal-aerosol studies and a band for cirrus cloud detection as well as two thermal bands. Landsat 8 collects reflectance data for a total of eleven spectral bands (Table 2.1), using 14 separate detector assemblies assigned in a push broom assembly (Franz et al., 2015). Each Landsat 8 OLI swath covers around 185 km width, which equates to ~7000 pixels (Franz et al., 2015). Both Landsat 7 and Landsat 8 have 16 day sampling intervals (USGS, 2015a).

Table 2.1 Landsat 8 Specifications

Sensors:	Band	Band Designations	Bandwidth (µm)	Spatial Resolution
Operational Land Imager (OLI)	Band 1	Coastal Aerosol	0.43-0.45	30 m
	Band 2	Blue	0.45-0.51	30 m
	Band 3	Green	0.53-0.59	30 m
	Band 4	Red	0.64-0.67	30 m
	Band 5	NIR	0.85-0.88	30 m
	Band 6	Short-wave IR	1.57-1.65	30 m
	Band 7	Short-wave IR	2.11-2.29	30 m
	Band 8	Panchromatic	0.50-0.68	15 m
	Band 9	Cirrus Detection	1.36-1.38	30 m
Thermal Infrared Sensor (TIRS)	Band 10	Thermal IR	10.60-11.19	100 m
	Band 11	Thermal IR	11.5-12.51	100 m

Landsat 8 contains two sensors sensing reflectance in a total of 11 bands. Only bands 1-7 are used in SPM modeling (USGS, 2015).

Landsat 8 provides the necessary spatial resolution for looking at small coastal and inland bodies of water. Landsat 8 OLI contains narrow enough spectral bands in the visible to shortwave infrared range, making it a suitable tool for ocean color radiometry (Franz et al., 2015). The disadvantage of using Landsat imagery was the lower temporal resolution when compared to satellites such as NOAA's MODIS. The lower temporal resolution limit the number of available field collection dates, and will provide a coarser temporal resolution when monitoring concentration changes. Additionally, Weeks Bay's proximity to the Gulf of Mexico makes it prone to frequent cloud cover. Images with high percentages of cloud cover are unusable due to the prevention of data extraction from the satellite imagery. The frequent cloud cover, coupled with the lower temporal resolution, further limits the availability of useful imagery. However, Weeks Bay is

visible within two separate scanning paths, therefore increasing the temporal resolution to two scans within each 16 day rotation. For the sake of modeling, if the Landsat-8 imagery contained cloud interference on an *in situ* collection date, reflectance values from a radiometer were used to determine the predicted Landsat-8 reflectance for that precise point and time. The relative spectral response (RSR) of each Landsat-8 band provides the sensitivity of each given wavelength for the various satellite bands.

2.5 Development of Bio-Optical Algorithms in Case-2 Waters

Due to the complexity of Case-2 waters, established bio-optical models are often site specific due to local variations in environmental conditions (Merritt, 2016). These variations may include differences in the size, shape, and mineralogy of the suspended particulates, concentrations of organics such as algal blooms, changes in fluvial, tidal, and wave dynamics, and variations in the size and depth of the body of water, as well as variations in the correlation between the three OACs (Tassan, 1994; Binding et al., 2005; Merritt, 2016). Furthermore, the development of bio-optical algorithms in Case-2 waters requires the proper satellite sensor to be chosen to fit the study area (Merrit, 2016). For smaller bodies of water such as small bays and estuaries, it is necessary to utilize sensors with the best possible spatial accuracy, such as Landsat. In larger bodies of water and the open ocean, a lower spatial resolution would be needed, allowing the use of sensors with higher spectral or temporal resolutions. Mapping more dynamic water bodies may require a higher temporal resolution than is provided by Landsat.

2.6 Review of Literature on SPM

Thomason (2008) compared land use data derived from Landsat TM imagery to suspended sediment concentrations in Weeks Bay, Alabama. She determined areas of high and low potential for erosion by looking at the distribution of urban development and then obtained *in situ* SSCs in order to verify the existence of high erosion sites. Thomason's study demonstrated that areas with high erosion potential resulted in higher SSCs, but the relationship between land use and suspended sediment ended up being much more complex than originally expected due to various components such as precipitation amounts, and tidal patterns.

By only relying on *in situ* field sampling to determine SSCs, Thomason had a very limited coverage both spatially and temporally. The limited nature of *in situ* data collection is only one of the disadvantages of relying solely on field data collection. *In situ* suspended sediment data collection is both expensive and time consuming, while allowing for only a discrete number of samples to be collected. It can also be inaccurate due to human error, sampling bias, improper operation or miscalibration of equipment, and the disturbance of the environment (Jenson, 2006).

Remote sensing has proved to be invaluable in a variety of water studies due to the wealth of information provided by the electromagnetic reflectance on the various OACs and the water itself (Roesler and Perry, 1994). Remote sensing systems provide a method of rapidly and repetitively collecting data on a synoptic scale without having to be present at the collection site. The use of remotely sensed data to study SSC relies on the fact that suspended sediment increases the reflectance of visible and NIR wavelengths from surface waters (Ritchie & Cooper, 2001; Doxaran et al., 2002; Devi et al., 2015).

The millions of microscopic particles found in a single liter of estuarine water are each capable of absorbing and scattering sunlight, therefore altering the reflectance seen by the satellite sensors (Bowers & Binding, 2006). It is known that the red band is the most sensitive of the visible bands to suspended sediment, while organic material that contains chlorophyll has an absorption in the red band (Zhao, 2009). Many studies have demonstrated the effectiveness of using red and/or near-infrared band reflectance data to observe suspended sediment remotely (Miller et al., 2004; Han et al., 2006; Chen et al., 2011; Zhao et al., 2011; Kaba et al., 2014). While the use of the red and infrared bands is most common when determining SSC, other band ratios have been used, such as a ratio between the green and NIR bands in the study by Zhang (2005).

Depending on the range of SSCs present, different relationships may be acceptable. If the range of SSCs is fairly low, ranging between 0 and 50 mg/l, the reflectance values from most wavelengths may successfully be related to SSCs with a linear relationship (Ritchie & Cooper, 2001). For larger ranges of SSCs such as from 0 to 200+ mg/l, a more complex curvilinear relationship between SSC and longer wavelengths must be used due to the fact that suspended sediment saturates the reflectance of lower wavelengths at lower SSCs (Ritchie & Cooper, 2001).

Different remote sensing systems have been used to study suspended sediment including NOAA's Advanced Very High Resolution Radiometer (AVHRR; Walker et al., 1993), Système Pour l'Observation de la Terre (SPOT; Doxaran et al., 2002; Pavelsky & Smith, 2009; Gernez et al., 2015), Landsat (Zhang et al., 2014; Zheng et al., 2015) and the MODIS instrument on the Terra and Aqua satellites (Hu et al., 2004; Miller et al., 2004; Chen et al., 2011; Espinoza et al., 2012; Liu et al., 2014; Vazyulya et al., 2014).

The remote sensing system used depends on the resolution required for each particular study. The satellite imagery must have sufficient temporal, spatial, spectral, and radiometric resolutions. Although designed for land studies, the Landsat satellites have been demonstrated to be effective for studying suspended sediment in smaller coastal and inland environments due to having sufficient resolutions for such regions.

When using remote sensing to study SPM, the establishment of a relationship between SPM concentrations and reflectance data, along with the resulting algorithm, is site specific. This site specific quality of suspended sediment algorithms is credited to the variations in suspended sediment within different bodies of water. This includes inorganic particle properties such as size, shape, and mineralogy (Binding et al., 2005). It has also been demonstrated that the applicability of an algorithm may diminish after several years if a watershed event alters the properties of the sediments delivered to the waterbody (Devi et al., 2015). Previous investigations have developed models to study SSCs in the Gulf of Mexico region, including in the Mississippi Sound (Merritt, 2016), Tampa Bay (Hu et al., 2004), the Mississippi Delta (Kaufman et al., 2003), and Mobile Bay (Zhao et al., 2011). Prior to this study, there has yet to be an investigation of this nature exclusively focused on Weeks Bay in Alabama.

Substantial research using remotely sensed imagery to study suspended sediment has been completed all over the world. Kaba et al. (2014) sought to produce historic sediment concentrations in Lake Tana using Terra MODIS images due to the erosion crisis in Ethiopia. Kaba et al. (2004) used MODIS imagery to determine the linear relationship between reflectance in the red and NIR band regions and total suspended sediments, turbidity and Secchi depth in the largest lake of Ethiopia.

Many studies have used remotely sensed reflectance data specifically in the Gulf of Mexico region. For example, Hu et al. (2004) explored three different methods to derive water quality parameters from remotely sensed imagery within the Tampa Bay estuary. Hu et al. (2004) tested a regression of *in situ* data against total radiance, single-scattering corrected total radiance, and multi-scattering corrected total radiance to determine that a simple regression with *in situ* data is satisfactory for synoptic studies of estuaries and that more complex atmospheric correction processes provide little gain (Hu et al., 2004). Similarly, Kaufman et al. (2003) used MODIS imagery to determine an empirical algorithm that can be used to identify areas with suspended sediment in shallow waters with bottom reflections and turbid waters in regions including the Mississippi Delta and the west coast of Florida.

Furthermore, the study by Haihong Zhao (2009) created a model for suspended sediment within Mobile Bay, Alabama using MODIS band 1 (red) imagery. Due to the larger size of Mobile Bay, MODIS imagery was acceptable for the study by Zhao et al. (2009). As a tributary estuary of Mobile Bay, Weeks Bay is significantly smaller than its parent, and therefore requires a satellite with a finer spatial resolution. Landsat meets this requirement, while still providing sufficient spectral bands for determining SSCs.

Numerous studies have used Landsat imagery when spatial distribution requires more precision (Amos & Alfoeldi, 1979; Mertes et al., 1993; Lodhi et al., 1998; Zhang, 2005; Wang et al., 2009; Qu, 2014; Montanher et al., 2014; Kong et al., 2015a; Lobo et al., 2015; Zheng et al., 2015) or a combination of Landsat and MODIS imagery (Min et al., 2012; Zhang et al., 2014). Gernez et al. (2015) used a combination of SPOT4 and Landsat 5, 7, and 8 imagery to study SPM concentrations in the turbid Gironde and Loire

estuaries in France. Lodhi et al. (1998), created twenty SSCs in a 7510 liter tank and used a high resolution spectroradiometer to obtain measurements that were then converted into the band widths of the Landsat- TM sensor. This study found that the wavelength range between 700 and 900 nm to be best for determine SSCs and that a second-order regression model to be the best estimator of SSC (Lodhi et al., 1998). Additionally, Lodhi et al. (1998) demonstrated that spectroradiometer data converted into Landsat band widths to may be used to accurately estimate SSC. More recently, Zhang et al. (2014) conducted an investigation on inter-annual and seasonal variations of SSC between 2000 and 2010 in the Yellow River estuary using Landsat TM and ETM+ data. Zhang used Terra MODIS data to make atmospheric corrections and *in situ* data to create a model for retrieving SSC from Landsat imagery. A regression analysis was used to establish a positive correlation between *in situ* TSM measurements and Landsat reflectance. Similarly, the study by Kong et al. (2015a) relied on Landsat TM images to determine SSC in the Caofeidian coastal waters. The study looked at various bands and band ratios, as well as numerous model types such as linear, logarithmic, quadratic, power, and exponential (Kong et al., 2015a). The study also took into account the ratio of the reflectance to the particle size, i.e. binary combination factors. Kong et al. (2015a) determined the best model to be a quadratic relationship with the 3/2 TM band ratio, which corresponds to a red/green band ratio.

Furthermore, the study by Zhang (2005) on SSC and turbidity in Old Woman Creek, Ohio relied on Landsat-7 imagery to observe a study area of only 0.3 km^2 (Zhang, 2005). Zhang (2005) calculated SSC using turbidity values from automated collection stations using a relationship determined in a previous study. The SSCs were then related

to Landsat-7 reflectance values using a multivariate regression method to establish a model for determining SSC remotely. Zhang (2005) considered a total of 21 predictor variables, consisting of six Landsat bands and their 15 band ratios. The best model for determining SSC from Landsat reflectance data was found to be based on band 2 and band 4 of Landsat-7, which correspond to the green and NIR spectral regions (Zhang, 2005).

Bowers & Binding (2006) stated that ratios between two reflection coefficients are not sufficient for detecting variations in scattering, and that a combination of satellite measurements of brightness as well as color will produce a more accurate estimate of SSC. They used Monte Carlo modeling to relate absorption and scattering to attenuation and reflection coefficients in the Irish Sea (Bowers & Binding, 2006). Similarly, Kong et al. (2015b) developed a model to determine SSC using Landsat-5 imagery in the Gulf of Bohai using a quadratic polynomial semi-analytical model. The model was based on the inherent and apparent optical properties of water (Kong et al., 2015b).

Han et al. (2016) sought to develop an algorithm for the remote sensing of SPM that was appropriate on a global scale. The GlobCoast project collected *in situ* SPM and Rrs data from multiple coastal environments in Europe, French Guiana, North Canada, Vietnam, and China in order to represent environments of different biogeochemical and physical processes (Han et al., 2016). The study tested various empirical and semi-analytical approaches, seeking to find a single approach that allowed for global application. While a single algorithm was unable to be developed for global use, a generic semi-analytical approach was developed based on two standard semi-analytical equations for low-to-medium and highly turbid waters, as well as a mixing law for

intermediate waters (Han et al., 2016). Algorithm coefficients were calculated for a number of different remote sensing sensors, with the performance of the algorithm varying only slightly between the different systems (Han et al., 2016).

2.7 Study Site

As small, inland, tributary estuary, Weeks Bay is an ideal study site for the research of bio-optical properties utilizing the Landsat satellite. Weeks Bay has been established as an area of high research activity, but has yet to have a study of this nature conducted upon it.

2.7.1 The National Estuarine Research Reserve System (NERRS)

In 1972, the Coastal Zone Management Act (CZMA) was passed by Congress. In this act, Congress officially recognized the value, as well as the loss and damage, of coastal zones due to their natural, commercial, recreational, ecological, industrial, and esthetic resources (NOAA, 2005). The CZMA defines a "coastal zone" as the coastal waters and the adjacent shore lands that are strongly influenced by each other, including islands, transitional and intertidal areas, salt marshes, wetlands, and beaches (NOAA, 2005). The CZMA was established to manage, develop, and protect these ecologically fragile coastal zones from the threat of the effects of population growth and economic development. In order to effectively protect these valuable resources, the CZMA states that coastal states must be encouraged to exercise authority over these areas, with the assistance of federal and local governments.

The National Estuarine Research Reserve System (NERRS) was included as part of the CZMA in section 315 in order to designate and protect estuarine systems of the

United States. Under the CZMA, an estuary is defined as "a part of a river or stream or other body of water having unimpaired connection with the open sea, where the sea water is measurably diluted with fresh water derived from land drainage" (NOAA, 2005). An estuary may be declared a national estuarine reserve if it is a representative estuarine ecosystem that is suitable for long-term research and contributes to the biogeographical and typological balance of the NERRS, the law of the coastal state can provide long-term protection for the estuarine resources, designation of a reserve will further public awareness and provide opportunities for public education, and the coastal state has complied with the requirements of the regulations issued by the Secretary (NOAA, 2005). There are currently 28 coastal sites, covering 1.3 million acres of land that have been designated as NERRS locations. Each NERRS site is run by local state or university management, and is both funded and overseen by the National Oceanic and Atmospheric Administration (NOAA). As a result of this act, in 1986, Weeks Bay in Alabama became the 16th site of the NERRS and was renamed as the Weeks Bay National Estuarine Research Reserve.

Through the NERRS, a framework has been established for the sharing of management approaches, research results, and techniques for estuarine education between programs within the nation (NOAA, 2007). This has allowed for an increase in understanding and national coordination in our knowledge of estuarine ecosystems. From this further understanding, we can devise improved methods of preserving estuarine environments.

2.7.2 The Weeks Bay NERR

The Weeks Bay NERR is located in Baldwin County, Alabama, approximately 30 miles southeast of Mobile. The reserve covers an area of 6,525 acres of both land and water habitats that include forested wetlands and swamps, marshes, and submerged aquatic vegetation (NOAA, 2007). Weeks Bay is a small, shallow, coastal estuary with an average depth of 1.6 meters and a surface area of approximately 4 square miles (NOAA, 2007). Weeks Bay is secondarily characterized as a tributary estuary due to being part of the greater Mobile Bay estuary system (Cartwright, 2002). The bay has a daily tidal pattern with a mean range of approximately 0.4 meters (Miller-Way et al., 1996). Freshwater discharges into the bay from the Fish and Magnolia Rivers, while an inflow of saltwater is provided by the Gulf of Mexico through Mobile Bay. The Fish River is the dominant source of freshwater, providing 73% of the approximately 9 m^3s^{-1} inflow (Miller-Way et al., 1996). The bottom of the bay is composed of a combination of silts and clays deposited from the Fish and Magnolia Rivers within the interior of the bay. In addition, Weeks Bay contains quartz sand deposits around the perimeter, most likely the result of erosion along the shoreline (Miller-Way et al., 1996).

2.7.2.1 Weeks Bay Watershed

The watershed of Weeks Bay covers an area of around 149,000 acres in Baldwin County, and includes parts of the city limits of Fairhope, Robertsdale, Foley, and Loxley (NOAA, 2007). It includes the watersheds of the Fish and Magnolia Rivers. The watershed of Weeks Bay has experienced substantial urban growth throughout its recent history. The population of Baldwin County has increased significantly between 1990 and 2010. The census populations for Baldwin County in 1990, 2000, and 2010 were

determined to be 98,280, 140,415, and 182,265 respectively (Forstall, 1995; U.S. Census Bureau, 2000, 2010). This equates to a 42.87% population increase between 1990 and 2000 and a 29.80% increase between 2000 and 2010. Corresponding to the population increase is a decrease in forested and herbaceous vegetation and an increase in urban/built-up land cover between 1990 and 2000 as depicted in Table 2.2 (Cartwright, 2002). Urban development has likely continued to increase since 2000, given the continued rise in population. Within the Weeks Bay watershed, in 2011 the percentage of land classified as "Urban/Built Up" was 14.73% according to the USGS 2011 National Land Cover Database (NLCD) and the classifications described by Cartwright (2002), while the percentage of "Forested Vegetation" was 32.58%, and "Herbaceous Vegetation" was 42.42%. The Economic Development Alliance (EDA) of Baldwin County describes Baldwin County's significant growth by stating that the county is tied for the 8th fastest growing metropolitan statistical area (MSA) in the nation in 2014, was the fastest growing county in Alabama in 2015, has had a 45% population growth since 2000, and has the largest projected population growth among all Alabama MSAs (Baldwin County EDA, 2017).

Table 2.2 Land Use/Land Cover Change Between 1990 and 2000 in Baldwin County

	1990			2000			
	Percent of Watershed	Acres	Hectares	Percent of Watershed	Acres	Hectares	Percent Change
Water	1.84%	2,302	932	1.89%	2,365	957	2.74%
Forested Vegetation	33.12%	41,468	16,781	31.49%	39,431	15,957	-4.91%
Herbaceous Vegetation	28.94%	36,235	14,664	21.00%	10,640	10,640	-27.44%
Seasonal Herbaceous Vegetation	19.72%	24,696	9,994	23.20%	11,753	11,753	17.60%
Transitional/ Mixed Vegetation	7.08%	8,864	3,587	12.22%	6,910	6,190	72.56%
Urban/ Built-Up	1.34%	1,677	679	2.58%	1,306	1,306	92.47%
Sparse/ Residual Vegetation	7.96%	9,969	4,034	7.63%	3,868	3,868	-4.13%

Baldwin County, Alabama has experienced a significant increase in urban/build-up land cover/land use (Cartwright, 2002)

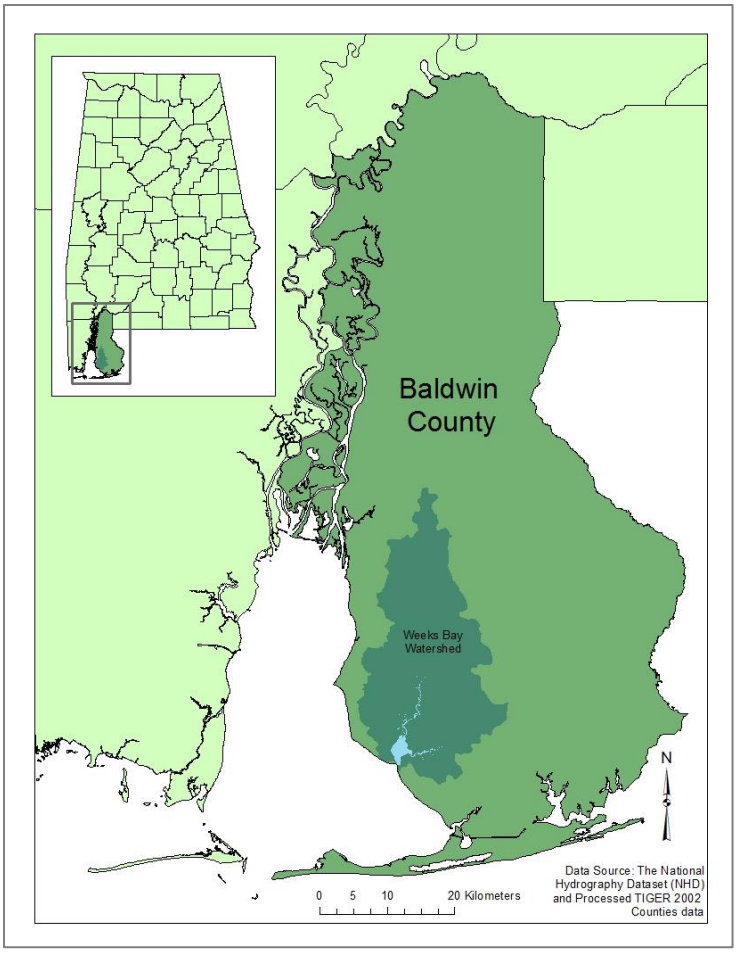

Figure 2.1 Weeks Bay Watershed in Baldwin County, Alabama

The Weeks Bay watershed covers 149,000 acres in Baldwin County (NOAA, 2007).

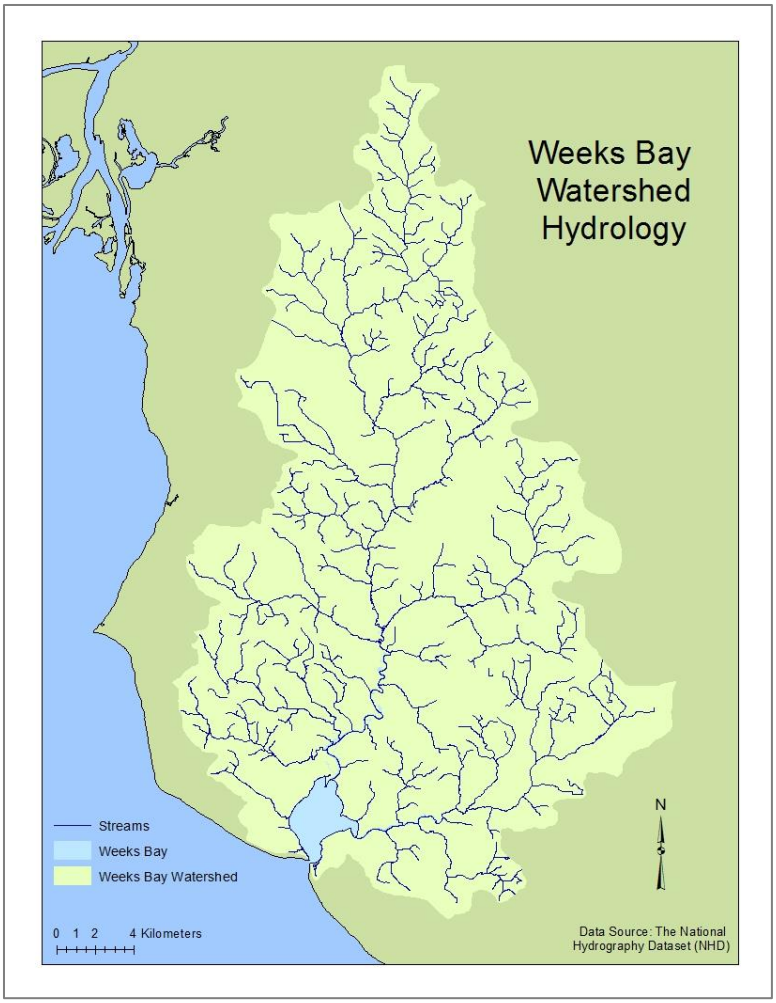

Figure 2.2 Weeks Bay Hydrology

The Weeks Bay watershed includes the watersheds for the Fish and Magnolia Rivers.

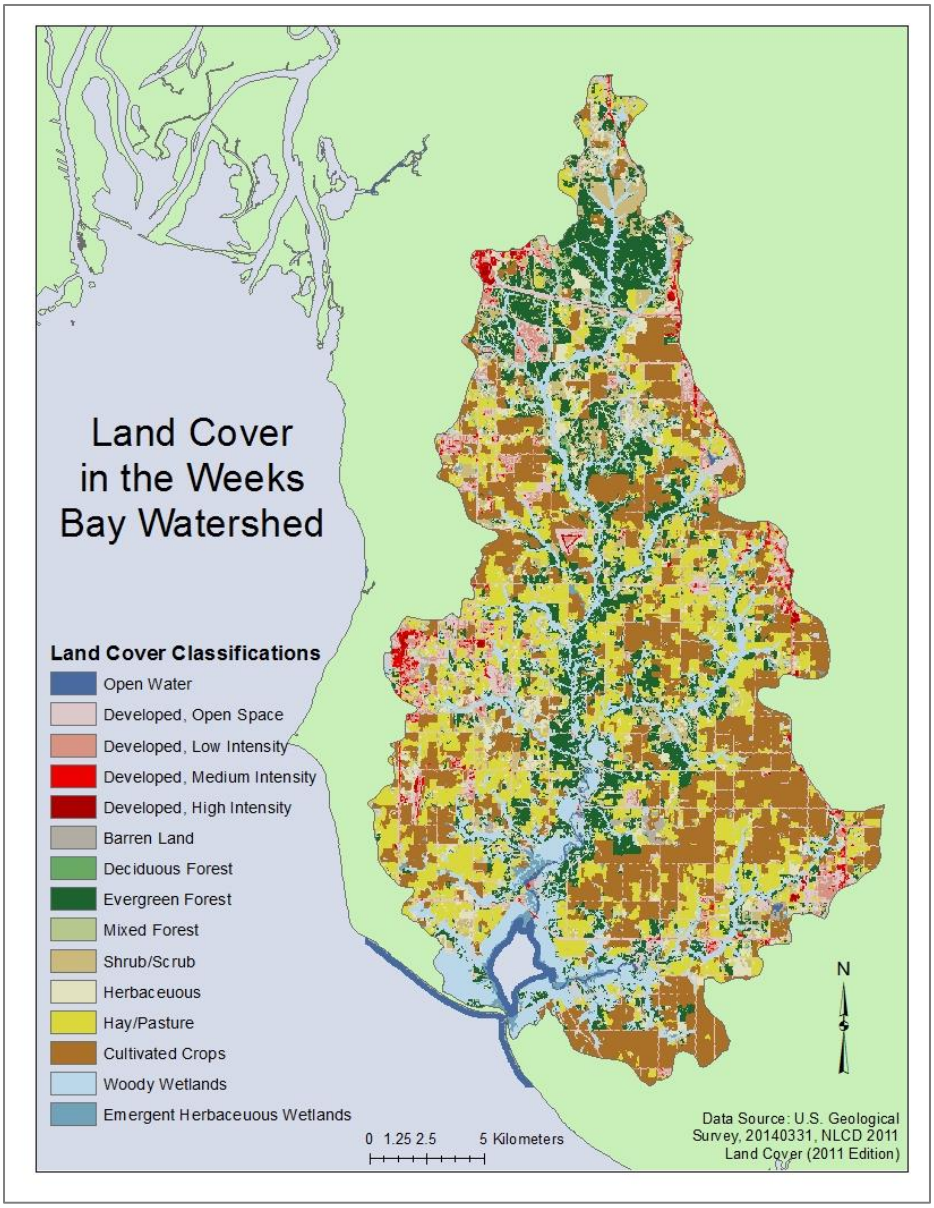

Figure 2.3 Land cover in the Weeks Bay watershed

2.7.2.2 Climate

The Weeks Bay watershed is located in a humid subtropical climate region with warm summers and relatively mild winters and occasional cold waves (Miller-Way et al., 1996). The Gulf of Mexico provides a relatively constant flow of usually unstable, humid

air that results in frequent thunderstorms during the summer months (Miller-Way et al., 1996). Strong winds from tropical storms and cold fronts reduce vertical stratifications and horizontal variations in sediment concentrations by causing an increase in turbulent mixing (Zhao, 2009). The western and eastern shores of Mobile Bay receive an average annual precipitation total of 165 centimeters (65 inches) from a combination of winter storms, thunderstorms, and tropical systems, making it one of the wettest regions along the Gulf Coast (Miller-Way et al., 1996). Maximum summer air temperatures typically vary between the upper 20°C (80 °F) the lower 30°C (90 °F) range, with thunderstorms usually limiting peak temperatures to this ranges (Miller-Way et al., 1996). High absolute humidity, however, occasionally allows the Mobile and Weeks Bay region to experience temperatures exceeding 38°C (100 °F) (Miller-Way et al., 1996)

.

CHAPTER III

DATA AND METHODS

3.1 *In Situ* Measurements

In situ water samples were collected on four days between May and September 2016. Collection corresponded to Landsat 8 passes over Weeks Bay as depicted in Table 3.1. Weeks Bay is visible in both path 20 and 21 along row 39. Twelve sampling locations were selected prior to the first date of collection such that the points were dispersed throughout Weeks Bay, with one point in Mobile Bay at the mouth of Weeks Bay (Figure 3.1). By planning to sample a transect of Weeks Bay from Fish River to the mouth of the estuary, it was expected that the samples would display a range of salinities, as well as a range of SSCs, due to river input being the most important source of sediment for most estuaries (Kennett, 1982). Sampling occurred between approximately 9:00 AM and 1:00 PM local time to coincide with the 11:25 AM (Path 21) or 11:19 (Path 20) overpass of the Landsat 8 satellite.

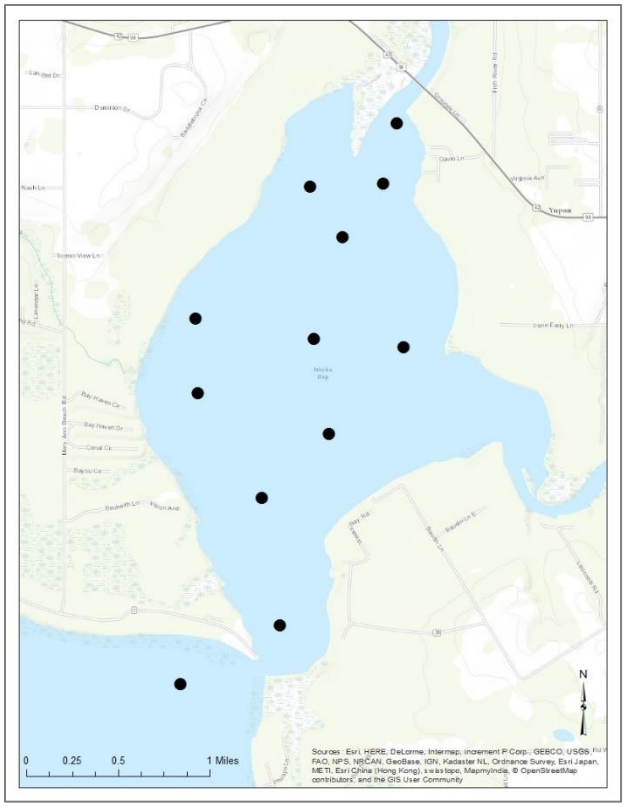

Figure 3.1 Predetermined Sampling Locations

Table 3.1 Landsat 8 scenes corresponding to periods of water sample collection

Date	Entry ID	Row	Path	Cloud Cover (%)	Sun Elevation (degrees)	Sun Azimuth (degrees)
5/9/16	LC80210392016130LGN00	39	21	82	66.80024	118.3639
6/19/16	LC80200392016171LGN00	39	20	35	68.81741	103.5181
6/26/16	LC80210392016178LGN00	39	21	10	68.46992	103.4206
9/30/16	LC80210392016274LGN00	39	21	0	51.72757	147.5127

3.1.1 Field Measurements

At each sampling location, GPS coordinates (+/- 3 m or less accuracy) were taken to ensure improved spatial accuracy when relating the *in situ* observations to observed satellite reflectance. Three surface water samples were taken in clean 32 ounce Nalgene bottles. Samples were collected from the upper 20-40 cm of the water column on behalf

of the assumption that light at 645 nm can penetrate the upper 40 cm of the water column (Zhao et al., 2011) and so the *in situ* water samples would reflect the view of the Landsat sensors as closely as possible. The samples were then immediately chilled at ~1-5℃ by placing them into a cooler with ice until lab processing.

A Geophysical and Environmental Research (GER) 1500 Radiometer was used to determine water surface reflectance in the region from 300 to 1050 nm. At each site location, two sets of scans were taken. Each set of scans including a reference scan of a 99% spectralon reference panel by Labsphere, three consecutive scans of the target surface water, and a scan of the sky such that the radiometer was held at a 45° angle directed away from the sun at a clear portion of the sky.

Additionally, a number of other measurements were recorded at each sampling location. An Eco-Triplet was used to determine the profiles of fluorescence for chlorophyll, phycocyanin, and phycoerythrin to account for the organic portion of the samples. Depth and Secchi depth observations were recorded at each sampling location. A calibrated Hanna multiparameter probe was used to record the vertical profiles of pH, dissolved oxygen, temperature, and salinity at each site.

3.1.2 Spectroradiometer Reflectance Measurements

Raw GER 1500 radiometer data collected from each sampling location was downloaded and then processed into Landsat-8 reflectance values. The raw radiometer values provided by the radiometer were converted into Rrs, by applying the following equation to each of the three target recordings at each wavelength:

$$Rrs = \frac{L_{target} - (0.02 L_{sky})}{99 L_{reference} \pi} \quad (3.1)$$

Where L_{target} is the radiance of the target surface water, $0.02L_{sky}$ is an approximation for the Rayleigh path radiance, and $99L_{reference}\pi$ is the incident solar energy as recorded by the 99% spectralon reflectance panel. The spectral curve for each target scan was plotted in order to visually assess the accuracy of each. If a particular target scan differed greatly, it was not included in an average of the target scans. This was done for both sets of scans taken at each site location. The two sets were then averaged together to calculate the final Rrs value for each wavelength at each site location.

The GER 1500 radiometer collects data in 512 bands that range from 284.84 nm to 1094.17 nm with an average interval of 1.58nm. In order to mimic Landsat 8 observations, the radiometer hyperspectral data must be converted into the multispectral bands associated with the satellite sensors. Landsat 8 collects in 11 spectral bands as previously described in Chapter 2.4. For the sake of SPM modeling, the hyperspectral data were only converted to bands 1-5, which are bands corresponding to visible and NIR wavelengths, as well as band 8 which is the panchromatic band.

Each band reports a single value for each pixel within the scene, which represents the reflectance received over a specific spectral range. To convert the hyperspectral data into six single readings, the hyperspectral data must first be interpolated such that the radiometer values are converted into whole integers, opposed to decimal values. This allows the RSR of the Landsat 8 OLI sensor to be applied to the radiometer data. The RSR reports the sensitivity of each given wavelength for the various satellite bands. The RSR value will be close to one at the band center, such that the sensor is most sensitive to those wavelengths, and will decrease as the wavelength values move away from the band center as the sensor's sensitivity decreases. The RSR function must be applied for each of

the six Landsat 8 bands to the radiometer data in order to derive the values given for each pixel observed by the satellite.

3.1.3 Particulate Backscattering

At each sampling location, an Eco-Triplet was used to record profiles of optical backscattering at wavelengths of 470, 532, and 650 nm. Following the precedent set by Reynolds et al. (2001), the value of backscattering at 555 nm was selected for the parameterization of our model. The value of backscattering at 555 nm was calculated by determining the unit b_{bp} value between $b_{bp}(532)$ and $b_{bp}(650)$. The b_{bp} value at 555 nm was then calculated through the addition of the unit b_{bp} value to $b_{bp}(532)$. Using the backscattering at 555 nm, b_{bp} was determined using the equation derived by Reynolds et al. (2001):

$$b_{bp}(\lambda) = b_{bp}(555)\left(\frac{555}{\lambda}\right)^{\gamma} \tag{3.2}$$

Where γ is the spectral slope and may be calculated using the equation (D'sa et al., 2007; Dash et al., 2011):

$$\gamma = -0.566 - \left[1.395\ log\{b_{bp}(555)\}\right] \tag{3.3}$$

3.2 Lab Methods

Directly after collection, the water samples were filtered and processed for the analysis of SPM, CDOM, High Performance Liquid Chromatography (HPLC), absorption, toxins, PC, toxic metals, nutrients, microscopy, and four different bacteria counts including Heterotrophic Plate Counts (HPC), E Coli, Enterococci (ENT), and

Total Coliform. Only SPM, CDOM, and PC were required for the modeling process. The remaining data was gathered for use in future research.

3.2.1 Suspended Particulate Matter (SPM)

Water samples were filtered for SPM within 24 hours of collection in order to limit the deterioration of organic particulate matter. SPM concentrations in mg/L were determined using the glass-fiber filter method (Guy and Norman, 1970; Merritt, 2016). Filtration was done using Whatman GF/F 47 mm glass microfiber filters (pore size 0.7μm). For each sampling date, enough filters for duplicates of each sample and two controls were combusted in aluminum foil at 500℃ for one hour to remove any contaminant matter. Once contaminants were eliminated from the filters, they were washed in distilled (DI) water, and then placed within individually in separate labeled 43 mm VWR International Aluminum Crinkle Dishes. The filters in the aluminum dishes were then dried at 105℃ for one hour. Filters were then weighed to four significant digits before being used to filter the water samples. Once the filters were prepared and weighed, 200 mL of water sample was filtered through the Whatman filter papers using a vacuum pump filtration system. Samples were filtered at a reduced pressure to avoid damaging any organisms present within the sample. The filter was dried once again at 105℃ for one hour, and then reweighed to four significant digits. This weight, minus the weight of the filter, represents the total concentrations of SPM in mg/L. The sample filters were then wrapped individually in foil, baked at 500℃ for one hour to fully combust organic material and then reweighed to determine the SPIM concentrations. The SPOM concentrations were then determined by subtracting the SPIM concentrations from the total SPM concentrations.

3.2.2 Color Dissolved Organic Material (CDOM)

Water samples were filtered for CDOM on the same day as collection to diminish the possible degradation of organic content. CDOM concentrations were determined using the method described by Dash et al. (2011). Subsamples (50 ml) of the surface water sample were filtered through Whatman Nuclepore Track-Etch Membrane filters with 47 mm diameter and 0.2 μm pore size using a low pressure water retaining vacuum. The 0.2 μm pore size removes all components of the water sample barring CDOM, such that the remaining water may be analyzed to determine the absorption solely due to CDOM. The samples were stored in amber colored bottles and refrigerated at 4°C until analysis could occur. Amber colored bottles were used to reduce the amount of light the samples were exposed to.

The analysis was performed using a PerkinElmer Lambda 850 spectrophotometer that records an absorption spectra between 200 nm and 750 nm at 2 nm intervals. Samples were allowed to reach room temperature before analysis. The spectrophotometer records a scan of both DI water and the sample water in order to subtract the DI absorption from the sample water absorption, therefore reporting the absorption of CDOM alone. Absorption between wavelengths of 702 nm to 750 nm is expected to be zero, making a baseline correction necessary to rectify the initial output of the spectrophotometer. The absorbance values between 702 nm and 750 nm were averaged and this average was subtracted from each wavelength between 400 nm and 700 nm. Any negative absorbance values were assumed to be zero. After the baseline correction, the absorption coefficient was calculated using the following equation:

$$\alpha(\lambda) = \frac{2.303A(\lambda)}{l} \tag{3.4}$$

Where, $a(\lambda)$ is the absorption coefficient at each wavelength, $A(\lambda)$ is the absorbance, and l is the path length in meters, which was 0.01m for the cubic used in the PerkinElmer Lambda 850 spectrophotometer.

3.2.3 Phycocyanin (PC)

The absorption of phycocyanin (PC) may be determined through the concentration measurement of PC at each sampling site. In order to determine the concentration measurement, 50 ml of sample water was filtered onto polycarbonate filters with 4.7 cm diameter and 0.2 µm pore size. The filtered samples were then frozen at -20°C until analysis. PC was extracted from the filtered samples using the method described by Horvath et al. (2013) using a 0.05 M phosphate buffer (pH 6.8). The filter papers were placed in 15 ml centrifuge tubes with 5 ml of the buffer solution and then vortexed for approximately one minute to displace cells from the filter paper into the buffer solution. The samples were then placed on ice and sonicated using a Misonix Sonicator 3000 at 30-40 W until the filter paper degraded (approximately 2 minutes). Samples were then incubated in a dark refrigerator set at 4°C for 1 hour. After incubation, the samples were centrifuged at 4000 RPM with a relative centrifugal force of 1,240g in an IEC Centra CL2 centrifuge for 10 minutes. The samples were then ready to be placed in a Horiba Jovin Yvon FloroMax®-4 Spectrofluorometer with $\lambda_{excitation}$=615 nm and $\lambda_{emission}$=647 nm to measure fluorescence. The sample fluorescence values were then interpolated using the following previously constructed standard PC curve equation that adjust for the volumes of both the sample water and buffer solution in order to determine PC concentrations:

$$PC\left(\frac{\mu g}{L}\right) = \frac{\frac{[F_S - F_b]}{R} * [467.52 - 0.3622] * V_b}{V_s} \quad (3.5)$$

Where F_s is the fluorescence of the filtered sample, F_b is the fluorescence of the buffer solution, V_b is the volume in liters of the buffer solution, V_s is the volume in liters of the filtered sample, and R is the Raman peak area.

3.2.4 Algal and Non-Algal Particulate Absorption

Suspended particulate matter (SPM) may be divided into both algal and non-algal particulate components. In order to determine the absorption of both components, within 24 hours of sample collection, 50 mL of sample water was filtered with a low pressure vacuum using Whatman GF/F glass fiber filters with 25 mm diameter and 0.7 µm pore size. The filter papers were than stored in tissue capsules and frozen at -80°C until analysis. The filter papers were kept in the dark as much as possible to inhibit the deterioration of the organic component.

Before processing began, samples were allowed to reach ambient room temperature by being placed in the dark at room temperature for approximately 30 minutes. Analysis of absorption was performed using the same PerkinElmer Lambda 850 spectrophotometer that was used to determine the absorption of CDOM. The absorbance between 200 nm and 750 nm at 1 nm intervals was determined for each of the samples, as well as for a filter paper filtered with 15 ml of distilled water.

Once each sample was run to determine the total absorbance, the filter papers were placed in 15 ml of methanol for a minimum of 30 minutes and then filtered to dissolve phytoplankton. The filter papers were run once again using the spectrophotometer to determine the non-algal particulate (NAP) absorbance. The NAP

absorbance value was subtracted from the total absorbance value in order to determine the absorbance of phytoplankton.

3.3 Satellite Processing

Landsat 8 OLI data is freely available from the USGS through the Earth Explorer user interface (https://earthexplorer.usgs.gov/). Landsat 8 images were downloaded for dates corresponding to *in situ* sampling, as expressed in Table 3.1. Files are provided in a compressed tape archive (tar) file, with each band in a separate GeoTIFF format. The bands are displayed using the Universal Transverse Mercator (UTM) projection. A Landsat Metadata file is included in each scene download, providing information such as correction coefficients, the sun elevation, and other collection information.

Landsat 8 data is provided as Digital Numbers (DN) in 16-bit unsigned integer format. These were then converted into Top Of Atmosphere (TOA) reflectance by using the provided radiometric rescaling coefficients (USGS, 2015). Using these coefficients, Equation 3.6 was applied to each band to convert into TOA Reflectance:

$$\rho\lambda' = M_\rho Q_{cal} + A_\rho \tag{3.4}$$

Where $\rho\lambda'$ is the TOA planetary reflectance, without correction for solar angle, M_ρ is the band specific multiplicative rescaling factor from the metadata (REFLECTANCE_MULT_BAND_x, where x is the band number), Q_{cal} is the standard product pixel values (DN), and A_ρ is the band-specific additive rescaling factor from the metadata (REFLECTANCE_ADD_BAND_x, where x is the band number) (USGS, 2015). The TOA reflectance was than corrected for variations in the solar angle with Equation 3.7:

$$\rho\lambda = \frac{\rho\lambda\prime}{\cos\theta_{SZ}} = \frac{\rho\lambda\prime}{\sin\theta_{SE}} \quad (3.5)$$

Where $\rho\lambda$ is the TOA planetary reflectance, θ_{SZ} is the local sun elevation angle in degrees from the metadata (SUN_ELEVATION), and θ_{SE} is the local solar zenith angle such that $\theta_{SZ} = 90° - \theta_{SE}$ (USGS, 2015).

3.4 SPM Retrieval Algorithm Development and Validation

Numerous previously developed models for SPM and SPIM retrieval using remote sensed reflectance were assessed to determine the functionality for Weeks Bay as depicted in Table 3.2. Each model was first tested exactly as published in the literature. The previously developed models were then adjusted by keeping the defined independent parameters, and altering the coefficients by running regressions with the Weeks Bay SPM/SPIM data. Two-thirds of the sample sites were used to develop the new coefficients, with one-third being reserved for the validation of the adjusted models. For each model, both original and adjusted, the R^2 and root mean square error (RMSE) statistics were provided. R^2 is the coefficient of determination and measures the proportion of the variance in the SPM/SPIM concentrations that is explained by the independent variables (Chapman, Lembo, & Monroe, 2014). Being a proportion, the most significant R^2 value is R^2=1, such that 100% of the variability is explained by the independent variables. The RMSE measures the difference between the predicted and observed values. RMSE was calculated in mg/L, as depicted in Equation 3.8, as well as a percent, as depicted in Equation 3.9.

$$RMSE\ \left(\frac{mg}{L}\right) = \sqrt{\frac{\sum_{i=1}^{n}(y_p - y_o)^2}{n}} \quad (3.8)$$

$$RMSE\ (\%) = \frac{RMSE\left(\frac{mg}{L}\right)}{observed\ maximum - observed\ minimum} * 100 \quad (3.9)$$

Once the previously developed models were tested, many additional possible reflectance parameters were tested as potential variables in a Weeks Bay SPM/SPIM retrieval algorithm. These reflectance parameters included single bands, the natural logs of single bands, band ratios, band combinations, and combinations of the previously listed. Both linear, and nonlinear models were tested for each reflectance parameter. As with the alteration of coefficients in preexisting models, 32 sites were used for model development, with 16 being reserved for validation. Exponential, logarithmic, power, 2nd order polynomial, and 3rd order polynomial equations were considered as potentials for the nonlinear modeling. The algorithm with the highest R^2 value was chosen for each reflectance parameter. A multiple linear regression was also considered for an SPM concentration retrieval algorithm.

In addition to the R^2 and RMSE statistics, the p-value, F-statistic, t-statistic, and Pearson's product moment correlation coefficient (R) were also reported. The p-value reports the statistical significance of the linear regression. The 95% level was used to assess significance, such that an algorithm with a p-value of less than 0.05 is considered significant and therefore a good fit for the data. Due to the nature of the p-value calculation, the p-values will not be provided for the nonlinear regression equations (Frost, 2014). The F-statistic is a ratio of two variances and assesses the difference of variances (Frost, 2016). The t-test compares two sample means for difference and may be used to determine if the predicted SPM/SPIM values coincide with the *in situ* observations (Chapman, Lembo, & Monroe, 2014). Pearson's product moment correlation coefficient measures the association of the linear relationship between two

variables with a strength between +1 and -1 (Chapman, Lembo, & Monroe, 2014). The stronger the association, the closer R is to +/- 1. A correlation greater than 0.8 is generally considered to be strong, while any correlation less than 0.5 would be described as weak (Roberts & Roberts, 2017).

A limited number of possible reflectance parameters for SPM were also analyzed for each sampling trip on an individual basis. Due to the small sample size per sampling trip (n=11, 12, or 13), four sites were reserved from each field cruise for validation. Both a linear and nonlinear model was considered for each reflectance parameter. For the nonlinear models, exponential, logarithmic, power, and 2nd order polynomial equations were considered. A 3rd order polynomial equation was not considered in order to limit the complexity when using such a small sample population.

Table 3.2 Previously Developed SPM/SPIM Retrieval Algorithms

Author	Model	x	Satellite	SPM Range (mg/L)	R^2	Error	Location
Doxoran et al, 2002	SPM=12.996*exp(x/0.1829)	x=NIR/Red	SeaWifs, MODIS, MERIS	0-2250	0.89	RE=+/-10%	Gironde
Han et al, 2006	Log_{10}(SSC)=0.892+6.2244(x)	x=[Green+Red]/[Green/Red]	MODIS	n/a	0.9147	n/a	Yangste
Kong et al, 2015a	SSC=70.939-272.62x+296.29x^2	x=Red/Green	Landsat TM	4.3-104.1	0.9773	RMSE=23.35%	Caofeid
Lobo et al, 2014	TSS=2.64*(x-2.27)$^{0.45}$	x=Red	Landsat TM and OLI	35.3-115.2	0.94	RMSE=1.33%	Tapajós
Lodhi et al, 1998	SSC=19.516+42.65+23.16x^2	x=NIR	Landsat TM	50-1000	0.99	RMSE= 31.880 mg/L	Large ta
Martinez et al, 2015	SPM=20.41[x]$^{1.173}$	x=Red	Landsat TM	5–620 g/m^3	0.81	RMSE= 114.1 g/m^3 to 61g/m^3	Amazor
Wang et al, 2009	Ln(SSC)=3.18236*x-1.40060	x=Ln(NIR)	Landsat ETM+	22-2610	0.88	MAE= –46 mg/L	Yangste
Zhang, 2005	Ln(SSC)=14.727+2.5228*x_1+1.3147*x_2	x_1=Ln(Green); x_2=Ln(NIR)	Landsat-7	0-284	0.749	MSPE=0.6502	Old Wo
Zhao et al, 2011	SSC=2.12*exp[45.92(x)]	x=Red	MODIS	0-87.8	0.78	n/a	Mobile
Zheng et al, 2015	TSM=6110.3*Rrs(x)-1.8242	x=NIR	Radiometer, Landsat OLI	4-101	0.81	RMSE= 5.79 mg/L	Dongtin

3.5 SPM Simulation

A semi-analytical simulation approach was attempted to determine the contribution of Rrs from the various OACs present in Weeks Bay, including SPM/SPIM. In order to simulate the Rrs of a water body, one must take into account the reflectance of all OACs within the water body being studied. The total reflectance of the water may be represented by the following equation:

$$Rrs_{total} = Rrs_{water} + Rrs_{Chla} + Rrs_{CDOM} + Rrs_{NAP} \quad (3.10)$$

Through inherent optical properties, Rrs may be determined by the following equation:

$$Rrs(\lambda) = 0.54(\frac{f}{Q})(\frac{b_b}{a+b_b}) \quad (3.11)$$

where 0.54 corrects for Fresnel reflectivity, f is the coefficient of anisotropy of the light field, and often takes a value of 0.33 for the sun at the zenith and a level sea surface; Q is the conversion factor between radiance and Rrs; b_b is the backscattering coefficient, such that all OACs of the water are accounted for, and a is the absorption coefficient such that all OACs of the water are accounted for (Reynolds et al., 2001; Dash et al., 2011). By including the backscattering and absorption coefficients of all OACs, Equation 3.11 may be modified the total Rrs such that

$$Rrs_{total} = 0.54\left(\frac{f}{Q}\right)\left(\frac{b_{bw}+b_{bp}}{(a_w+cdom+a_{chla}+a_{NAP}+a_{pc})+(b_{bw}+b_{bp})}\right) \quad (3.6)$$

Where b_{bw} is the backscattering of water, b_{bp} is the backscattering of all particulate matter, and a_w, a_{cdom}, a_{chl}, a_{NAP}, and a_{pc}, are the absorption coefficients of water, CDOM, Chl a, SPIM, and PC respectively.

The components of non-algal (NAP) and algal (Chl a and PC) particulates may then be removed from the simulation equation to simulate the Rrs of all components except the suspended particulate matter, such that the equation only includes the backscattering and absorption for water, CDOM, and PC. This value was then subtracted from the Landsat reflectance data in order to obtain the reflectance solely from SPM. Additionally, only the inorganic OAC (NAP) may be removed from the simulation to simulate the Rrs of the water body without the presence of inorganic suspended sediment. This value was then subtracted from the Landsat reflectance data in order to obtain the reflectance solely from SPIM.

3.6 Precipitation Data

As a NERR, Weeks Bay has a meteorological station located within the grounds of the reserve. Meteorological data is available for download from the NERR Centralized Data Management Office through the Advanced Query System. Meteorological data was downloaded for the date of each sampling trip and the 7 days prior to collection for the Safe Harbor Met Station.

CHAPTER IV

RESULTS

4.1 *In Situ* Measurements

4.1.1 Field Measurements

Water and optical Secchi depth were measured at each site for each of the four sampling trips. On May 9, 2016, the water depth ranged from 1.22 to 3.35 m, while the Secchi depth ranged from 0.26 to 0.68 m. On the June 19, 2016 trip, the water depth ranged from 0.91 to 2.50 m, and the Secchi depth ranged from 0.46 to 0.61 m. On the June 26, 2016 trip, the water depth ranged from 0.76 to 2.83 m, with the Secchi depth only ranging from 0.37 to 0.46 m. On the September 30, 2016 trip, the water depth ranged from 0.97 to 2.74 m, while the Secchi depth ranged from 0.20 to 0.43 m. A comparison of these depths may be seen in Figures 4.1, 4.2, 4.3, and 4.4.

The Secchi depth varied by as much as 1.83 at the mouth of the Fish River, ranging from 1.52 m on June 26 to 3.35 m on May 9, 2016. The collection sites central in the Bay varied by as much as 0.60 m. Variation increased for sites towards the influx of the Fish River, as well as those located nearest the mouth of Mobile Bay, with variations of 0.9 to 1.2 m per site.

Overall, Secchi depth was fairly consistent both temporally and spatially. The Secchi depth typically varied by less than 0.3 m per site. Only the site directly at the

mouth of the Fish River and a site towards the mouth of Mobile Bay varied by over 0.3 m. Variation of Secchi depth tended to increase with proximity to Mobile Bay.

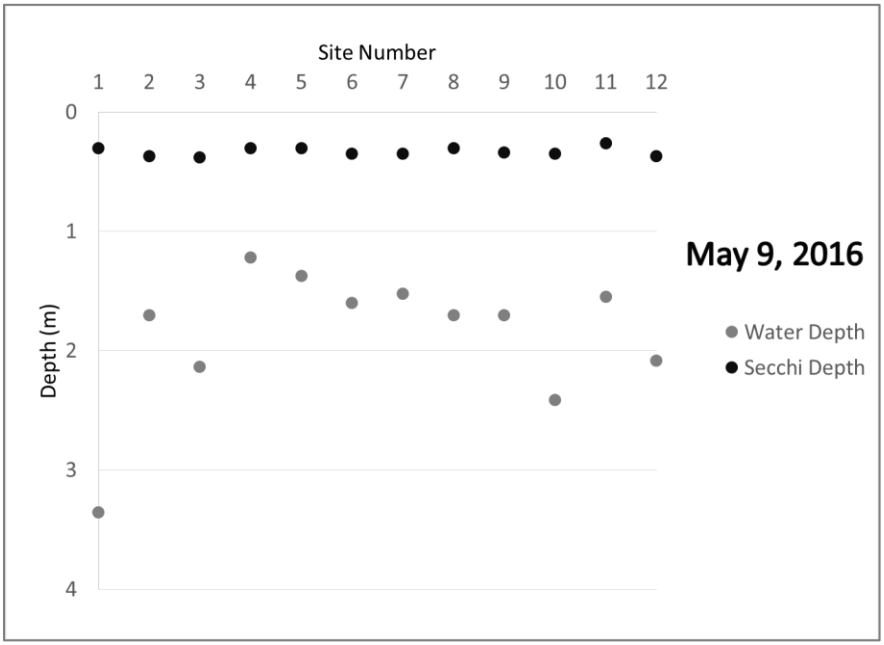

Figure 4.1 Water Depth and Secchi Depth on May 9, 2016

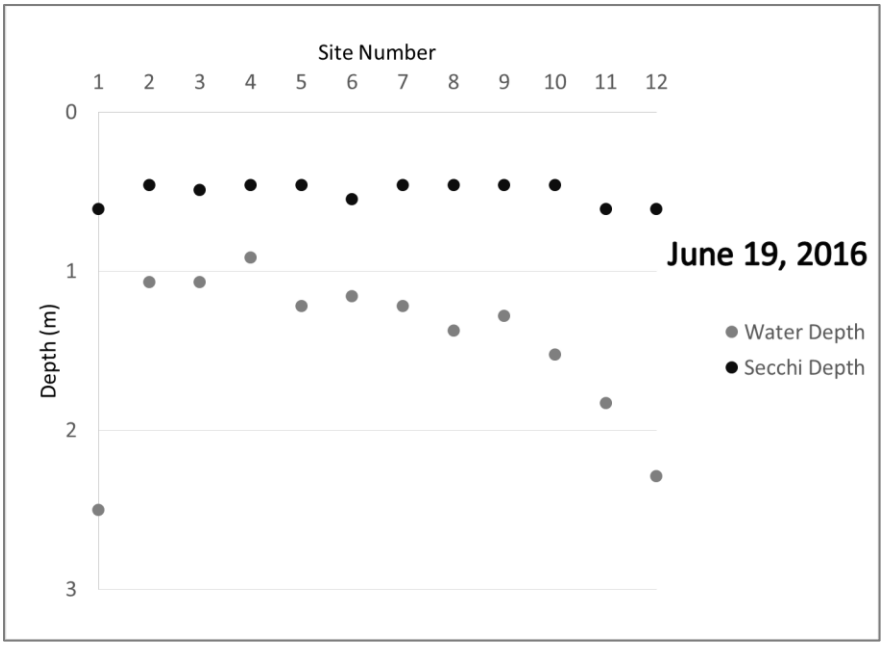

Figure 4.2 Water Depth and Secchi Depth on June 19, 2016

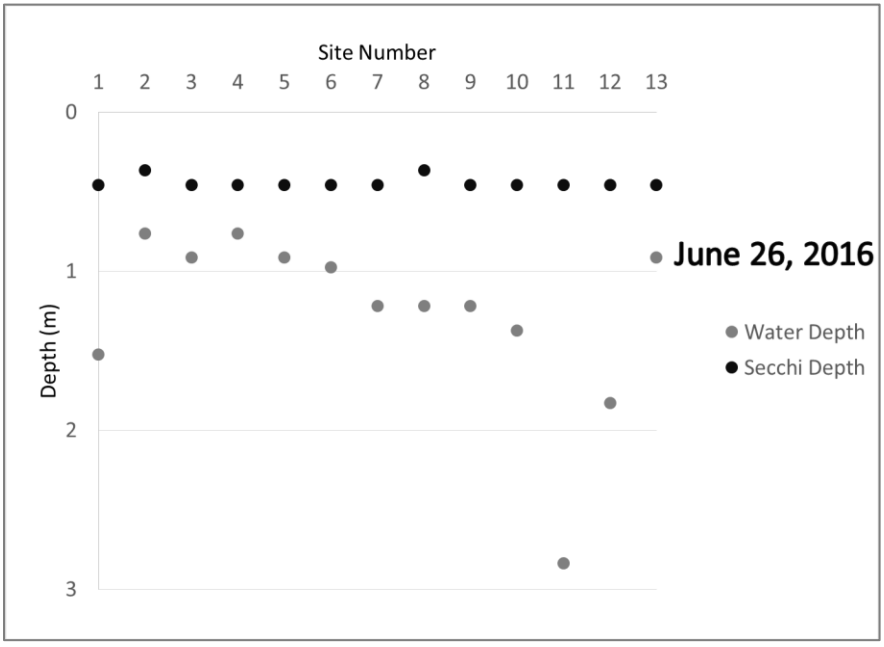

Figure 4.3 Water Depth and Secchi Depth on June 26, 2016

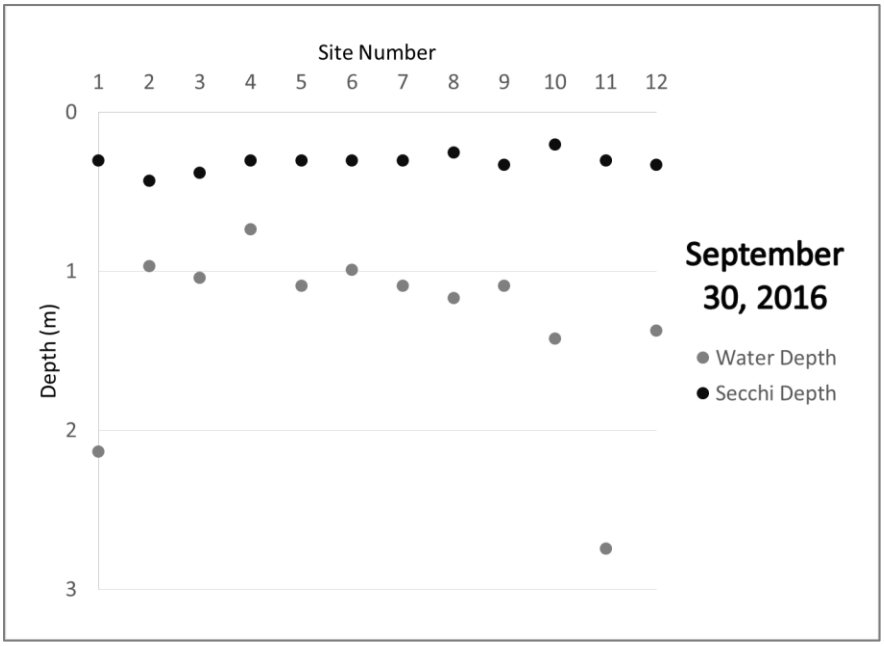

Figure 4.4 Water Depth and Secchi Depth on September 30, 2016

The Hanna multiparameter probe collected pH, DO, temperature, and salinity data for the entire water column at 48 of the 49 sites collected over the duration of the four sampling trips. There is no Hanna data for site 8 on June 26, 2016. The pH values ranged from 7.28 to 8.99, with the lowest pH occurring on May 9, 2016, and the highest occurring on September 30, 2016. May 9, 2016 had the greatest variation in pH values, ranging from 7.28 to 8.67, while June 19, 2016 had pH values from 7.66 to 8.55, June 26, 2016 had pH values from 8.00 to 8.90, and September 30, 2016 had pH values from 8.03 to 8.99 as depicted in Figure 4.5.

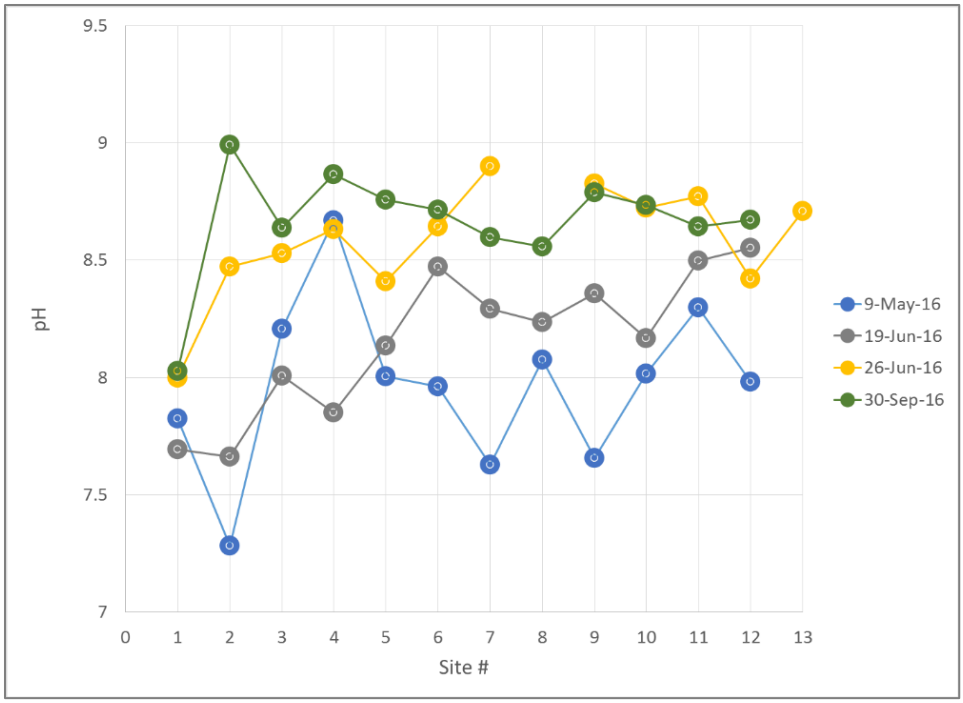

Figure 4.5 pH Measurements

pH measurements for 48 sample sites during four field cruises.

DO values ranged from 0.29 to 10.91 parts per million (ppm), with the highest DO value occurring on September 30, 2016, and the lowest DO value occurring on May 9, 2016. Only the May 9, 2016 collection trip reported DO levels over 2 ppm. May 9, 2016 had DO levels ranging from 2.22 to 10.91 ppm, demonstrating the greatest variability in DO across the bay. The remaining field cruises depicted much less variation in DO values throughout the bay. June 19, 2016 ranged from 1.06 to 1.70 ppm, June 26, 2016 ranged from 0.98 to 1.59 ppm, and September 30, 2016 ranged from 0.29 to 0.38 ppm as depicted in Figure 4.6. Due to the low recorded values of DO by the Hanna instrument, the NERR water quality station data was used to assess the validity of the

Hanna recordings. The NERR water quality station data typically indicates much higher DO values, and therefore the inaccuracy of the Hanna instrument DO data.

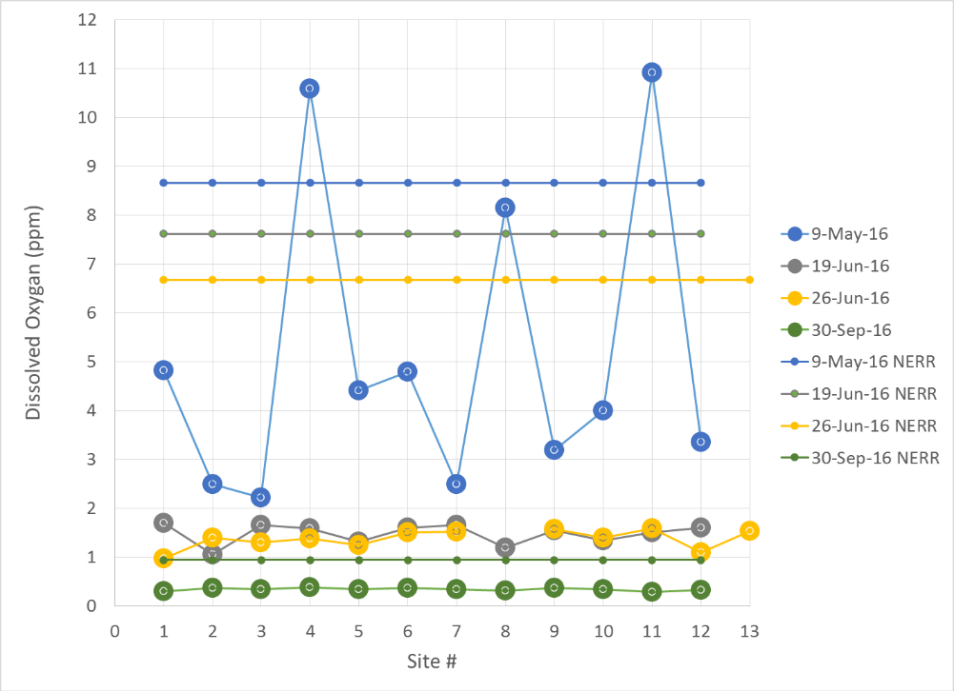

Figure 4.6 DO (ppm) Measurements

DO (ppm) measurements for 48 sample sites during four field cruises.

Salinity values ranged from 0.42 to 22.98 Practical Salinity Units (PSU), with the highest value occurring on September 30, 2016 at the mouth of Weeks Bay, and the lowest value occurring on May 9, 2016 in the northern portion of the bay. May 9, 2016 has salinity values that range from 0.42 to 12.76 PSU, June 19, 2016 has values that range from 3.42 to 14.24 PSU, June 26, 2016 has values that range from 5.39 to 11.86 PSU, and September 30, 2016 has values that range from 11.95 to 22.98 PSU as depicted in Figure 4.7.

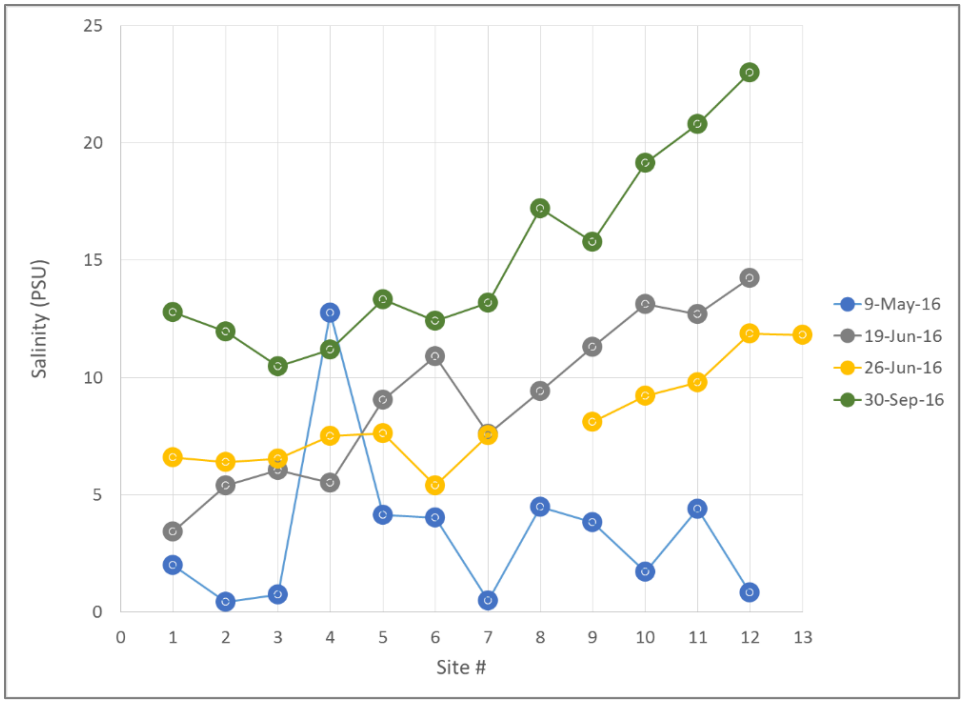

Figure 4.7 Salinity (PSU) Measurements

Salinity (PSU) measurements for 48 sample sites from four field cruises.

Temperature values ranged from 23.89 to 31.49 ℃ as depicted in Figure 4.8. Temperature values were on average the lowest on May 9, 2016, ranging from 23.39 to 28.64 ℃. May 9, 2016 depicted the highest variation in temperatures. Temperature values were consistently the highest on June 26, 2016, ranging from 30.48 to 31.49 ℃. Temperatures ranged from 27.84 to 29.99 ℃ on June 19, 2016 and from 25.24 to 27.35 ℃ on September 30, 2016.

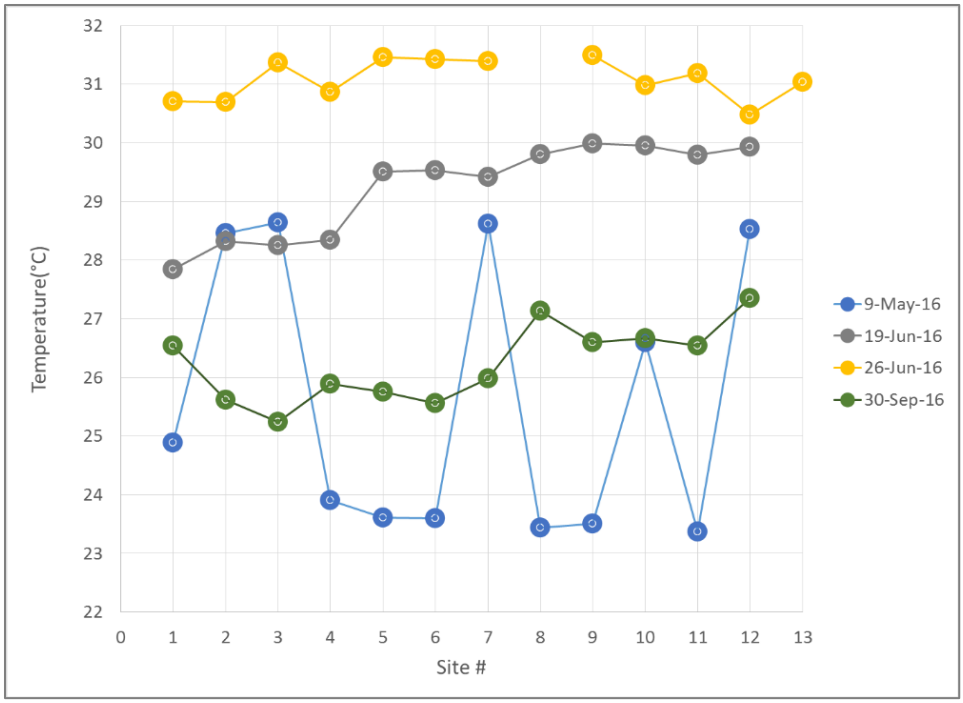

Figure 4.8 Temperature (℃) Measurements

Temperature (℃) measurements for 48 sample sites from four field cruises.

4.1.2 Spectroradiometer Reflectance Values

Hyperspectral Rrs values were derived from raw GER 1500 radiometer data for each sampling location. The hyperspectral values were then converted into multispectral values in order to mimic Landsat-8 bands 1-5 and 8. The Rrs values for each trip may be seen in Figures 4.9, 4.10, 4.11, and 4.12. There is no radiometer data for site 1 radiometer data on June 19, 2016. The Rrs values typically peak at Band 3 which represents the green portion of the EMS.

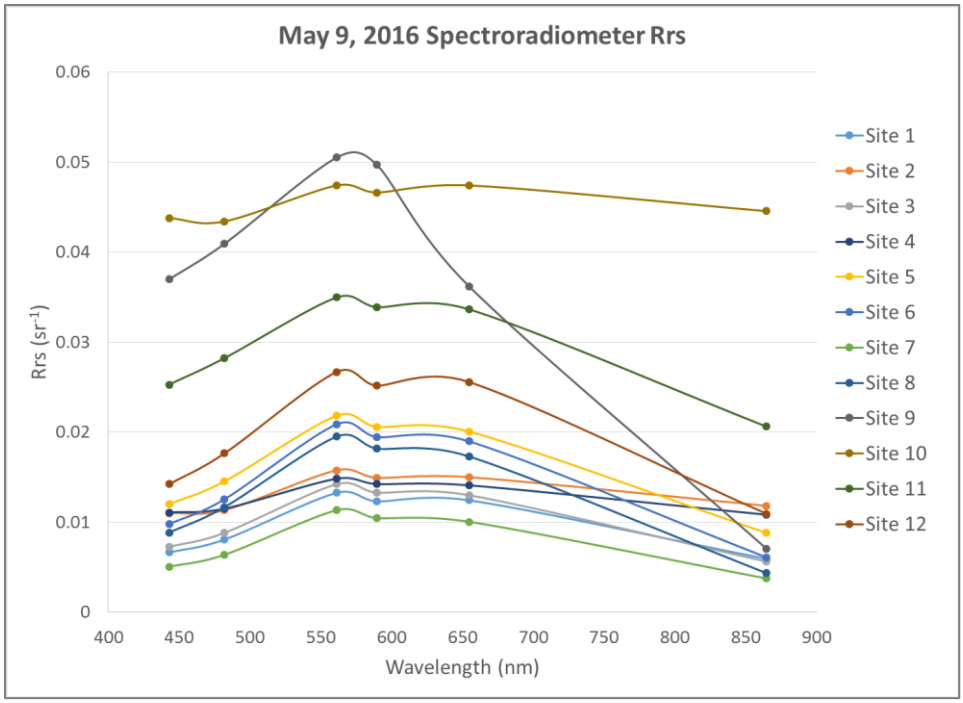

Figure 4.9 *In Situ* Radiometer data collected on May 9, 2016

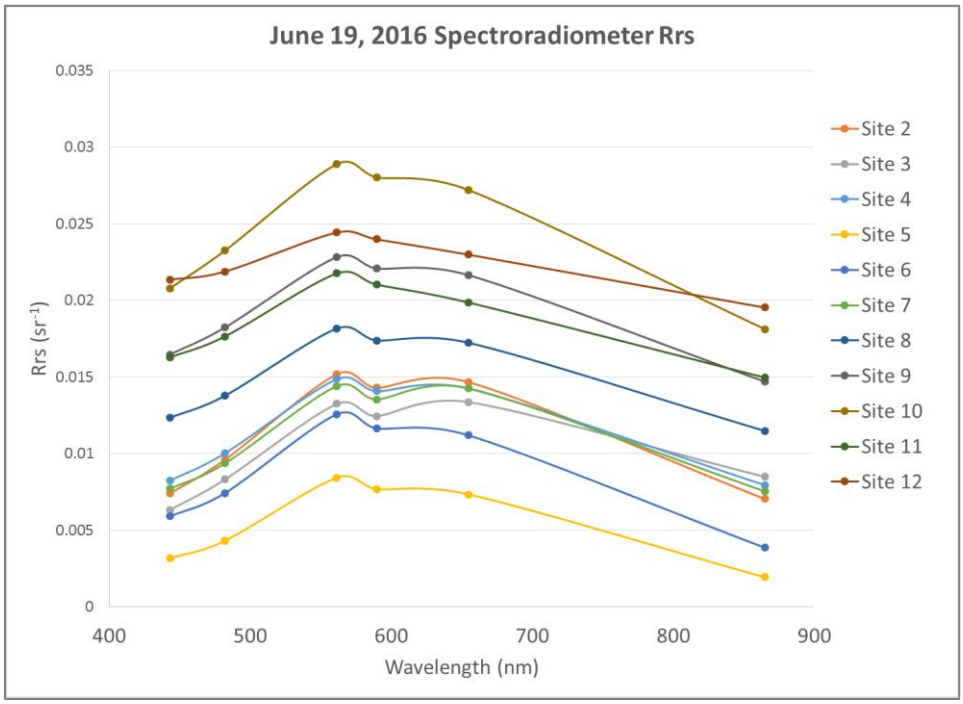

Figure 4.10 *In Situ* Radiometer data collected on June 19, 2016

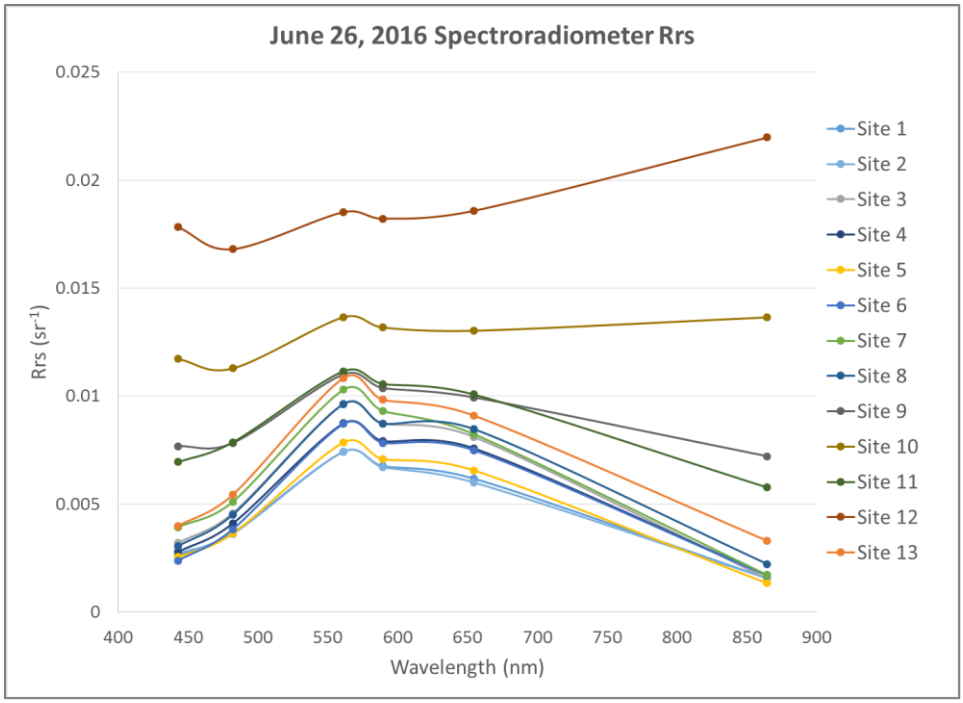

Figure 4.11 *In Situ* Radiometer data collected on June 26, 2016

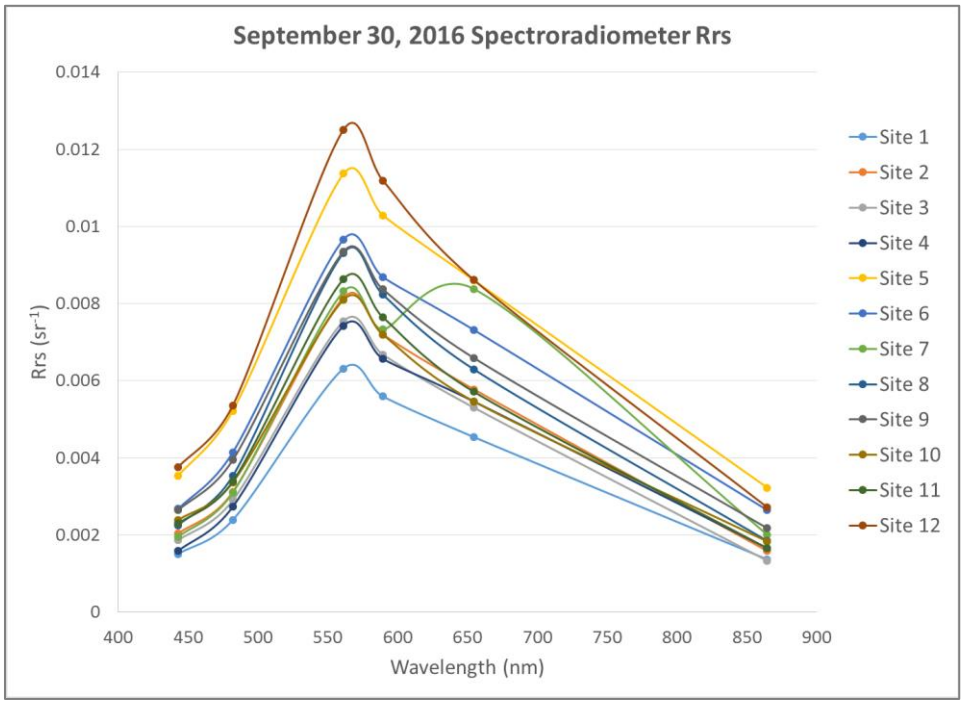

Figure 4.12 *In Situ* Radiometer data collected on September 30, 2016

4.2 Lab Results

4.2.1 SPM Concentration Measurements

Total SPM, as well as SPIM and SPOM concentrations were measured at 49 sampling sites over the duration of 4 sampling trips. The total SPM concentrations ranged from 19.5 mg/L to 85.5 mg/L. SPIM ranged from 6.5 mg/L to 21.5 mg/L representing an average of 29% of the total SPM. SPOM ranged from 11.8 mg/L to 66.25 mg/L representing an average 71% of the total SPM. The sites demonstrating peak concentrations vary between sampling trips, but higher concentrations were found in the southern and/or central portion of the bay, while lower concentrations were found in the northern portion where the Fish River flows into Weeks Bay. The spatial variability of the total SPM concentrations may been seen in Figures 4.14, 4.16, 4.18, and 4.20. The concentrations of total SPM, SPIM, and SPOM for each sampling trip may be seen in Figures 4.13, 4.15, 4.17, and 4.19.

On May 9, 2016, total SPM concentrations range from 21.55 to 50.55 mg/L, with SPIM concentrations ranging from 8.5 to 11 mg/L. On average, SPIM accounts for 28% of the total SPM on May 9, while SPOM represents 72%. On June 19, 2016, total SPM concentrations range from 22.25 to 56.25 mg/L, with SPIM concentrations ranging from 6.5 to 13.25 mg/L. On average, SPIM accounts for only 24% of the total SPM on June 19, with 76% belonging to the SPOM fraction. On June 26, 2016, total SPM concentrations range from 19.5 to 42.25 mg/L, with SPIM concentrations ranging from 7 to 13 mg/L. On average, SPIM makes up 33% of the total SPM concentration, while SPOM accounts for 67%. On September 30, 2016, total SPM concentrations range between 42.75 and 85.5 mg/L, while SPIM ranges from 13 to 21.25 mg/L. Out of the

total SPM concentrations, SPIM, on average, accounts for 31%, while SPOM accounts for 69%

The relationships between SPM and both SPIM and SPOM may be seen in Figures 4.21 and 4.22. A significant linear relationship (p-value = $1.77937*10^{-44}$) exists between SPOM and total SPM, were R^2=0.9579 (n=49). A significant relationship (p-value = $3.74545*10^{-24}$) also exists between SPIM and total SPM, where R^2=0.6641 (n=49). The histogram distribution of both SPM and SPIM may be seen in Figures 4.23 and 4.24. The SPM concentrations more closely follow a normal distribution curve, while the SPIM concentrations have a bimodal distribution with the largest peak at around 10 mg/L, and a lesser peak at approximately 20 mg/L.

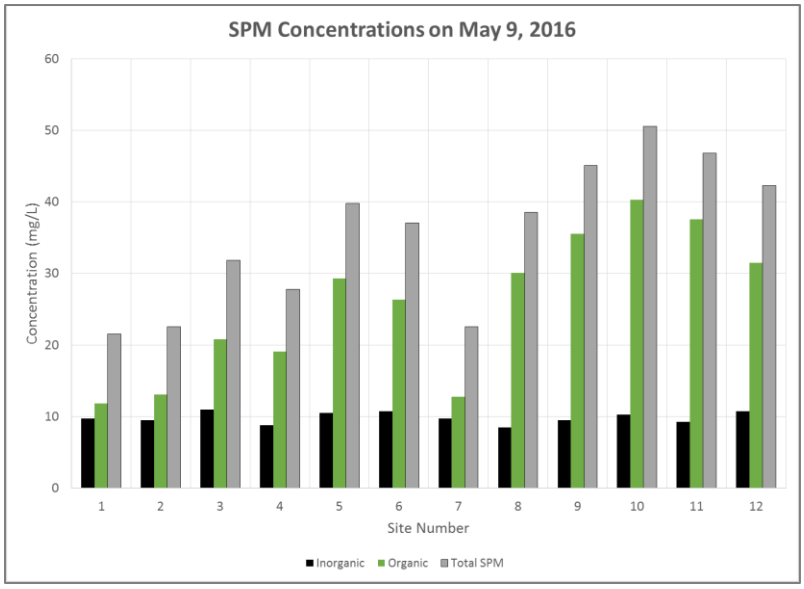

Figure 4.13 SPOM, SPIM, and Total SPM Concentrations on May 9, 2016

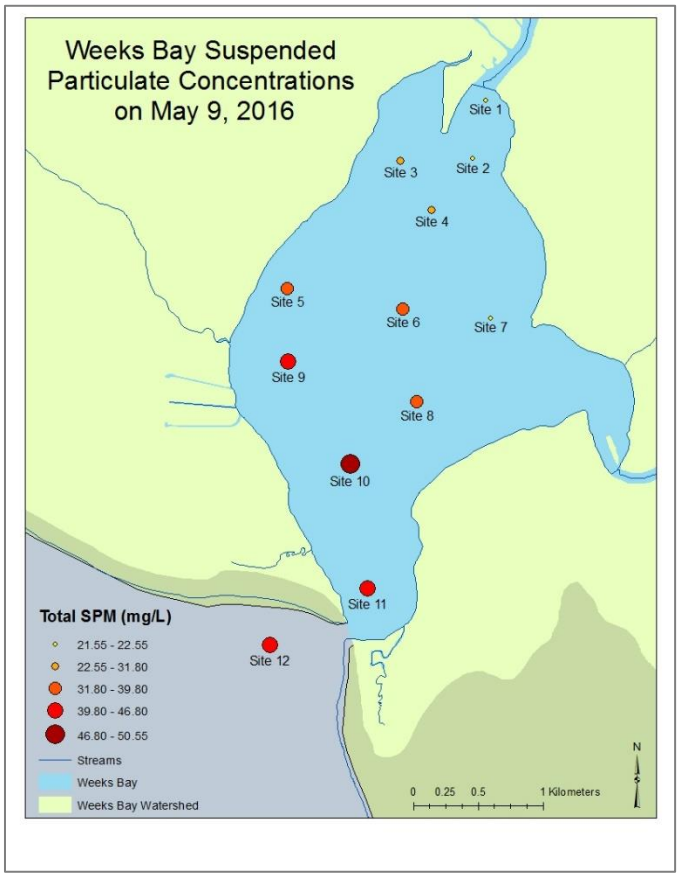

Figure 4.14 Spatial Variability of Total SPM Concentrations on May 9, 2016

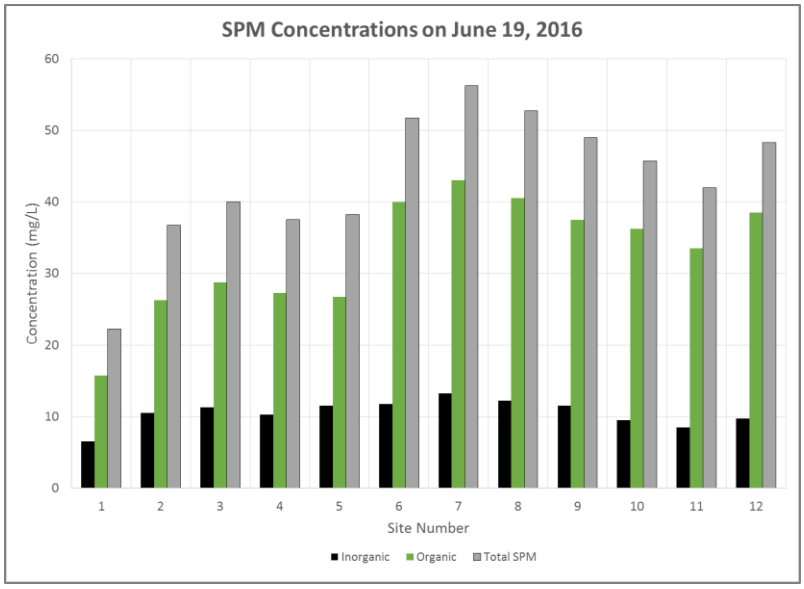

Figure 4.15 SPOM, SPIM, and Total SPM Concentrations on June 19, 2016

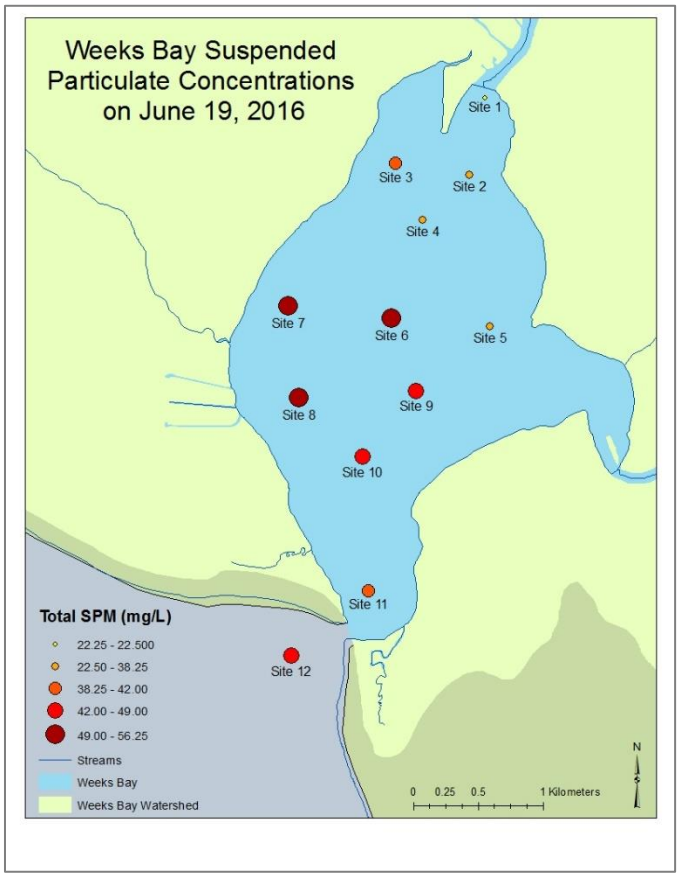

Figure 4.16 Spatial Variability of Total SPM Concentrations on June 19, 2016

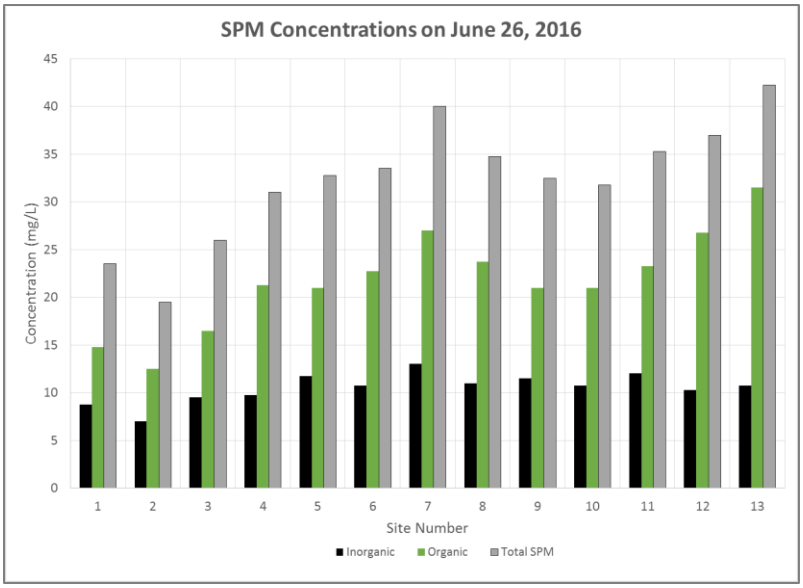

Figure 4.17 SPOM, SPIM, and Total SPM Concentrations on June 26, 2016

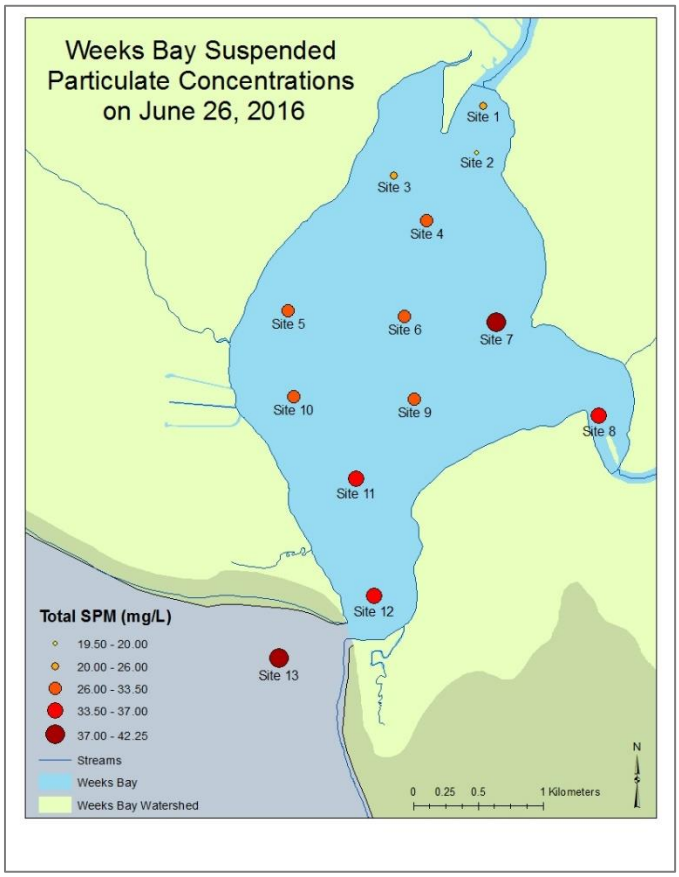

Figure 4.18 Spatial Variability of Total SPM Concentrations on June 26, 2016

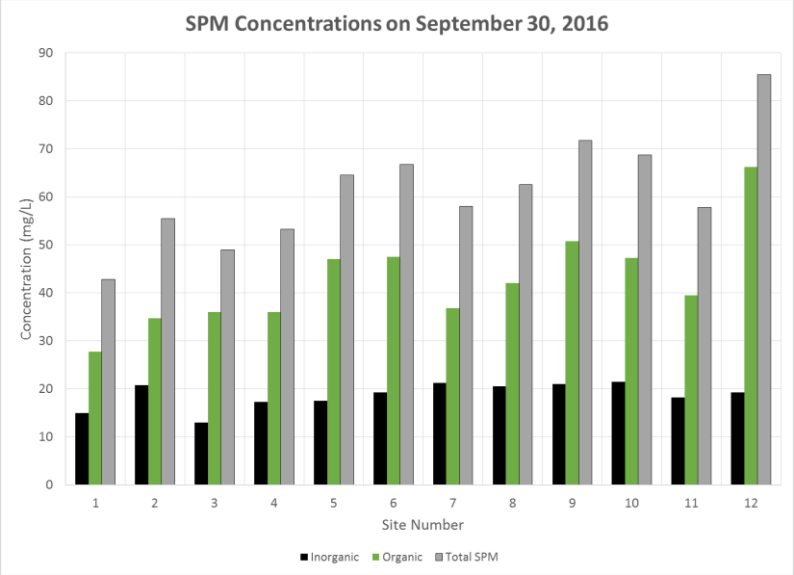

Figure 4.19 SPOM, SPIM, and Total SPM Concentrations on September 30, 2016

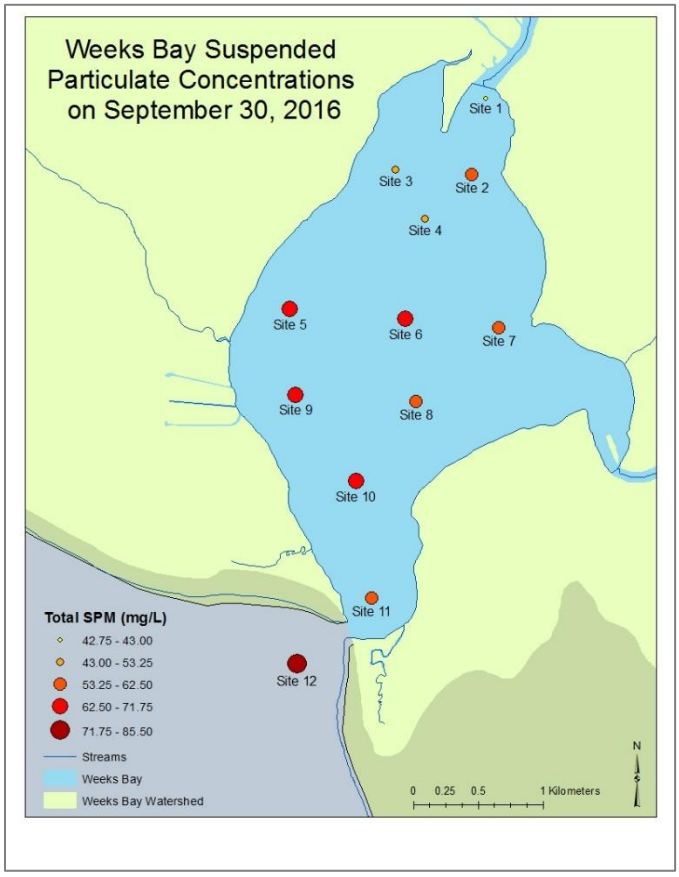

Figure 4.20 Spatial Variability of Total SPM Concentrations on September 30, 2016

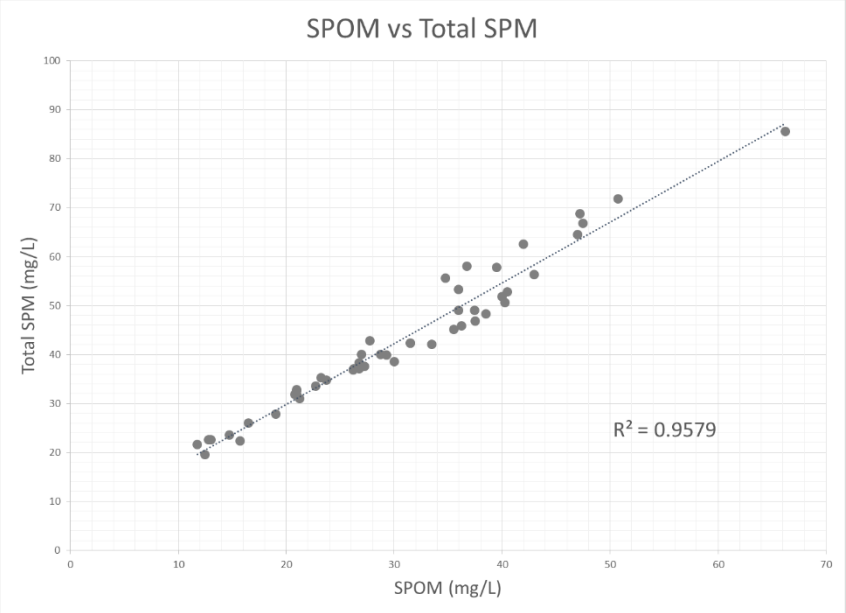

Figure 4.21 Relationship between SPOM and Total SPM concentrations for all sampling dates.

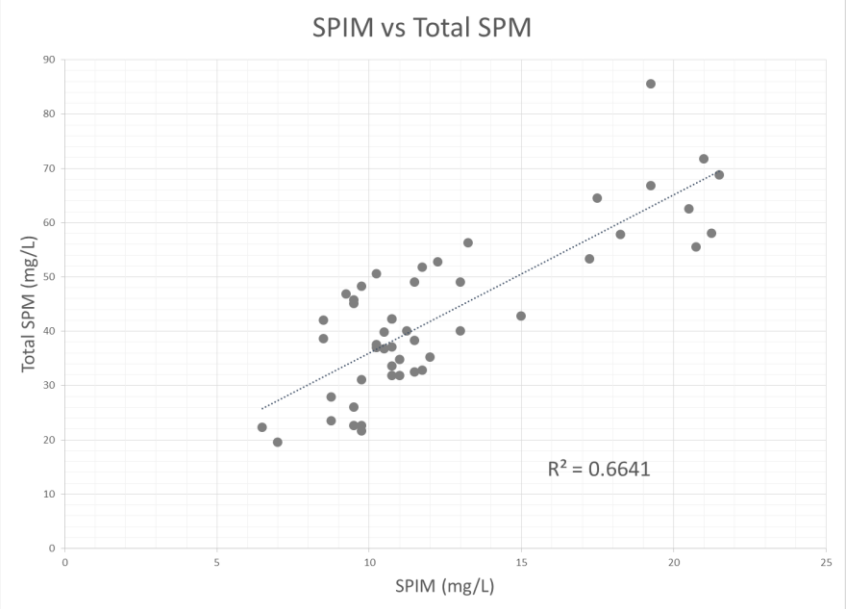

Figure 4.22 Relationship between SPIM and Total SPM concentrations for all sampling dates.

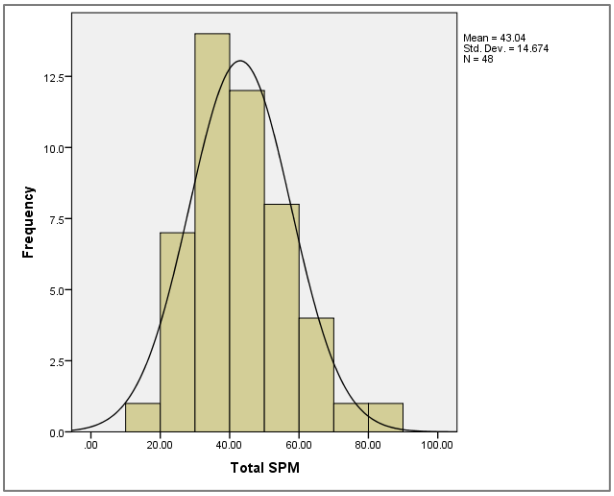

Figure 4.23 Histogram plot of SPM Concentrations

The black line depicts a normal distribution curve.

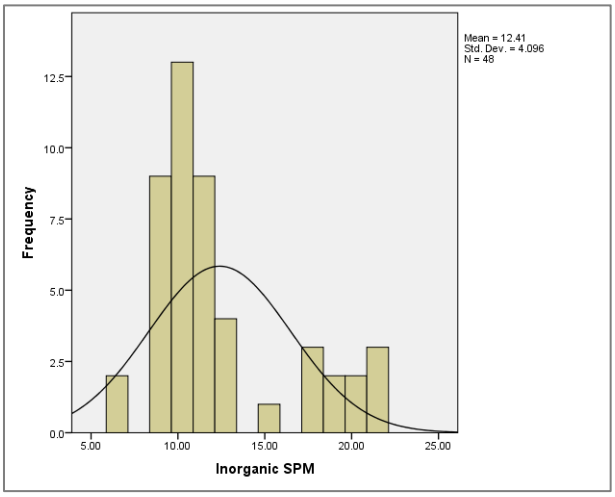

Figure 4.24 Histogram plot of SPIM Concentrations

The black line depicts a normal distribution curve.

The multiple sampling trips were compared for statistical differences between the measured concentrations of SPM and SPIM. A general linear model univariate analysis was run in SPSS software to test the means of the various sampling trips. A Tukey Post

Hoc was used to determine which field collection dates varied significantly from one another. Both the SPM and SPIM concentrations observed on September 30, 2016 differed significantly from the three previous sampling trips, as is demonstrated by the varying means depicted in Tables 4.1 and 4.2

Table 4.1 SPM statistics for each sampling trip

	5/9/2016	6/19/2016	6/26/2016	9/30/2016
Mean	35.53	43.98	32.29	61.33
Variance	102.19	90.12	39.98	128.09
Observations	12	11	13	12

Table 4.2 SPIM statistics for each sampling trip

	5/9/2016	6/19/2016	6/26/2016	9/30/2016
Mean	9.85	10.54	10.51	18.71
Variance	0.65	3.63	2.36	7.05
Observations	12	11	13	12

4.3 SPM and SPIM Retrieval Algorithms

The Rrs values calculated from the GER 1500 radiometer were used for the development and validation of the various SPM and SPIM retrieval algorithms. Lodhi et al. (1998), as well as Merritt (2016), demonstrated that the use of field spectrometer data, integrated into satellite band widths, allows for accurate estimation of SPM and SPIM.

4.3.1 Previously Developed Model Results

Previously developed models for SPM or SPIM retrieval using Rrs were evaluated as published in the literature to predict SPM/SPIM concentrations in Weeks Bay, as listed in Table 3.2. The R^2 and RMSE (% and mg/L) statistics for each model

tested is provided in Table 4.3. Models were evaluated using all 48 sampling sites. Only Wang et al. (2009) produced an R^2 of greater than 0.2 (R^2= 0.2203). Han et al. (2006), and Kong et al. (2015) produced R^2 values of greater than 0.1 (0.1729 and 0.1681 respectively). With the lowest RMSE (%) of 66.96% (10.04 mg/L) given by Zhao et al. (2015), none of the preexisting models were a good fit.

The previously developed models were adjusted by keeping the defined independent variable reflectance parameters, and altering the coefficients by running regressions with the Weeks Bay SPM/SPIM data. A total of 49 sites were visited over the course of the four sampling trips. Due to the loss of the radiometer data for site 1 on June 19, 2016, that site was excluded from the modeling process, leaving a total of 48 sites. Thirty-two of the 48 sites were used to develop the new coefficients, while 16 sites were used for the validation of the adjusted models. The R^2 and RMSE statistics, as well as the adjusted model, are provided in Table 4.4. All models improved when the coefficients were adjusted specifically for Weeks Bay. The algorithm developed by Kong et al. (2015a) produced the highest R^2 value with R^2 = 0.5173. All other algorithms yielded an R^2 of less than 0.25. The RMSE (%) values given by the adjusted models were all under 40%, with the lowest RMSE of 13.67% (1.74 mg/L) being yielded by Kong et al. (2015a). The model by Kong et al. (2015a) uses a ratio of the red and green bands to determine the SSC using a second order polynomial algorithm.

Table 4.3 Statistics of the evaluated existing models for SPM

Author	Model		R^2	% RMSE	RMSE in mg/L
Doxoran et al, 2009	SPM=12.996*exp(x/0.1829)	x=NIR/Red	0.0146	2131%	1406.21
Han et al, 2006	$Log_{10}(SSC)=0.892+6.2244(x)$	x=[Green+Red]/[Green/Red]	0.1729	2.53E+68	1.32E+68
Kong et al, 2015a	$SSC=70.939-272.62x+296.29x^2$	x=Red/Green	0.1681	69.02%	54.52
Lobo et al, 2014	$TSS=2.64*(x-2.27)^{0.45}$	x=Red	Inapplicable due to negative (x-2.27) values		
Lodhi et al, 1998	$SSC=19.516+42.65+23.16x^2$	x=NIR	0.0427	331.09%	49.66
Martinez et al, 2015	$SPM=20.41[x]^{1.173}$	x=Red	0.0002	105.0%	45.49
Wang et al, 2009	Ln(SSC)=3.18236*x-1.40060	x=Ln(NIR)	0.2203	88.7%	13.31
Zhang, 2005	$Ln(SSC)=14.727+2.5228*x_1+1.3147*x_2$	x_1=Ln(Green); x_2=Ln(NIR)	0.0194	88.5%	13.27
Zhao et al, 2011	SSC=2.12*exp[45.92(x)]	x=Red	0.0995	66.96%	10.04
Zheng et al, 2015	TSM=6110.3*Rrs(x)-1.8242	x=NIR	0.0012	76.5%	50.46

Table 4.4 Statistics of existing models for SPM with adjusted coefficients

Author	Model		R^2	% RMSE	RMSE mg/L
Doxoran et al, 2009	$SPM = 44.474e^{-0.116x}$	x=NIR/Red	0.0076	30.84%	14.25
Han et al, 2006	$Log10(SPIM)= -3.9752x + 1.1818$	x=[Green+Red]/[Green/Red]	0.2229	24.91%	3.18
Kong et al, 2015a	$SPIM = 227.73x^2 - 402.92x + 188.4$	x=Red/Green	0.5173	13.67%	1.74
Lobo et al, 2014	$SPM = 37.355x^{-0.028}$	x=Red	0.0022	33.97%	15.69
Lodhi et al, 1998	$SPIM = 20062x^2 - 683.62x + 15.509$	x=NIR	0.1865	36.87%	4.70
Martinez et al, 2015	$SPM = 37.355x^{-0.028}$	x=Red	0.0022	33.97%	15.69
Wang et al, 2009	$Ln(SPIM) = -0.1302x + 1.7822$	x=Ln(NIR)	0.1563	23.80%	3.03
Zhang, 2005	$Ln(SPIM)=1.4602-0.17071x_1-0.05395x_2$	x_1=Ln(Green); x_2=Ln(NIR)	0.1831	24.01%	3.06
Zhao et al, 2011	SPIM = 15.142e-16.91x	x=Red	0.2076	25.15%	3.21
Zheng et al, 2015	SPM = -317.27x + 46.524	x=NIR	0.0158	31.66%	14.63

4.3.2 SPM Retrieval Algorithm Results

Once the previous models for SPM were tested and modified, the previously utilized variables were modified to consider alternative formula types. Additional possible reflectance parameters and algorithm forms were then tested as potential variables in a Weeks Bay SPM retrieval algorithm. These reflectance parameters include single bands, the natural logs of single bands, band ratios, band combinations, and combinations of the previously listed. Both a linear, and nonlinear model were tested for each variable- those previously used in SPM models, and those not. The equations for each tested model, as well as the associated statistics may be seen in Table 4.5 for the previously utilized variables, and Table 4.6 for the additionally tested variables. Three out of the 29 reflectance parameters tested as possible variables in a linear model were significant ($p<0.05$). This included Band 4/Band 3, Ln(Band 4)/Ln(Band 3), and (Band 3 – Band 5)/(Band 3 + Band 5) with p-values of 0.0070, 0.0055, and 0.0489 respectively. The RMSE (%) reported for each of these statistically significant linear models were 26.48%, 25.89%, and 27.23% respectively. None of these predictive variables produce a Pearson Correlation of $R > 0.8$. The nonlinear models for Band 4/Band 3, Ln(Band 4)/Ln(Band 3), and (Band 3 – Band 5)/(Band 3 + Band 5) resulted in R^2 values of 0.4644, 0.4827, and 0.3032 with RMSE (%) values of 21.70%, 18.78%, and 139.02% respectively. None of the nonlinear models have a significant Pearson correlation coefficient.

With the development and validation of (Band 3 – Band 5)/(Band 3 + Band 5) as a possible variable in an SPM retrieval algorithm, both Sites 1 and 2 from May 9, 2016 may be removed as outliers. With the removal of these sites, the linear algorithm using

the (Band 3 – Band 5)/(Band 3 + Band 5) variable improves in performance to an R^2 of 0.2131, p-value of 0.0089, and RMSE (%) of 23.34%. The nonlinear algorithm improves in performance to an R^2 of 0.4744, and RMSE (%) of 17.65%. The Pearson correlation coefficient was significant and positive (R=0.8).

A multiple regression was also considered as a potential for modeling SPM concentrations in Weeks Bay, however due to the high degree of correlation between the Landsat-8 band Rrs values (Table 4.7), a multiple regression was not valid.

Table 4.5 Statistics of previously used variables with modified model types for an SPM Retrieval Algorithm

Reflectance Parameter	Relationship with SPM	R^2	p-value	F	t	R	RMSE (%)	RMSE in mg/L
Band 5	$y = -317.27x + 46.524$	0.0158	0.49	0.00	0.48	-0.12	31.66%	14.63
	$y = 2E+06x^3 - 47458x^2 - 189.02x + 46.737$	0.0194		0.00	0.16	0.20	48.32%	22.32
Band 4	$y = -164.84x + 46.72$	0.0083	0.62	0.00	0.34	-0.10	30.91%	14.28
	$y = -1E+06x^3 + 98687x^2 - 2405.9x + 59.083$	0.0339		0.00	0.16	0.43	28.54%	13.19
Band 5/Band 4	$y = -7.4105x + 47.715$	0.0158	0.49	0.00	0.40	0.07	30.07%	13.89
	$y = 279.76x^3 - 591.98x^2 + 351.77x - 11.466$	0.1660		0.03	0.34	0.07	33.63%	15.54

Table 4.6 Statistics of additional single band and band combinations for an SPM Retrieval Algorithm

Reflectance Parameter	Relationship with SPM	R^2	p-value	F	t	R	RMSE (%)	RMSE in mg/L
Band 5	$y = -317.27x + 46.524$	0.0158	0.49	2E-06	0.48	-0.12	31.66%	14.63
	$y = 2E+06x^3 - 47458x^2 - 189.02x + 46.737$	0.0194		2E-01	0.16	0.20	48.32%	22.32
Band 4	$y = -164.84x + 46.72$	0.0083	0.62	2E-10	0.34	-0.10	30.91%	14.28
	$y = -1E+06x^3 + 98687x^2 - 2405.9x + 59.083$	0.0339		1E-04	0.16	0.43	28.54%	13.19
Band 3	$y = -31.807x + 45.074$	0.0004	0.91	9E-11	0.37	-0.14	30.91%	14.28
	$y = 594604x^3 - 44495x^2 + 843.32x + 40.474$	0.0039		6E-15	0.31	-0.30	31.09%	14.36
Band 2	$y = -137.38x + 45.905$	0.0063	0.67	8E-12	0.34	-0.12	30.86%	14.26
	$y = -2E+06x^3 + 164161x^2 - 2975.4x + 56.318$	0.0477		3E-02	0.11	0.39	30.13%	13.92
Band 1	$y = -182.27x + 46.057$	0.0098	0.59	8E-10	0.36	-0.12	31.03%	14.33
	$y = -3E+06x^3 + 212620x^2 - 3379.7x + 55.159$	0.0668		4E-03	0.14	0.47	27.94%	12.91
Band 4/Band 1	$y = 4.9268x + 34.052$	0.0612	0.17	9E-07	0.21	0.47	29.25%	13.51
	$y = -0.5205x^3 + 4.597x^2 - 7.0978x + 43.277$	0.0627		9E-07	0.47	0.25	28.97%	13.39
Band 4/Band 2	$y = 7.0437x + 33.501$	0.027	0.37	6E-10	0.40	0.10	29.97%	13.85
	$y = 5.0571x^3 - 23.365x^2 + 39.944x + 19.696$	0.0317		2E-12	0.39	0.08	30.06%	13.89
Band 4/Band 3	$y = -66.147x + 101.05$	0.2183	0.00	1E-02	0.62	0.45	26.48%	12.24
	$y = -1345.5x^3 + 4205.9x^2 - 4257.9x + 1443.1$	0.4644		1E-01	0.62	0.75	21.70%	10.03
Band 4/Band 5	$y = -0.6602x + 46.603$	0.0033	0.75	5E-17	0.24	-0.06	30.92%	14.29
	$y = 0.3135x^3 - 7.0912x^2 + 32.623x + 8.8692$	0.207		3E-04	0.18	0.14	31.65%	14.62
Band 3/Band 5	$y = 0.6249x + 42.295$	0.0055	0.69	8E-15	0.37	0.23	29.80%	13.77
	$y = 0.2007x^3 - 3.959x^2 + 20.454x + 18.037$	0.1048		5E-05	0.38	0.00	31.62%	14.61
Band 2/Band 5	$y = -1.2742x + 47.056$	0.0064	0.66	3E-18	0.23	-0.03	30.91%	14.28
	$y = 4.8834x^3 - 45.19x^2 + 110.56x - 30.298$	0.2497		2E-05	0.11	0.25	31.15%	14.39

Table 4.6 (continued)

Reflectance Parameter	Relationship with SPM	R^2	P-value	F	t	R	RMSE (%)	RMSE in mg/L
Band 1/Band 5	$y = -2.4135x + 48.132$	0.0169	0.48	1E-18	0.22	0.17	30.79%	14.22
	$y = 6.4772x^3 - 49.743x^2 + 91.241x - 0.9242$	0.1407		1E-12	0.08	0.34	31.68%	14.63
Band 3 + Band 1	$y = -48.708x + 45.713$	0.0032	0.76	5E-14	0.32	-0.13	30.75%	14.21
	$y = -96935x^3 + 16124x^2 - 750.57x + 52.756$	0.0155		1E-10	0.32	0.38	29.20%	13.49
Band 3 + Band 2	$y = -40.017x + 45.575$	0.0023	0.79	2E-15	0.32	-0.13	30.70%	14.18
	$y = -65521x^3 + 11818x^2 - 599.22x + 51.723$	0.0113		1E-11	0.31	0.37	29.42%	13.59
Band 3 + Band 4	$y = -45.266x + 45.855$	0.0029	0.77	2E-14	0.32	-0.12	30.72%	14.19
	$y = 8568.8x^3 + 1915.7x^2 - 263.88x + 49.423$	0.0103		2E-10	0.28	0.27	29.76%	13.75
Band 3 + Band 5	$y = -72.532x + 46.117$	0.0046	0.71	2E-11	0.35	-0.13	30.89%	14.27
	$y = 834876x^3 - 74314x^2 + 1748.3x + 34.337$	0.0264		9E-05	0.20	0.18	94.98%	43.88
Band 4 + Band 1	$y = -88.796x + 46.452$	0.0092	0.60	5E-10	0.35	-0.11	30.98%	14.31
	$y = -368290x^3 + 48700x^2 - 1803.3x + 60.412$	0.0514		7E-01	0.01	0.12	31.18%	14.41
Band 4 + Band 2	$y = -76.448x + 46.31$	0.0073	0.64	5E-11	0.34	-0.11	30.89%	14.27
	$y = -279958x^3 + 39567x^2 - 1576.1x + 59.753$	0.0413		3E-05	0.48	0.26	28.92%	13.36
Band 4 + Band 5	$y = -128.09x + 47.024$	0.0128	0.54	1E-07	0.41	-0.11	31.31%	14.46
	$y = 76106x^3 + 6013.2x^2 - 612.94x + 51.691$	0.0332		7E-01	0.14	0.24	41.16%	19.01
Band 5 + Band 1	$y = -135.14x + 46.5$	0.014	0.52	2E-07	0.42	-0.12	31.42%	14.52
	$y = -222365x^3 + 30900x^2 - 1079.1x + 51.389$	0.0391		1E-07	0.38	0.42	28.19%	13.02
Band 5 + Band 2	$y = -118.89x + 46.45$	0.0114	0.56	4E-01	0.00	-0.12	31.25%	14.44
	$y = -25747x^3 + 15404x^2 - 785.08x + 50.884$	0.0344		2E-01	0.16	0.28	33.46%	15.46
Band 1 + Band 2	$y = -79.539x + 45.992$	0.0079	0.63	9E-11	0.35	-0.12	30.94%	14.29
	$y = -366948x^3 + 47352x^2 - 1606.8x + 55.95$	0.0573		8E-05	0.51	0.27	28.72%	13.27
Ln(Band 1)	$y = -2.9848x + 29.033$	0.0314	0.33	9E-08	0.38	0.11	30.06%	13.89
	$y = 1.6237x^3 + 27.101x^2 + 144.12x + 287.72$	0.0589		2E-05	0.31	0.46	27.51%	12.71

Table 4.6 (continued)

Reflectance Parameter	Relationship with SPM	R^2	P-value	F	t	R	RMSE (%)	RMSE in mg/L
Ln(Band 2)	$y = -2.7502x + 30.997$	0.0193	0.45	3E-09	0.36	0.08	30.24%	13.97
	$y = 2.4288x^3 + 36.989x^2 + 181.55x + 330.54$	0.0398		5E-07	0.31	0.41	28.39%	13.11
Ln(Band 3)	$y = -0.4998x + 42.43$	0.0003	0.93	5E-23	0.30	-0.03	30.50%	14.09
	$y = 14.47x^3 + 172.88x^2 + 678.1x + 916.37$	0.0306		3E-09	0.29	-0.29	32.20%	14.88
Ln(Band 4)	$y = -3.2956x + 29.724$	0.0157	0.49	1E-09	0.34	0.08	30.29%	13.99
	$y = 10.436x^3 + 140.36x^2 + 619.19x + 938.97$	0.0422		2E-04	0.25	0.28	29.61%	13.68
Ln(Band 5)	$y = -1.6078x + 35.734$	0.01	0.59	5E-11	0.38	0.08	30.11%	13.91
	$y = 12.468x^3 + 192.24x^2 + 968.59x + 1638.4$	0.2117		4E-01	0.15	0.21	44.47%	20.54
Ln(Band 4) / Ln(Band 3)	$y = 246.07x - 210.72$	0.2297	0.00	6E-03	0.66	0.48	25.89%	11.96
	$y = -211487x^3 + 669574x^2 - 705947x + 247908$	0.4827		2E-01	0.42	0.78	18.78%	8.68
(Band 3 - Band 5) / (Band 3 + Band 5)	$y = 27.311x + 17.141$	0.1231	0.05	3E-03	0.38	0.40	27.73%	12.81
	$y = 2190.5x^3 - 4372.3x^2 + 2173.9x + 47.919$	0.3032		2E-06	0.29	-0.29	139.02%	64.23

Table 4.7 Correlation between Landsat-8 bands

	Band 1	Band 2	Band 3	Band 8	Band 4	Band 5
Band 1	1					
Band 2	0.994987	1				
Band 3	0.968141	0.987194	1			
Band 8	0.973186	0.990486	0.999694	1		
Band 4	0.969741	0.980501	0.977562	0.97804	1	
Band 5	0.865941	0.829541	0.75795	0.765538	0.853616	1

All Landsat-8 bands were highly correlated.

Given the statistical variability between SPM concentrations during the separate field cruises, numerous possible reflectance parameters were tested as potential variables in a Weeks Bay SPM algorithm for each sampling trip on an individual basis. The tested algorithms and associated statistics may be found in Tables 4.8, 4.9, 4.10, and 4.11. Four sites were reserved from each sampling trip for validation of the algorithms. Eight sites were used for the development of May 9 and September 30, while seven sites were used for the development of June 19 and nine for June 26.

The relationship between the reflectance parameters and SPM concentrations improves when observed on a trip-by-trip basis for the May 9 and September 30, 2016 sampling trips. Out of the 12 reflectance parameters analyzed for a relationship with SPM concentrations on May 9, 2016, 10 of the linear equations had a reported p-value of 0.05 or less. Out of those 10 reflectance parameters, 8 had both a linear and nonlinear relationship with a Pearson correlation coefficient of 0.8 or greater, with a 9th parameter, Ln(Band 1), having a strong Pearson coefficient reported for only the linear model. Out of these reflectance parameters, the lowest RMSE and highest R^2 was reported as 22.74% (5.12 mg/L) and R^2=0.9310 for the second order polynomial equation associated with the

variable Ln(Band 3). Out of the 12 reflectance parameters analyzed for a relationship with SPM concentrations on September 30, 2016, 6 had a reported p-value of 0.05 or less associated with the linear relationship. All of those 6 reflectance parameters had both a linear and nonlinear relationship with a strong Pearson correlation coefficient of 0.8 or greater. Out of the significant reflectance parameters, the lowest RMSE of 13.18% (3.16) was reported for the second order polynomial equation using Band 2 as the predictive variable. The highest R^2 of 0.6616 was reported with the second order polynomials associated with both Band 1 and Ln(Band 1).

The relationships between the various reflectance parameters and SPM concentrations for the two June 2016 sampling trips are not strong like with the May and September sampling trips. Neither the June 19 nor June 26 trips reveal any significant p-values for any of the 12 reflectance parameters analyzed. Similarly, neither the June 19 nor June 26 trips produce a strong Pearson correlation coefficient for any of the reflectance parameters tested.

Table 4.8 Statistics of single bands and band combinations for the May 9, 2016 sampling trip using 8 sites for development and 4 sites for validation

Reflectance Parameter	Relationship with SPM	R^2	p-value	F	t	R	RMSE (%)	RMSE in mg/L
Band 5	y = 467.69x + 32.296	0.505	0.05	0.46	0.02	0.98	48.81%	10.98
	$y = -21291x^2 + 1505x + 25.705$	0.6052		0.66	0.01	0.94	54.08%	12.17
Band 4	y = 651.15x + 23.207	0.7388	0.01	0.60	0.05	0.97	30.18%	6.79
	$y = -26645x^2 + 2223.4x + 4.2309$	0.8707		0.94	0.08	0.95	23.52%	5.29
Band 3	y = 690.17x + 21.391	0.7735	0.00	0.78	0.02	0.98	37.14%	8.36
	$y = -27294x^2 + 2331.1x + 0.5933$	0.9025		0.97	0.12	0.96	19.91%	4.48
Band 2	y = 613.18x + 27.435	0.677	0.01	0.88	0.00	0.98	39.64%	8.92
	$y = -31901x^2 + 2238x + 12.518$	0.8439		0.99	0.03	0.95	31.86%	7.17
Band 1	y = 553.13x + 29.707	0.614	0.02	0.63	0.01	0.98	42.45%	9.55
	$y = -30595x^2 + 2076.1x + 17.516$	0.7864		0.98	0.02	0.93	41.88%	9.42
Ln(Band 1)	y = 12.217x + 91.655	0.7819	0.00	0.92	0.03	0.92	40.62%	9.14
	$y = -8.4907x^2 - 57.175x - 46.408$	0.8908		0.74	0.21	0.75	45.79%	10.30
Ln(Band 2)	y = 14.248x + 97.943	0.8317	0.00	0.94	0.02	0.95	34.55%	7.77
	$y = -9.3064x^2 - 59.987x - 47.102$	0.9215		0.77	0.25	0.84	34.75%	7.82
Ln(Band 3)	y = 19.605x + 112.63	0.8821	0.00	0.75	0.06	0.97	28.83%	6.49
	$y = -11.282x^2 - 63.934x - 40.131$	0.931		0.78	0.30	0.93	22.74%	5.12
Ln(Band 4)	y = 18.035x + 107.91	0.8519	0.00	0.90	0.07	0.95	24.11%	5.42
	$y = -11.09x^2 - 64.916x - 45.042$	0.9081		0.84	0.37	0.90	24.18%	5.44
Ln(Band 5)	y = 8.6957x + 78.865	0.5797	0.03	0.20	0.32	0.00	54.30%	12.22
	$y = -0.2821x^2 + 6.2809x + 73.885$	0.58		0.22	0.32	0.01	54.53%	12.27
Band 4 / Band 5	y = -3.2724x + 46.25	0.105	0.43	0.37	0.38	-0.87	72.05%	16.21
	$y = 5.1299x^2 - 29.566x + 76.175$	0.3765		1.00	0.01	0.86	79.73%	17.94
Band 4 / Band 3	y = 131.49x - 84.493	0.2821	0.18	0.62	0.93	0.90	94.80%	21.33
	$y = 2961.9x^2 - 5457.2x + 2548.2$	0.4625		0.02	0.22	0.97	257.13%	57.85

Table 4.9 Statistics of single bands and band combinations for the June 19, 2016 sampling trip using 7 sites for development and 4 sites for validation

Reflectance Parameter	Relationship with SPM	R^2	p-value	F	t	R	RMSE (%)	RMSE in mg/L
Band 5	y = 551.14x + 36.06	0.1433	0.40	0.04	0.28	-0.38	59.20%	9.62
	$y = 119755x^2 - 2083.5x + 45.5$	0.2651		0.06	0.12	-0.40	77.61%	12.61
Band 4	y = 485.27x + 33.55	0.1142	0.46	0.02	0.22	-0.15	59.00%	9.59
	$y = 58103x^2 - 1536x + 48.619$	0.165		0.01	0.14	-0.33	68.47%	11.13
Band 3	y = 520.97x + 32.354	0.1406	0.41	0.05	0.22	-0.16	60.88%	9.89
	$y = 38973x^2 - 945.92x + 44.349$	0.1652		0.03	0.17	-0.31	66.55%	10.81
Band 2	y = 565.03x + 34.173	0.1727	0.35	0.08	0.22	-0.17	61.85%	10.05
	$y = 64571x^2 - 1276.9x + 44.174$	0.2156		0.04	0.15	-0.43	71.17%	11.56
Band 1	y = 609.38x + 34.569	0.2001	0.31	0.12	0.23	-0.14	62.38%	10.14
	$y = 55490x^2 - 813.85x + 40.993$	0.2257		0.05	0.16	-0.38	69.80%	11.34
Ln(Band 1)	y = 5.5022x + 67.302	0.15	0.39	0.08	0.26	-0.04	57.34%	9.32
	$y = 7.3008x^2 + 74.321x + 226.22$	0.2363		0.17	0.18	-0.25	69.74%	11.33
Ln(Band 2)	y = 5.809x + 67.698	0.1261	0.43	0.05	0.26	-0.10	57.55%	9.35
	$y = 9.8447x^2 + 95.175x + 267.17$	0.2192		0.13	0.17	-0.27	70.50%	11.46
Ln(Band 3)	y = 5.809x + 67.698	0.1261	0.46	0.01	0.42	-0.10	49.79%	8.09
	$y = 9.8447x^2 + 95.175x + 267.17$	0.2192		0.19	0.36	-0.17	57.55%	9.35
Ln(Band 4)	y = 6.3867x + 68.36	0.0824	0.53	0.01	0.25	-0.10	56.32%	9.15
	$y = 15.739x^2 + 139.92x + 348.65$	0.1639		0.04	0.15	-0.23	68.09%	11.07
Ln(Band 5)	y = 3.1187x + 56.86	0.0686	0.57	0.01	0.30	-0.37	54.82%	8.91
	$y = 6.65x^2 + 70.015x + 220.64$	0.2151		0.14	0.20	-0.37	69.80%	11.34
Band 4 / Band 5	y = -1.7881x + 45.577	0.0266	0.73	0.00	0.31	-0.66	53.62%	8.71
	$y = 4.9296x^2 - 26.306x + 71.688$	0.1266		0.08	0.38	-0.65	60.39%	9.81
Band 4 / Band 3	y = -98.865x + 133.88	0.1215	0.44	0.33	0.14	-0.09	75.84%	12.32
	$y = -11682x^2 + 21342x - 9688.4$	0.8966		0.01	0.23	0.15	341.41%	55.48

Table 4.10 Statistics of single bands and band combinations for the June 26, 2016 sampling trip using 9 sites for development and 4 sites for validation

Reflectance Parameter	Relationship with SPM	R^2	p-value	F	t	R	RMSE (%)	RMSE in mg/L
Band 5	$y = 231.19x + 32.579$	0.0642	0.51	0.03	0.22	0.30	50.59%	7.08
	$y = 51.527x^{0.0763}$	0.1412		0.20	0.27	0.33	47.40%	6.64
Band 4	$y = 607.86x + 28.017$	0.1354	0.33	0.07	0.23	0.50	46.44%	6.50
	$y = -201536x^2 + 5722x + 0.0553$	0.3244		0.82	0.23	0.64	41.88%	5.86
Band 3	$y = 820.96x + 24.985$	0.1903	0.24	0.12	0.25	0.50	44.76%	6.27
	$y = -254909x^2 + 7562.2x - 15.635$	0.4253		0.86	0.32	0.62	39.92%	5.59
Band 2	$y = 445.05x + 30.837$	0.0924	0.43	0.05	0.24	0.33	49.00%	6.86
	$y = -116804x^2 + 2836.4x + 21.907$	0.174		0.46	0.27	0.36	48.41%	6.78
Band 1	$y = 337.96x + 31.832$	0.0745	0.48	0.04	0.23	0.28	49.98%	7.00
	$y = 60.915x^{0.1126}$	0.1429		0.22	0.33	0.25	47.07%	6.59
Ln(Band 1)	$y = 3.3367x + 51.711$	0.1243	0.35	0.16	0.27	0.25	48.90%	6.85
	$y = -4.9484x^2 - 46.653x - 72.223$	0.2172		0.39	0.43	0.17	47.50%	6.65
Ln(Band 2)	$y = 4.745x + 58.176$	0.1442	0.31	0.17	0.26	0.36	47.23%	6.61
	$y = -8.3364x^2 - 76.59x - 137.89$	0.2511		0.45	0.35	0.44	42.86%	6.00
Ln(Band 3)	$y = 11.787x + 87.638$	0.2592	0.16	0.26	0.26	0.55	42.06%	5.89
	$y = -27.585x^2 - 233.36x - 454.92$	0.4258		0.72	0.28	0.72	34.69%	4.86
Ln(Band 4)	$y = 8.4511x + 73.58$	0.1978	0.23	0.21	0.22	0.58	43.39%	6.07
	$y = -19.105x^2 - 164.55x - 315.71$	0.3536		0.72	0.20	0.77	34.66%	4.85
Ln(Band 5)	$y = 2.264x + 46.766$	0.1232	0.35	0.14	0.23	0.33	49.35%	6.91
	$y = -2.0676x^2 - 19.684x - 9.4838$	0.1925		0.17	0.26	0.39	46.75%	6.54
Band 4 / Band 5	$y = -1.1896x + 37.665$	0.1047	0.40	0.09	0.24	0.13	51.85%	7.26
	$y = -0.5087x^2 + 1.935x + 34.112$	0.127		0.03	0.25	-0.19	54.02%	7.56
Band 4 / Band 3	$y = 13.714x + 21.834$	0.0188	0.73	0.01	0.20	0.66	50.22%	7.03
	$y = 377.71x^2 - 668.45x + 328.22$	0.0792		0.02	0.29	-0.70	55.30%	7.74

Table 4.11 Statistics of single bands and band combinations for the September 30, 2016 sampling trip using 8 sites for development and 4 for validation

Reflectance Parameter	Relationship with SPM	R^2	p-value	F	t	R	RMSE (%)	RMSE in mg/L
Band 5	y = 10417x + 43.191	0.3468	0.12	0.45	0.04	0.96	38.07%	9.14
	$y = -3E+07x^2 + 156511x - 118.42$	0.8642		0.19	0.55	0.94	59.03%	14.17
Band 4	y = 5268.4x + 30.343	0.4416	0.07	0.85	0.05	0.83	46.39%	11.13
	$y = -1E+06x^2 + 20929x - 23.328$	0.4507		0.62	0.04	0.87	60.38%	14.49
Band 3	y = 4623.9x + 21.66	0.5928	0.03	0.45	0.13	0.99	23.52%	5.65
	$y = 435123x^2 - 4097.2x + 64.011$	0.6027		0.15	0.19	0.98	32.81%	7.87
Band 2	y = 8201.7x + 33.504	0.5698	0.03	0.39	0.18	0.96	27.76%	6.66
	$y = -3E+06x^2 + 32067x - 13.523$	0.6		0.81	0.21	0.97	13.18%	3.16
Band 1	y = 11318x + 55.859	0.5362	0.02	0.52	0.20	0.99	27.12%	6.51
	$y = 933.84x^{0.446}$	0.6616		0.42	0.20	0.96	24.19%	5.80
Ln(Band 1)	y = 29.241x + 243.42	0.6414	0.02	0.53	0.17	0.96	22.05%	5.29
	$y = 933.84e^{0.446x}$	0.6616		0.42	0.20	0.96	24.19%	5.80
Ln(Band 2)	y = 33.668x + 253.15	0.5903	0.03	0.62	0.10	0.97	21.82%	5.24
	$y = -25.482x^2 - 248.3x - 525.53$	0.6031		0.97	0.10	0.97	15.18%	3.64
Ln(Band 3)	y = 45.039x + 275.97	0.5823	0.03	0.67	0.09	0.98	18.46%	4.43
	$y = 41.921x^2 + 433.55x + 1174.9$	0.5935		0.24	0.16	0.99	30.25%	7.26
Ln(Band 4)	y = 37.029x + 251.64	0.4463	0.07	1.00	0.05	0.85	43.73%	10.50
	$y = 22.673x^2 + 181.51x + 308.28$	0.4483		0.83	0.06	0.88	40.80%	9.79
Ln(Band 5)	y = 26.228x + 227.63	0.4197	0.08	0.76	0.02	0.96	32.20%	7.73
	$y = -136.82x^2 - 1643.2x - 4855.4$	0.791		0.15	0.81	0.92	65.46%	15.71
Band 4 / Band 5	y = -14.764x + 112.27	0.1929	0.28	0.87	0.40	0.35	47.19%	11.33
	$y = -46.156x^2 + 276.73x - 343.92$	0.3808		0.12	0.50	0.01	125.26%	30.06
Band 4 / Band 3	y = -65.487x + 110.83	0.0416	0.63	0.85	0.62	-0.38	62.29%	14.95
	$y = -2594.4x^2 + 3614x - 1191.1$	0.0914		0.00	0.47	-0.28	508.11%	121.95

4.3.3 SPIM Retrieval Algorithm Results

Once the previous models for SPIM were tested and modified, the previously utilized variables were modified to consider alternative formula types. Additional possible reflectance parameters and algorithm forms were then tested as potential variables in a Weeks Bay SPIM retrieval algorithm. These reflectance parameters include single bands, the natural logs of single bands, band ratios, band combinations, and combinations of the previously listed. Both a linear, and nonlinear model were tested for each reflectance parameter. The equations for each tested model, as well as the associated statistics may be seen in Table 4.12 for the previously utilized variables, and Table 4.13 for the new variables.

Table 4.12 Statistics of previously used variables with modified model types for an SPIM Retrieval Algorithm

Reflectance Parameter	Relationship with SPIM	R^2	p-value	F	t	R	RMSE (%)	RMSE in mg/L
Band 5	$y = -286.87x + 14.495$	0.1595	0.02	0.48	0.86	0.37	29.79%	3.80
	$y = -760786x^3 + 44988x^2 - 891.18x + 15.849$	0.1874		0.88	0.61	0.37	33.07%	4.22
Band 4	$y = -235.12x + 15.778$	0.2073	0.01	0.13	0.67	0.42	27.07%	3.45
	$y = -534292x^3 + 43640x^2 - 1200.3x + 21.026$	0.2586		0.22	0.82	0.59	23.34%	2.98
Band 4/Band 3	$y = -20.644x + 30.374$	0.2619	0.00	0.05	0.84	0.83	17.48%	2.23
	$y = 475.87x^3 - 985.16x^2 + 618.59x - 95.695$	0.525		0.58	0.29	0.90	12.95%	1.65
Ln(Band 5)	$y = -1.8859x + 2.3545$	0.1693	0.02	0.01	0.90	0.57	23.54%	3.00
	$y = 2.6794x^3 + 41.555x^2 + 209.2x + 353.49$	0.2752		0.88	0.38	0.21	36.25%	4.62
(Band 3 + Band 4) / (Band 3/Band 4)	$y = -127.77x + 15.842$	0.2243	0.01	0.24	0.76	0.43	27.38%	3.49
	$y = -120550x^3 + 16592x^2 - 759.68x + 21.816$	0.2824		0.43	0.70	0.45	34.09%	4.35

Table 4.13 Statistics of additional single band and band combinations for an SPIM Retrieval Algorithm

Reflectance Parameter	Relationship with SPIM	R^2	p-value	F	t	R	RMSE (%)	RMSE in mg/L
Band 3	$y = -172.03x + 15.306$	0.1481	0.03	0.01	0.49	0.38	27.02%	3.44
	$y = 6198x^2 - 478.1x + 17.958$	0.1891		0.01	0.47	0.53	24.73%	3.15
Band 2	$y = -214.31x + 14.789$	0.1876	0.01	0.05	0.65	0.39	27.08%	3.45
	$y = -721699x^3 + 54097x^2 - 1238.8x + 18.788$	0.2879		0.06	0.76	0.64	21.98%	2.80
Band 1	$y = -230.73x + 14.598$	0.1932	0.01	0.12	0.74	0.38	27.65%	3.52
	$y = -1E+06x^3 + 69652x^2 - 1347x + 17.926$	0.3038		0.04	0.68	0.65	22.01%	2.81
Band 4/Band 1	$y = 3.3281x + 5.6304$	0.3441	0.00	0.04	0.97	0.57	23.42%	2.99
	$y = -0.521x^3 + 4.5095x^2 - 8.2808x + 14.419$	0.3591		0.05	0.93	0.56	23.76%	3.03
Band 4/Band 2	$y = 6.5101x + 2.497$	0.2842	0.00	0.01	0.88	0.51	24.60%	3.14
	$y = -1.0523x^3 + 6.9102x^2 - 7.2651x + 10.972$	0.2888		0.00	0.92	0.51	24.60%	3.14
Band 4/Band 5	$y = 0.3697x + 11.638$	0.0129	0.54	0.00	0.57	0.45	27.79%	3.54
	$y = -0.2892x^3 + 1.4836x^2 + 0.2124x + 8.3444$	0.2264		0.01	0.45	0.57	24.12%	3.08
Band 3/Band 5	$y = 0.5315x + 10.795$	0.0491	0.22	0.00	0.74	0.62	25.48%	3.25
	$y = -0.1225x^3 + 0.9009x^2 - 0.4363x + 9.5677$	0.219		0.01	0.77	0.59	23.29%	2.97
Band 2/Band 5	$y = -0.5817x + 13.878$	0.0165	0.48	0.00	0.29	-0.38	30.49%	3.89
	$y = 1.1276x^3 - 10.811x^2 + 27.502x - 6.6329$	0.2013		0.00	0.05	0.03	5127.91%	653.81
Band 1/Band 5	$y = -1.3323x + 14.706$	0.0633	0.16	0.00	0.23	-0.09	30.31%	3.86
	$y = 1.0571x^3 - 8.0341x^2 + 13.467x + 7.1789$	0.1107		0.00	0.13	0.04	30.96%	3.95
Band 3 + Band 1	$y = -100.81x + 15.055$	0.1712	0.02	0.03	0.60	0.38	27.16%	3.46
	$y = -38933x^3 + 7437.1x^2 - 460.23x + 18.879$	0.2361		0.02	0.57	0.61	23.10%	2.95
Band 3 + Band 2	$y = -96.46x + 15.101$	0.1675	0.02	0.02	0.56	0.39	26.98%	3.44
	$y = -31690x^3 + 6525.1x^2 - 435.99x + 19.03$	0.2303		0.01	0.53	0.61	23.19%	2.96

Table 4.13 (continued)

Reflectance Parameter	Relationship with SPIM	R^2	p-value	F	T	R	RMSE (%)	RMSE in mg/L
Band 3 + Band 4	$y = -101.49x + 15.565$	0.1768	0.02	0.03	0.56	0.40	26.93%	3.43
	$y = -15175x^3 + 4249.1x^2 - 364.45x + 19.176$	0.2209		0.01	0.47	0.61	23.19%	2.96
Band 3 + Band 5	$y = -132.76x + 15.528$	0.1881	0.01	0.26	0.82	0.37	28.60%	3.65
	$y = 75503x^3 - 4409.3x^2 - 103.33x + 15.864$	0.2075		0.69	0.24	0.12	42.13%	5.37
Band 4 + Band 1	$y = -119.29x + 15.242$	0.205	0.01	0.14	0.72	0.40	27.44%	3.50
	$y = -107871x^3 + 15262x^2 - 688.46x + 20.051$	0.2833		0.58	0.92	0.53	26.07%	3.32
Band 4 + Band 2	$y = -113.9x + 15.3$	0.2001	0.01	0.09	0.67	0.41	27.10%	3.46
	$y = -84800x^3 + 12994x^2 - 640.49x + 20.223$	0.2744		0.18	0.85	0.60	22.98%	2.93
Band 4 + Band 5	$y = -149.35x + 15.58$	0.2147	0.01	0.54	0.98	0.39	29.38%	3.75
	$y = -90913x^3 + 11934x^2 - 547.86x + 18.563$	0.2421		0.81	0.74	0.42	31.97%	4.08
Band 5 + Band 1	$y = -147.52x + 14.828$	0.2055	0.01	0.53	0.98	0.37	29.76%	3.79
	$y = -355908x^3 + 30340x^2 - 834.68x + 17.892$	0.2608		0.00	0.36	0.19	148.18%	18.89
Band 5 + Band 2	$y = -144.7x + 15.006$	0.2071	0.01	0.45	0.96	0.38	29.27%	3.73
	$y = -245994x^3 + 23590x^2 - 748.66x + 18.238$	0.2541		0.40	0.23	0.00	86.77%	11.06
Band 1 + Band 2	$y = -111.42x + 14.703$	0.1908	0.01	0.08	0.70	0.39	27.34%	3.49
	$y = -109936x^3 + 15355x^2 - 647.29x + 18.395$	0.2959		0.00	0.00	-0.33	141.15%	18.00
Ln(Band 1)	$y = -2.6178x - 0.8981$	0.2972	0.00	0.09	0.77	0.61	22.71%	2.90
	$y = -0.1637x^3 - 1.4045x^2 - 4.1078x + 5.5073$	0.3252		0.08	0.74	0.70	20.51%	2.61
Ln(Band 2)	$y = -2.9541x - 1.8569$	0.2743	0.00	0.06	0.68	0.60	23.05%	2.94
	$y = 0.0928x^3 + 2.388x^2 + 13.334x + 30.961$	0.2944		0.70	0.65	0.05	20.91%	2.67
Ln(Band 3)	$y = -3.5142x - 2.5252$	0.1759	0.02	0.01	0.49	0.50	25.12%	3.20
	$y = 4.266x^3 + 51.923x^2 + 204.44x + 271.16$	0.2068		0.01	0.44	0.49	25.42%	3.24
Ln(Band 4)	$y = -3.71x - 3.9922$	0.2452	0.00	0.06	0.58	0.60	23.02%	2.94
	$y = 2.4453x^3 + 32.746x^2 + 140.91x + 206.41$	0.2617		0.02	0.46	0.65	22.39%	2.85

Table 4.13 (continued)

Reflectance Parameter	Relationship with SPIM	R^2	p-value	F	T	R	RMSE (%)	RMSE in mg/L
Ln(Band 4) / Ln(Band 3)	y = 66.182x - 55.914	0.2046	0.01	0.01	0.80	0.84	18.84%	2.40
	$y = -84393x^3 + 266348x^2 - 279970x + 98029$	0.6504		0.59	0.85	0.90	12.50%	1.59
(Band 3 - Band 5)/ (Band 3 + Band 5)	y = 4.3465x + 8.3873	0.0384	0.28	0.00	0.47	0.27	28.02%	3.57
	$y = 59.966x^3 - 67.058x^2 + 7.7731x + 9.8539$	0.2103		0.01	0.81	0.84	18.60%	2.37

The reflectance parameters produced much more significant results when being related to SPIM, opposed to SPM. Out of the 29 reflectance parameters tested as possible predictive variables in a SPIM retrieval algorithm for Weeks Bay, 25 were significant ($p<0.05$). Out of the 25 variables statistically significant p-values, only two reflectance parameters produced linear algorithms with a significant Pearson correlation coefficient ($R \geq 0.8$). Similarly, only three variables produced nonlinear algorithms with a significant Pearson correlation coefficient ($R \geq 0.8$).

Both the linear and non-linear algorithms for Band 4/Band 3 and Ln(Band 4)/Ln(Band 3), and the nonlinear algorithm for (Band 3 – Band 5)/(Band 3 + Band 5) had strong Pearson correlation coefficients, such that the linear algorithms had reported R values of 0.83, and 0.84 respectively, and the nonlinear algorithms had reported R values of 0.90, 0.90, and 0.84 respectively. The linear algorithms for Band 4/Band 3, and Ln(Band 4)/Ln(Band 3) had RMSE (%) of 17.48% (2.23 mg/L), and 18.84% (2.40 mg/L) respectively. The nonlinear algorithms for Band 4/Band 3, Ln(Band 4)/Ln(Band 3), and (Band 3 – Band 5)/(Band 3 + Band 5) were 12.95% (1.65 mg/L), 12.50% (1.59 mg/L), and 18.60% (2.37 mg/L) respectively. The R^2 increase significantly between the linear and nonlinear algorithms for each significant band. The R^2 value increases from 0.2619 to 0.5250 for Band 4/Band 3 when the equation is changed from a simple linear equation into a third order polynomial, while the R^2 value increases from 0.2046 to 0.6504 for Ln(Band 4)/Ln(Band 3) when the equation is changed from a simple linear equation into a third order polynomial.

With the development and validation of (Band 3 – Band 5)/(Band 3 + Band 5) as a possible variable in an SPIM retrieval algorithm, both Sites 1 and 2 from May 9, 2016

may be removed as outliers. With the removal of these sites, the linear algorithm using the (Band 3 – Band 5)/(Band 3 + Band 5) variable improves in performance to an R^2 of 0.0384 to 0.1951, a p-value of 0.28241 to 0.01, and RMSE (%) of 28.02% to 19.39%. The nonlinear algorithm improves in performance to an R^2 of 0.2103 to 0.6444, RMSE (%) of 18.60% to 12.85, and R of 0.85 to 0.90.

Plots for the predicted SPIM concentrations derived from each of the three significant linear models versus the *in situ* SPIM concentrations may be seen in Figures 4.25, 4.27, and 4.29. Plots for the predicted SPIM concentrations derived from each of the three significant nonlinear models versus the *in situ* SPIM concentrations may be seen in Figures 4.26, 4.28, and 4.30. Figure 4.35 and 4.36 depicts the results from the (Band 3 – Band 5)/(Band 3 + Band 5) variable with the removal of May 9, 2016 Sites 1 and 2 removed from the development and validation.

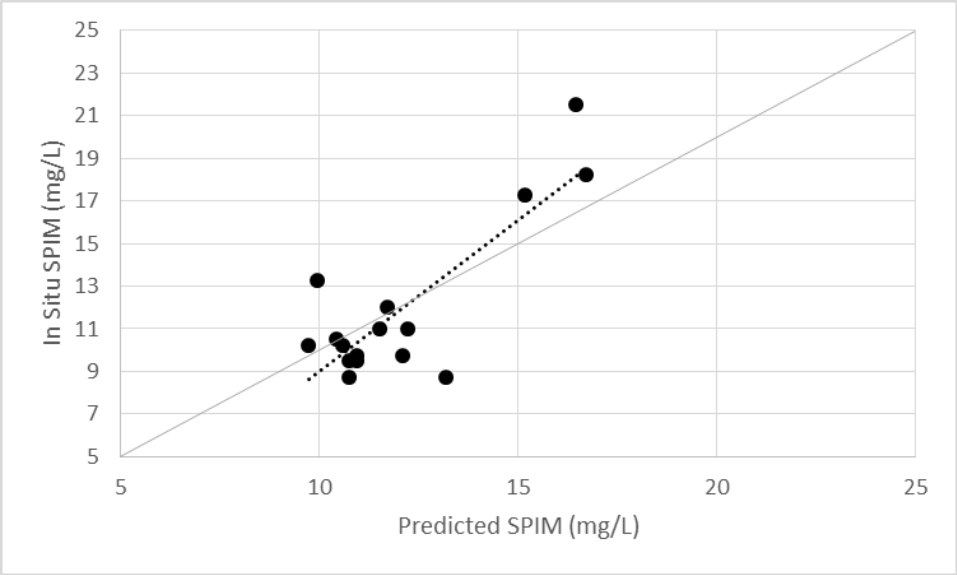

Figure 4.25 Predicted SPIM based on the developed linear model using Band 4/Band 3 as the predictive variable.

Based on the linear equation using the variable Band 4/Band 3 as depicted in Table 4.12. The solid line depicts a 1:1 relationship, while the dashed line represents the linear trend.

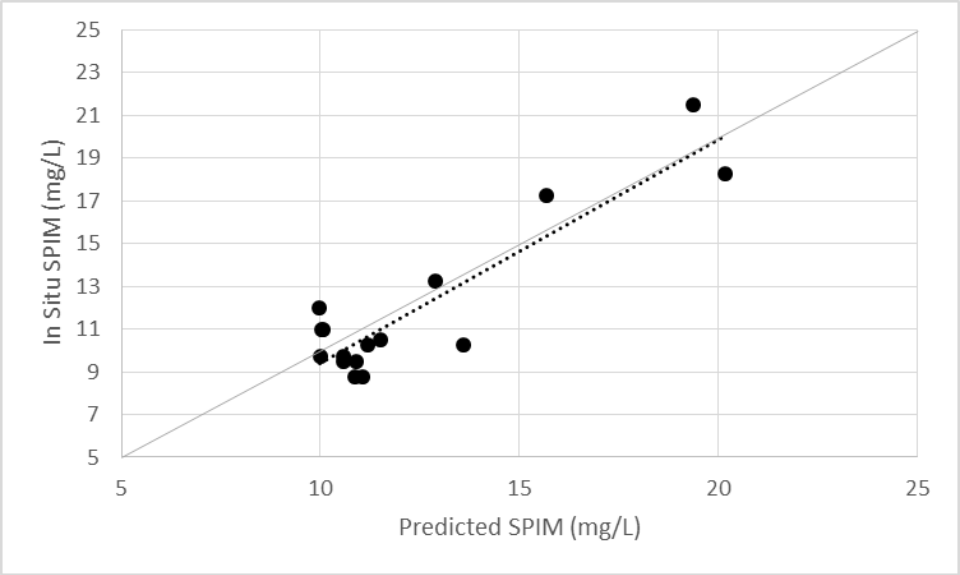

Figure 4.26 Predicted SPIM based on the developed nonlinear model using Band 4 /Band 3 as the predictive variable.

Based on the nonlinear mode using Band 4/Band 3 as the predictive variable as presented in Table 4.12. The solid line depicts a 1:1 relationship, while the dashed line represents the linear trend.

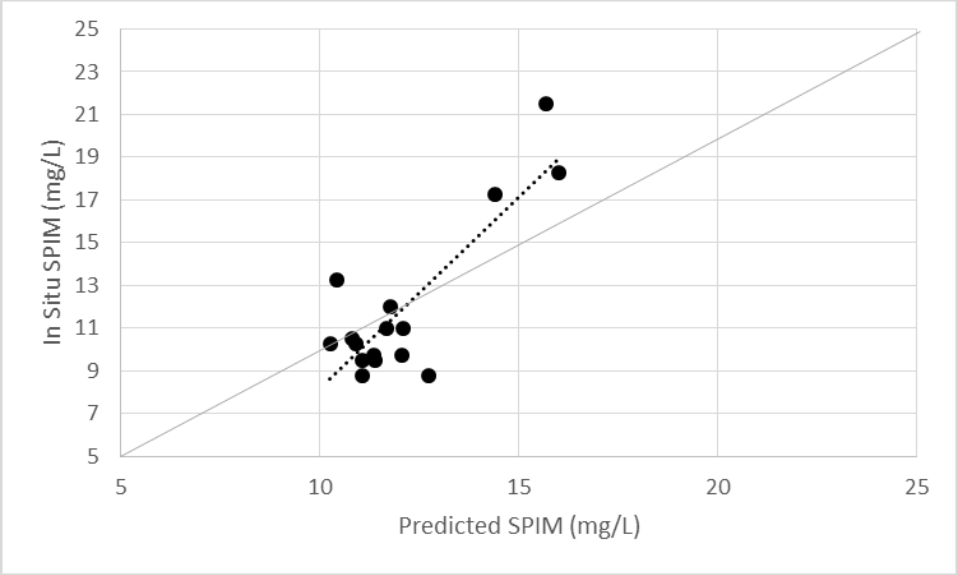

Figure 4.27 Predicted SPIM based on the developed linear model using Ln(Band 4)/Ln(Band 3) as the predictive variable.

Based on the linear equation using the variable Ln(Band 4)/Ln(Band 3) as depicted in Table 4.13. The solid line depicts a 1:1 relationship, while the dashed line represents the linear trend.

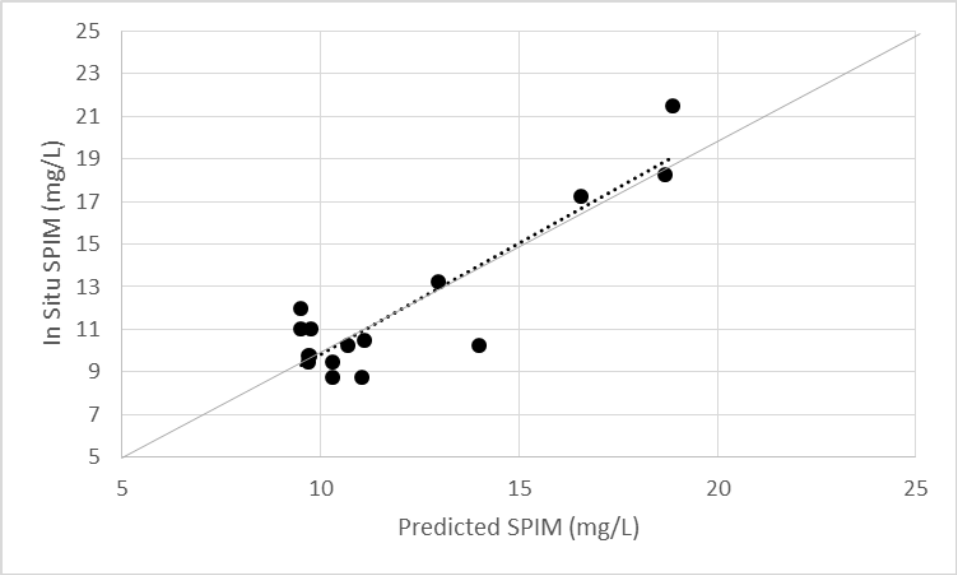

Figure 4.28 Predicted SPIM based on the developed nonlinear model using Ln(Band 4)/Ln(Band 3) as the predictive variable.

Based on the nonlinear equation using the variable Ln(Band 4)/Ln(Band 3) as depicted in Table 4.13. The solid line depicts a 1:1 relationship, while the dashed line represents the linear trend.

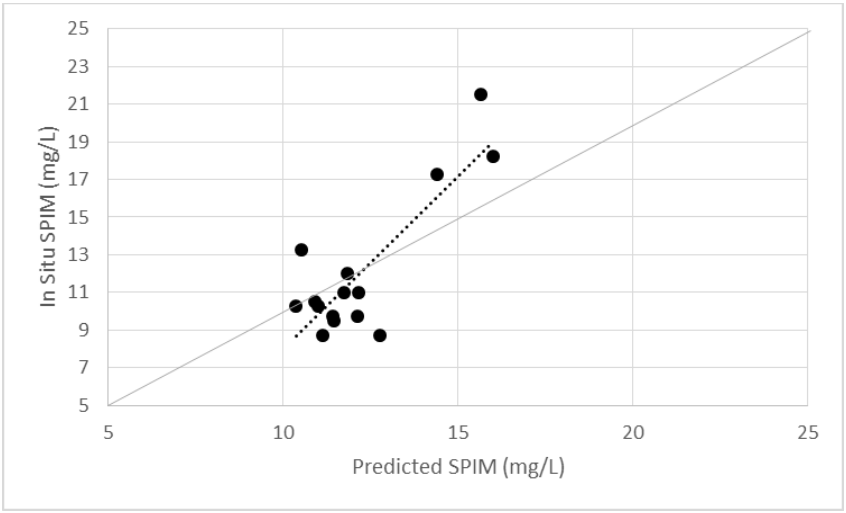

Figure 4.29 Predicted SPIM based on the developed linear model using (Band 3 – Band 5)/(Band 3 + Band 5) as the predictive variable.

Based on the linear equation using the variable (Band 3-Band 5)/(Band 3+Band 5). The solid line depicts a 1:1 relationship, while the dashed line represents the linear trend. This equation was developed and validated with the removal of May 9, 2016 Sites 1 and 2.

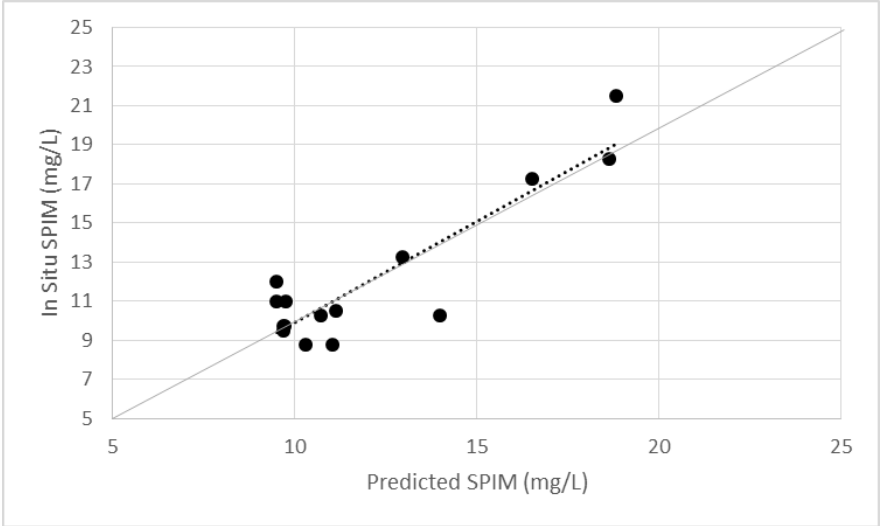

Figure 4.30 Predicted SPIM based on the developed nonlinear model using (Band 3 – Band 5)/(Band 3 + Band 5) as the predictive variable.

Based on the nonlinear equation using the variable (Band 3 – Band 5)/(Band 3 + Band 5). The solid line depicts a 1:1 relationship, while the dashed line represents the linear trend. This equation was developed and validated with the removal of May 9, 2016 Sites 1 and 2.

4.4 Simulation Results

A semi-analytical simulation approach was used to determine the contribution of Rrs from the various OACs present in Weeks Bay, particularly from SPM alone. For Equation 3.5, the b_{bw} values were derived from those published by Smith and Baker (1981). Smith and Baker (1981) derived the scattering coefficients for both fresh and saltwater between 200 and 800 nm. Weeks Bay is a brackish estuary, with an average salinity of 4.69‰ recorded by the NERR Weeks Bay water quality station between May and September 2016 (NERRS). Being a brackish water estuary, it is neither suitable to use the pure freshwater, nor the pure saltwater (35-39‰) coefficients as determined by Smith and Baker (1981). An average of the fresh and saltwater backscattering coefficients was used to represent the brackish water of Weeks Bay. Figure 4.25

demonstrates the limited variation between the simulated Rrs results using the various backscattering coefficients. The average variation in the simulated Rrs values between using the fresh water, ocean water, or averaged b_{bw} coefficients was 5.25×10^{-6} sr^{-1}. The a_w values used in the simulation approach were taken from Mueller et al. (2003). The b_{bp}, values were determined for each site using the procedure described in Section 3.1.4. The a_{cdom} values were determined using the procedure described in Section 3.2.2. PC concentrations were derived using the procedure described in Section 3.2.3. To obtain a_{pc}, the PC concentrations for each site were multiplied by the specific absorption coefficient of PC as determined by Dash et al. (2011). The a_{NAP} and a_{Chla} were determined using the procedure described in Section 3.2.4.

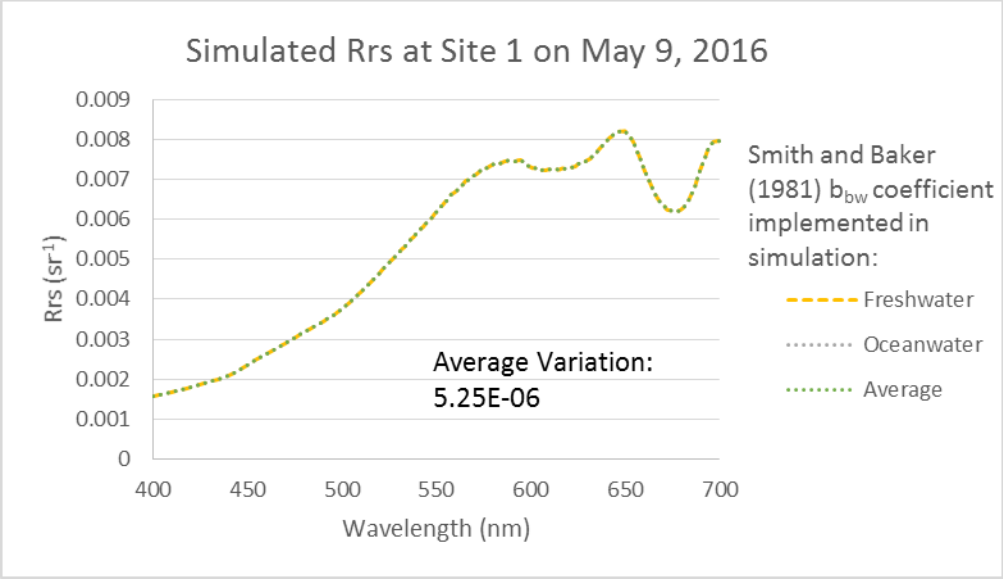

Figure 4.31 Simulated Rrs results at site 1 on May 9, 2016 using various b_{bw} coefficients

The simulated Rrs results at site 1 on May 9, 2016 using the backscattering coefficients of for pure fresh and ocean water derived by Smith and Baker (1981), as well as using an average of both the fresh and ocean water coefficients.

The Rrs simulation created for Weeks Bay presents modeled spectra curves that generally coincide with the spectra curves observed by the *in situ* radiometer data. While the spectra curves of the simulated Rrs match those observed by the radiometer, the magnitude of the simulated Rrs values tend to be low. Once the total Rrs was simulated using Equation 4.1, the equation was modified to determine the Rrs when there is no SPM present. By removing the absorption coefficients of the OACs that make up SPM including chlorophyll (Chl a and PC) and mineral particulates (NAP) (Gohin, 2011), the following equation may be derived:

$$Rrs_{SPM=0} = 0.54\left(\frac{f}{Q}\right)\left(\frac{b_{bw}+b_{bp}}{(a_w+cdom)+(b_{bw}+b_{bp})}\right). \quad (4.1)$$

By removing the absorption of NAP, Chl a, and PC, the simulated Rrs values increase from the simulated total Rrs values, as depicted for May 9, 2016 Site 1 in Figure 4.26. To obtain the Rrs of SPM alone, the Rrs values determined for SPM=0 were subtracted from the total Rrs values. This was done using both the simulated total Rrs and radiometer Rrs values. The resultant Rrs values for SPM alone often resulted in negative values (Figure 4.26).

Similarly, using Equation 4.1, the equation was modified to determine the Rrs when there is no SPIM present. By removing the absorption coefficients of the OACs that make up SPIM (NAP) (Gohin, 2011), the following equation may be derived:

$$Rrs_{SPIM=0} = 0.54\left(\frac{f}{Q}\right)\left(\frac{b_{bw}+b_{bp}}{(a_w+cdom+a_{chla}+a_{pc})+(b_{bw}+b_{bp})}\right) \quad (4.2)$$

By removing the absorption of NAP alone, the simulated Rrs values increase from the simulated total Rrs values. In 43 out of the 48 sites, the Rrs value increase is not as great as when NAP, Chl a, and PC are removed. To obtain the Rrs of SPIM alone, the Rrs values determined for SPIM=0 were subtracted from the total Rrs values. This was done using both the simulated total Rrs and radiometer Rrs values. The resultant Rrs values for SPIM are greater than those for SPM (Figure 4.26).

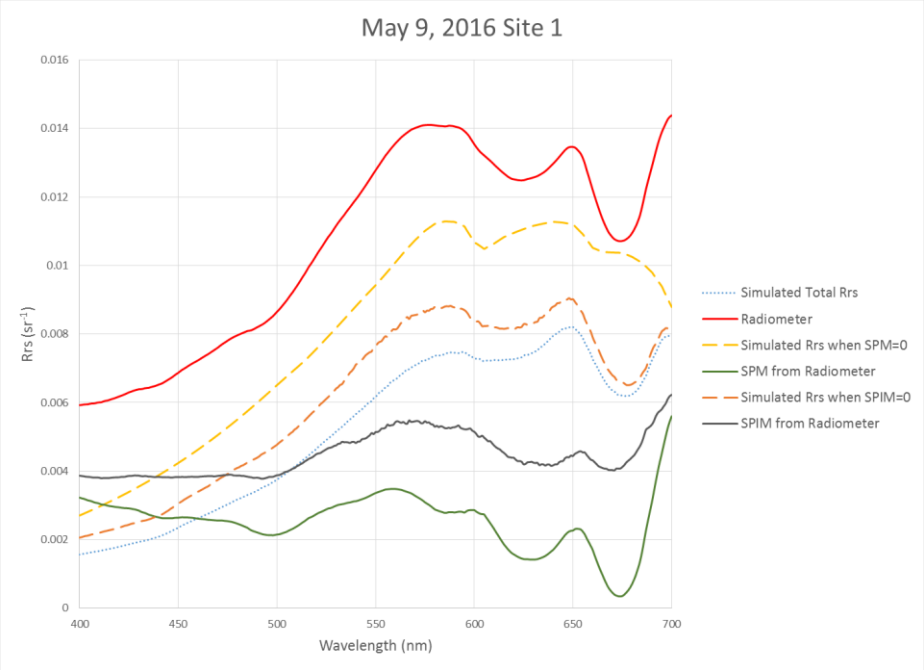

Figure 4.32 Semi-Analytical Simulation Results for May 9, 2016 Site 1

4.5 Precipitation Data

Meteorological data was downloaded for the entire field sampling season, from May to September 2016, for the Safe Harbor Met Station, looking at the Weeks Bay NERR.

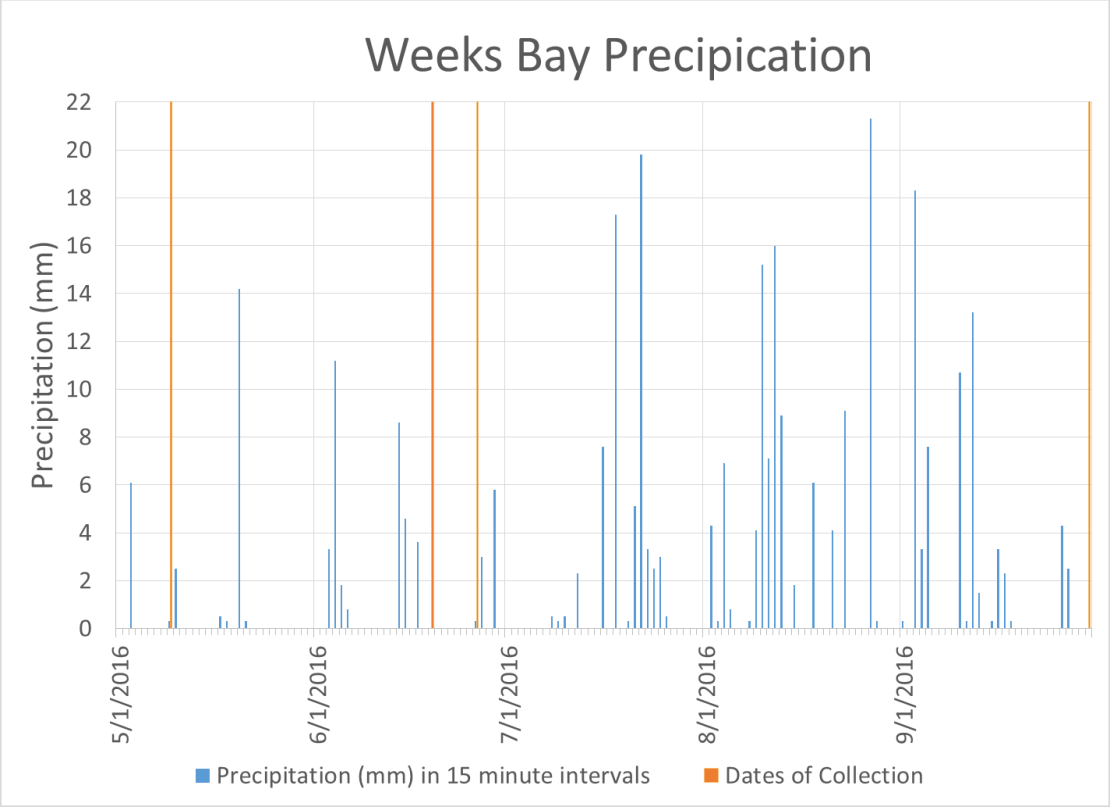

Figure 4.33 Precipitation in Weeks Bay from May to September 2016

CHAPTER V

DISCUSSION

5.1 *In Situ* Measurements

5.1.1 Field Measurements

The pH of estuarine waters typically range between 7.0 and 7.5 in lower salinities, and between 8.0 and 8.6 in the more saline portions (Ohrel & Register, 2006). Pure seawater has a pH average of 8.0 (Ohrel & Register, 2006). Estuarine organisms prefer pH values between 6.5 and 8.5 (Ohrel & Register, 2006). Most aquatic organisms may survive in waters with a pH between 5.0 and 9.0, with the values less than 7 being slightly acidic, and those above 7 being slightly basic (Ohrel & Register, 2006; NOAA, 2008). Algal blooms may cause dramatic fluctuations in pH over short periods of time, stressing other aquatic organisms. The range of pH values in Weeks Bay between 7.28 and 8.99 fall within the range of acceptable values for aquatic organisms (Figure 4.6). The average pH values increased with each consecutive field cruise, with average pH values of 7.97, 8.16, 8.59, and 8.67 respectively for the May 9, June 19, June 26, and September 30, 2016 sampling trips.

Salinity levels vary throughout the estuary depending on the location. Salinity levels will typically be higher near the mouth of the estuary, which serves as the source of saline water, and lower near the freshwater input, such as a river. Pure seawater has a salinity of around 35 parts per thousand (ppt), while pure water contains <0.5 ppt

(NOAA, 2008). Estuarine salinity levels may range anywhere between 0.5 and 30.0 ppt (Orthel & Register, 2006). Salinity has an important role with suspended sediment by causing particle aggregation, otherwise known as flocculation (Orthel & Register, 2006). June 19, June 26, and September 30, 2016 generally increase in salinity as the sample sites move closer to the mouth of Weeks Bay, and the source of seawater. Salinity levels in Weeks Bay ranged between 0.42 and 22.98 PSU during the four field cruises (Figure 4.7). The average measured salinity was 3.32, 9.05, 8.19, and 15.10 PSU respectively for the May 9, June 19, June 26, and September 30, 2016 sampling trips. The June 19, June 26, and September 30 field cruises demonstrated an increase in salinity as sampling moved south, towards the mouth of Weeks Bay, as would be expected. On May 9, 2016, the highest salinity value was found at site 4, located at the northern portion of the bay. Weeks Bay receives its source of saline water from Mobile Bay, which is also an estuary with its own fluctuating salinity values. Previous field cruises in Weeks Bay demonstrated significant variations both temporally and spatially (Miller-Way et al., 1996). The observed variability is due to flashy local runoff from the Fish and Magnolia Rivers, as well as from exchanges with the variable salinity of regime of Mobile Bay (Miller-Way et al., 1996).

The National Oceanographic Data Center (NODC) has reported water temperature averages that peak in July and reach a minimum in January for the Mobile Bay region (NODC, 2017). Water temperatures in Weeks Bay were coolest on May 9, 2016 with an average water temperature of 25.60 ℃. Temperatures were slightly warmer on June 19, 2016 with an average of 29.23 ℃, reaching a peak on June 26, 2016 with an average water temperature of 31.09. Water temperatures declined to an average of 26.24

℃ on September 30, 2016. This reflects the trends reported for the Mobile Bay by demonstrating a peak in late June.

DO levels are influenced by both temperature and salinity, varying seasonally with the highest values typically found in the late summer when temperatures are typically the highest (NOAA, 2008). The DO levels observed in Weeks Bay fail to exhibit this typical seasonal variability, by peaking on May 9, 2016 with an average DO value of 5.12 ppm when temperatures were the lowest. The lowest DO values were recorded on September 30, 2016 with an average value of 0.34 ppm. June 19 and June 26, 2016 reported average DO values of 1.48 and 1.38 ppm respectively. Aquatic organisms must have adequate DO levels in order to survive, making DO one of the best indicators of estuarine health (Ohrel & Register, 2006). In order for most aquatic organisms to function unimpaired, DO levels must typically exceed 5 ppm (Ohrel & Register, 2006). DO levels between 3 and 5 ppm may cause aquatic organisms to become stressed and is known as hypoxia, while levels below 3 ppm, otherwise known as anoxia, will force organisms to either move to new waters or perish (Orthel & Register, 2006). Only sites 4, 8, and 11 recorded on May 9, 2016 were above 5 ppm, and therefore at a level suitable for aquatic organisms to function unimpaired. Sites 1, 5, 6, 9, 10, and 12 on May 9, 2016 fell within the hypoxic range. The remaining three sites from May 9, 2016, and all sites from June 19, June 26, and September 30, 2016 fall within the anoxic range.

The Weeks Bay NERR contains four water quality sampling stations that record data continuously at 15 minute intervals. Out of those four water quality stations, only the Fish River water quality station has reported DO values that are neither missing nor flagged as suspect for all dates of collection. The Weeks Bay water quality station

produced DO values for May 9, but none of the other collection dates. With the removal of suspect values, May 9 has a reported average DO of 8.66 ppm, June 19 has a reported average DO of 7.62 ppm, June 26 has a reported average DO of 6.68 ppm, and September 30 has a reported average DO of 0.94 ppm. The reported values of the NERR water quality stations indicate that the DO sensor of the Hanna instrument used during the field sampling trips for this project was invalid and produced erroneous results. The reported DO values by the NERR water quality stations, for all but the September 30 sampling trip, are over 5 ppm and therefore of healthy levels for aquatic life

5.1.2 Spectroradiometer Reflectance Values

The Rrs spectra of all 48 sites may be seen in Figures 4.9, 4.10. 4.11, and 4.12. The curves of a standard reflectance curve in algae-laden water may be seen in Figure 5.3. A majority of the field radiometer Rrs curves depict similar peaks to those in the standard reflectance curve. A peak is commonly present in the green portion of the EMS due to the lower absorption, and higher reflection of green light caused by algae (Jenson, 2006). Additionally, visible in the hyperspectral *in situ* reflectance curves, is a peak around 700 nm due to increased chlorophyll reflectance, and minimal pigment and water absorption (Jenson, 2006). In the standard reflectance curve, reflectance increases as SPM concentrations increase (Jenson, 2006). As depicted in Figures 5.3 and 5.4, this relationship was not consistently true with the SPM and SPIM concentrations of Weeks Bay. With SPM concentrations, the highest SPM concentrations were found to generally coincide with the lowest Rrs values (Figure 5.1). This is most likely due to the abundance of organic material comprising the SPM concentrations, therefore increasing the

absorption of the samples. Similarly, the highest SPIM concentrations resulted in the lowest Rrs (Figure 5.2).

The sites that fail to produce the expected reflectance curves, such as May 9, 2016 site 10 and June 26, 2016 site 13, display the highest SPM and SPOM concentrations for the corresponding sampling trips. The unexpected spectra curves could in part be due to the high concentrations of particulate matter. Additionally, these sites could have experienced sun glint. Sun glint occurs when sunlight is reflected off the surface water at the same angle that the sensor is viewing the surface water.

The Rrs values are mostly low values, with only 10 sites with Rrs values greater than 0.2 sr^{-1}. Out of those 10 sites, only 3 sites have Rrs values greater than 0.3 sr^{-1}. The lowest Rrs value occurred in Landsat-8 band 5 with a value of 0.001333 sr^{-1}. The maximum Rrs value occurred in Landsat-8 band 3 with a value of 0.050529 sr^{-1}.

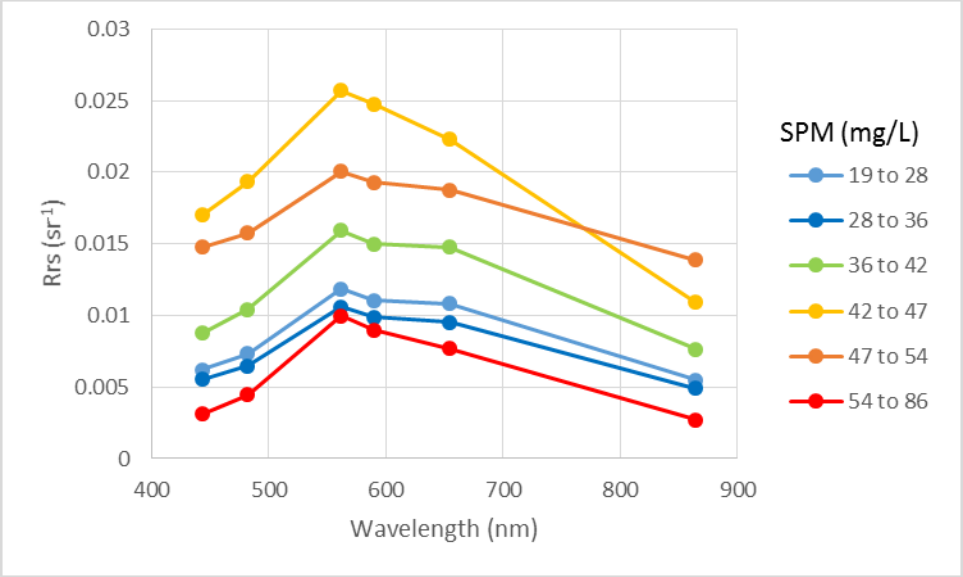

Figure 5.1 Spectral variation of Rrs (sr^{-1}) averaged over categories of SPM concentrations

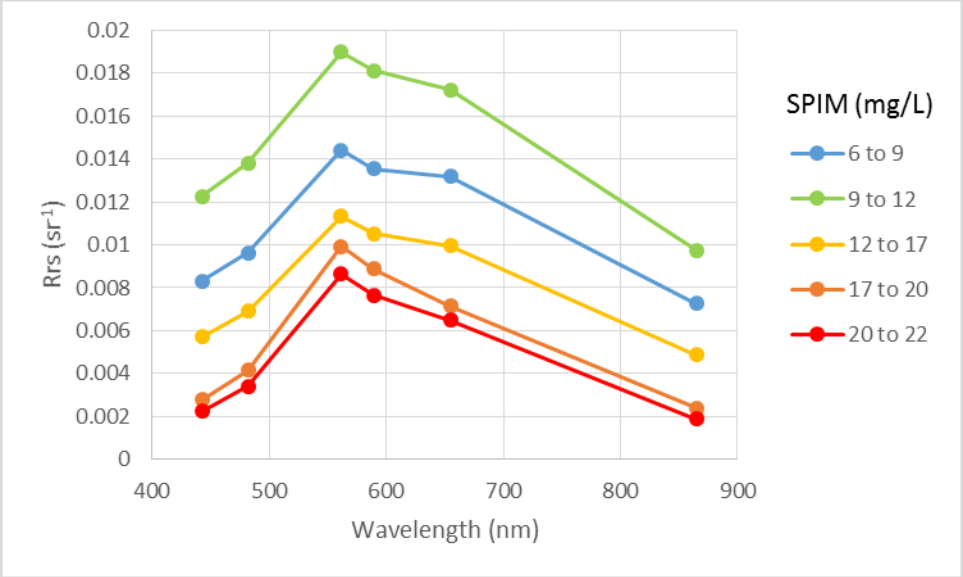

Figure 5.2 Spectral variation of Rrs (sr-1) averaged over categories of SPIM concentrations

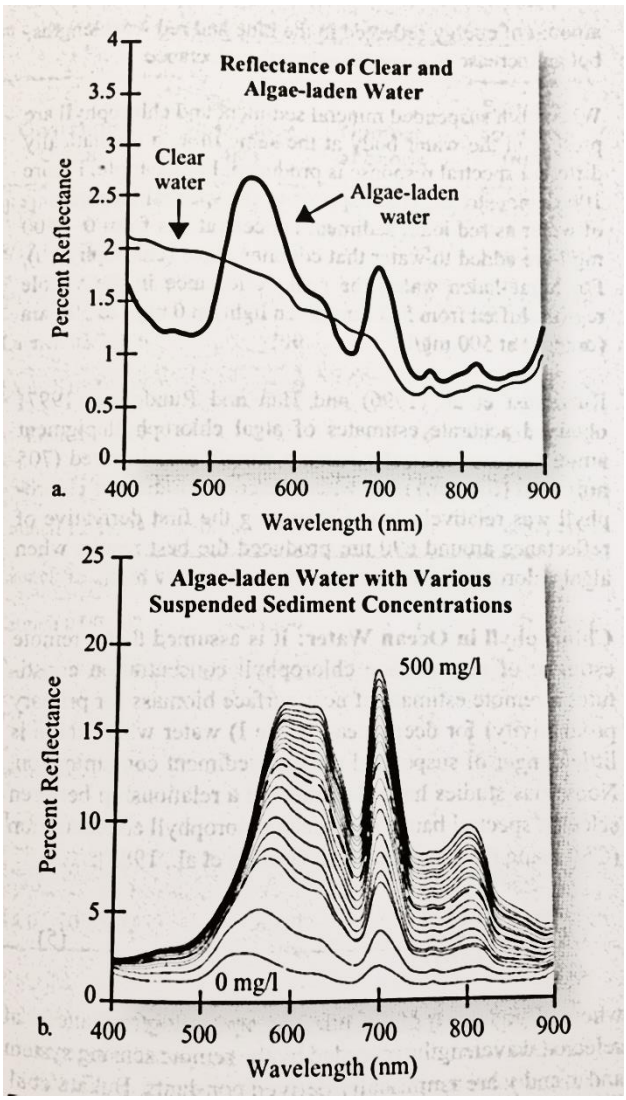

Figure 5.3 Standard reflectance spectra for clear and algae-laden waters. Source: (Jenson, 2006).

5.2 Lab Procedures

5.2.1 SPM Concentrations

SPM concentrations are measured to include both the organic (SPOM) and inorganic (SPIM) components. 48 *in situ* SPM concentrations were collected over the course of four sampling trips. Only site 12 on 9/30/2016, located at the mouth of Weeks Bay in Mobile Bay, exceeded 75 mg/L, with a concentration of 85.5 mg/L. All of the

September 30, 2016 sample sites had an SPM concentration above the 50th percentile, with the lowest SPM concentration being 42.75 mg/L at site 1, located at the mouth of the Fish River. The lowest SPM value occurred at site 2 on 6/26/2016, located in the northern portion of the bay, with a concentration of 19.5 mg/L.

Figures 4.13, 4.15, 4.17, and 4.19 depict the relationship between total SPM, SPOM, and SPIM for each field cruise. SPOM accounts for 71% of the total SPM, while SPIM accounts for only 29%. Total SPM exhibits positive correlation with both SPOM and SPIM. The total SPM concentrations more closely follows the SPOM concentrations with an R^2 value of 0.9579, while the relationship of total SPM with SPIM produces an R^2 of 0.6641 (Figures 4.21 and 4.22). SPOM consists primarily of phytoplankton, while SPIM is comprised of inorganic particulates of various sizes, shapes, and mineral compositions (Binding et al., 2005). Depending on the severity of tidal influences and river discharge, different inorganic particulates will be suspended in varying concentrations. The Weeks Bay estuary bottom is made up of primarily silty clay, with a section of clayey-silt in the northern tip, and clayey-sand by the mouth of the bay (Miller-Way et al., 1996). The shorelines are comprised of a quartz sand that is a result of shoreline erosion (Miller-Way et al., 1996).

The May 9, 2016 sampling trip SPM and SPIM concentrations were statistically similar to the June sampling trips, while the September 30, 2016 sampling trip differed significantly. On both the May 9 and June 26, 2016 collection date, a small amount precipitation of precipitation (<0.6) was recorded prior to collection (Figure 4.36). The similarity of the day of collection precipitation on May 9 and June 26, 2016 may be a possible explanation for their statistically similarity in SPM concentrations. June 26 and

September 30, 2016 did not receive any precipitation on the day of collection, but received a larger amount of precipitation throughout the seven days prior to collection (Figure 4.36). May 9, 2016 also received a large amount of precipitation during the seven days prior to collection, while June 26, 2016 did not (Figure 4.36).

Variable SPM concentrations could be attributed to the complex water exchange of the Weeks Bay estuary. Weeks Bay receives saline water from the Gulf of Mexico through Mobile Bay. Tides have been measured to produce current just inside the mouth of the bay of up to 40 cm/s, while in the narrow mouth, currents have been estimated to be as fast as 105 cm/s (Miller-Way et al., 1996). Freshwater input comes from both the Fish and Magnolia Rivers. The mean combined discharge of both rivers has been estimated at 9 m^3/s, with 73% of the flow coming from the Fish River (Miller-Way et al., 1996). East-West wind-stress influences the filling/emptying of Mobile Bay, and consequently the filling/emptying of Weeks Bay (Schroeder et al., 1986). River discharge into Weeks Bay tends to be flashy in nature, with individual flooding events (Miller-Way et al., 1996).

5.3 SPM and SPIM Concentration Retrieval Algorithms

5.3.1 Previously Developed Models

Numerous models (Table 3.2) were selected to be evaluated in their performance of retrieving SPM/SPIM concentrations from reflectance values. Algorithms were selected from published research on other optically complex Case 2 waters that have been proven successful. Algorithms were evaluated using 48 sample sites, providing RMSEs ranging from 76.5% to 2131% for algorithms producing SPM concentrations, and 66.96% to $2*10^{68}$ % for algorithms determining SPIM concentrations. None of the

algorithms produced significant results in their original forms (Table 4.3). Once the coefficients of the previously developed models were modified, performance was much better (Table 4.4). The previously developed models with altered coefficients produced RMSEs ranging from 31.66% to 33.97% for SPM retrieval algorithms, and 13.67% to 36.87% for SPIM retrieval algorithms.

The best modified SPM retrieval algorithm using Weeks Bay SPM and reflectance data was that of Zheng et al. (2015) as depicted in the following equation:

$$SPM = -317.27 * x + 46.524 \quad (5.1)$$

Where x is Band 5. While performing the best out of the attempted previously developed SPM algorithms, this model does not produce significant results. The reported RMSE was 31.66% (14.63 mg/L) and R^2 was 0.0158. The best modified SPIM retrieval algorithm using Weeks Bay SPIM and reflectance data was that of Kong et al. (2015b) as depicted in the following equation:

$$SPIM = 227.73 * x^2 - 402.92 * x + 188.4 \quad (5.2)$$

Where x is the ratio of Band 4/Band 3. The reported RMSE was 13.67% (1.74 mg/L) and R^2 was 0.5173. The published results for the SPIM algorithm by Kong et al. (2015b) reported an R^2 of 0.9773 and a mean relative error of 25.35% for the Caofeidian coastal water dataset used to develop the model.

5.3.2 Empirical SPM and SPIM Concentration Retrieval Algorithms

Many possible reflectance parameters were analyzed as potential variables in both linear and nonlinear SPM and SPIM retrieval algorithms. The selection of the best retrieval algorithms was made by considering the R^2, p-value, Pearson correlation coefficient (R), and the RMSE (%) of the estimate. The majority of the SPM retrieval

algorithms developed using the *in situ* data collected during the four field cruises resulted in insignificant p-values. All significant SPM retrieval algorithms include Band 3, or the green band, of Landsat-8.

Differences in SPM concentrations between field cruises (Table 4.1) may have played a role in the minimal number of significant regressions with reflectance values. Similarly, variations in the composition, both inorganic and organic, may have influenced the regression as well. Weeks Bay may receive suspended sediment from the Fish and Magnolia Rivers, as well as from the Mobile Bay and through resuspension within Weeks Bay itself, causing this variation (Miller-Way et al., 1996).

The best possible SPM retrieval algorithm developed for Weeks Bay is the third order polynomial utilizing the reflectance parameters (Band 3 – Band 5)/(Band 3 + Band 5) as given in the following equation:

$$SPM = -204473 * x^3 + 647570 * x^2 - 682964 * x + 239916 \quad (5.3)$$

Where *SPM* is the concentration of SPM measured in mg/L, and x is the combination of Landsat-8 Rrs values such that

$$X = (\text{Band 3} - \text{Band 5}) \Big/ (\text{Band 3} + \text{Band 5}). \quad (5.4)$$

Equation 5.3 is the only SPM retrieval algorithm developed for Weeks Bay with a significant p-value (p-value=0.0089), and Pearson correlation coefficient that may be considered strong, at least when rounded (R=0.7976). The reported RMSE is 17.65% (8.15 mg/L). However, this algorithm was developed by removing an outlier from both the development phase (May 9, 2016 Site 1) and the validation phase (May 9, 2016 Site 2).

The reflectance parameter (Band 3 – Band 5)/(Band 3 + Band 5) is similar to what is referred to as the Normalized Differential Water Index (NDWI). The NDWI is calculated with the band combination of Equation 5.4, using TOA values. The NDWI maximizes reflectance of a water body through the use of the green band, and minimizes low reflectance in the NIR region (Ko, Kim, & Nam, 2015).

Unlike with SPM, the majority of the SPIM retrieval algorithms developed using the *in situ* data collected during the four field cruises resulted in significant p-values. Out of the 29 reflectance parameters tested as possible predictive variables in a SPIM retrieval algorithm for Weeks Bay, 25 produced p-values of less than 0.05, and are therefore statistically significant. Merritt (2016) similarly found that SPIM, opposed to SPM, has a more significant relationship with reflectance values. Out of the 25 statistically significant reflectance parameters, only three reflectance parameters produced both linear nonlinear algorithms with a Pearson correlation coefficient of greater than 0.8.

The three reflectance parameters sensitive to SSCs all contain Landsat-8 Band 3, or the green band. Two of the reflectance parameters sensitive to SSCs contain Landsat-8 Band 4, or the red band. The red portion of the EMS has been demonstrated to be the most sensitive of the visible portion to suspended sediment, and the least affected by organic material containing chlorophyll (Zhao, 2009). Because CDOM has a minimal influence at longer wavelengths, it is supposed that a SPIM algorithm may be more successful with the use of bands selected from the red region of the EMS (Binding et al., 2005). In this study, the developed relationships with individual visible bands demonstrated the greatest proportion of explained variance (R^2 value) in relation with

Landsat-8 Band 4 (Table 4.11). Many studies have demonstrated the effectiveness of using red and/or near-infrared band reflectance data to observe suspended sediment remotely (Chen et al., 2011; Han et al., 2006; Kaba et al., 2014; Miller et al., 2004; Zhao et al., 2011). While the red band was included in two of the significant retrieval algorithms the NIR band was only found to possess a strong relationship with the Weeks Bay *in situ* SPM/SPIM concentrations when the reflectance parameter (Band 3 – Band 5)/(Band 3 + Band 5) was developed and validated without the use of May 9, 2016 Sites 1 and 2.

Zhang (2005) determined the strongest SSC retrieval algorithm for the Old Woman Creek estuary to utilize a ratio of the green and NIR band of Landsat-7. Similar to Zhang (2005), this study found the green band to be a stronger parameter for predicting both SPIM, as well as SPM. Unlike Zhang (2005), a combination of the green band with the red band is better suited for predicting the SPM/SPIM concentrations of Weeks Bay. Kong et al. (2015a), the best performing previously existing model with modified coefficients (R^2=0.5173, RMSE=13.67%), similarly found the utilization of a combination of the red and green bands from a Landsat satellite to be the best predictor of SPIM. Kong et al. (2015a) used a ratio of the red and green band in a quadratic equation.

Ritchie & Cooper (2001) report that suspended sediments between 0 to 50 mg/L will significantly relate to almost any wavelength, whereas higher ranges of suspended sediment between 0 to 200+ mg/L require a curvilinear relationship with longer wavelengths in order to be significant. Many studies have demonstrated that despite this claim, a curvilinear relationship might be necessary in lower ranges between 0 to 100+ mg/L as well (Zhao et al, 2011; Lobo et al., 2014; Kong et al., 2015a; Zheng et al., 2015).

Out of the six significant linear and nonlinear algorithms with a strong Pearson correlation coefficient, the best performing model was the third order polynomial equation utilizing Ln(Band 4)/Ln(Band 3) as the predictive variable as given in the following equation:

$$SPIM = -84393 * x^3 + 266348 * x^2 - 279970 * x + 98029 \quad (5.5)$$

Where *SPIM* is the concentration of SPIM measured in mg/L, and x is the combination of Landsat-8 Rrs values such that

$$x = {Ln(Band\ 4)}\Big/{Ln(Band\ 3)}. \quad (5.6)$$

This model resulted in the lowest RMSE (12.50% or 1.59 mg/L), and highest R^2 (R^2=0.6504). The validation of Equation 5.5 with 16 sample sites using a paired t-test resulted in a p-value of greater than 0.05, allowing us to not reject the null that the predicted and *in situ* SPIM concentration means are statistically similar. In order to reject the null hypothesis that the modeled and *in situ* concentration means are statistically similar, the resultant p-value must be less than 0.05. Similarly, validation using an F-test resulted in a p-value of greater than 0.05, allowing us to not reject the null that the predicted and *in situ* SPIM concentration variances are statistically similar. As depicted in Figure 3.4, the modeled SPIM concentrations are strongly related to the measured field SPIM concentrations.

While polynomial models have been reported by previous studies (Lodhi et al., 1998; Kong et al., 2015a), there is the threat of overfitting the model and creating misleading R^2, Pearson correlation coefficient, and p-values. An over fit model is too complicated for the given data set, accommodating itself to the random noise of the specific sample, rather than the general population (Frost, 2015). By using a separate

sample set for both the development and validation of the reported polynomial model, it has been the goal to avoid the thread of overfitting, but this cannot be guaranteed. Further testing of the model is necessary to detect this potential error. In the event that Equation 5.5 is over fit to the noise of the specific sample set used, a linear model may more accurately determine SPIM concentrations from reflectance.

Out of the three significant linear algorithms with a strong Pearson correlation coefficient, the best performing model was the equation utilizing Band 4/Band 3 as the predictive variable as given in the following equation:

$$SPIM = -20.644x + 30.374 \quad (5.7)$$

Where SPIM is the concentration of SPIM measured in mg/L, and x is the combination of Landsat-8 Rrs values such that

$$x = {Band\ 4}/{Band\ 3}. \quad (5.8)$$

This model resulted in the lowest RMSE (17.48% or 2.23 mg/L), and highest R^2 (R^2=0.2619). The validation of Equation 5.7 with 16 sample sites using a paired t-test resulted in a p-value of greater than 0.05, allowing us to not reject the null that the predicted and *in situ* SPIM concentration means are statistically similar. Similarly, validation using an F-test resulted in a p-value of greater than 0.05, allowing us to not reject the null that the predicted and *in situ* SPIM concentration variances are statistically similar. As depicted in Figure 3.25, the modeled SPIM concentrations are strongly related to the measured field SPIM concentrations, although not as strongly related as when SPIM concentrations are predicted using the nonlinear model (Figure 3.26).

Despite the significant p-values and Pearson correlation coefficients of the reported SPM/SPIM retrieval algorithms, none have R^2 values that stand up to those of

the models published in the literature. Published SPM/SPIM retrieval algorithms typically report an R^2 value of 0.75 or greater, as depicted in Table 3.2 containing the previously developed models evaluated in this study. The highest R^2 value reported in this paper was for Equation 5.5 with a reported R^2 of 0.6504.

While SPIM concentration is the most important factor in impacting the reflectance of the sediment, the sediment particle size and composition has a strong influence as well (Kong et al., 2015a). Reflectance curves have been demonstrated to vary significantly for SPIM of different particle sizes, even with a constant concentration (Binding et al., 2005; Kong et al., 2015a). The complexity of the combined influence from both sediment concentration and particle size may explain the improved performance of a polynomial algorithm and justify the increased complexity of the equation.

5.4 Rrs Simulation

The Rrs simulation created for Weeks Bay presents modeled spectra curves that generally correspond with the spectra curves observed by the *in situ* radiometer data. While the spectra curves of the simulated Rrs reflect those observed by the radiometer, the magnitude of the simulated Rrs values tend to be lower than the radiometer values.

By removing the absorption of NAP, Chl a, and PC from Equation 4.1 to obtain Equation 4.2, the Rrs of Weeks Bay without the presence of SPM was simulated. When the SPM OACs are removed, the Rrs curve increases in magnitude from the simulated total Rrs. This increase in reflectance is due to the total SPM concentration being made up of 71% SPOM, and only 29% SPIM. The organic component of SPM (SPOM) is made up primarily of phytoplankton, and therefore chlorophyll. Chlorophyll has a high

absorption in the red and blue portion of the EMS (Jenson, 2006). By removing the absorption of NAP alone from Equation 4.1 to obtain Equation 4.3, the simulated Rrs without the presence of SPIM was simulated. When SPIM=0, the Rrs values are larger than the simulated total Rrs values, although not as large as when SPM=0. This is due to the lack of absorption by the organic particulate matter. Additionally, when the Rrs of Weeks Bay is simulated without the presence of SPM by removing the effects of both organic and inorganic material, the trough around 670nm, that is visible in both the total Rrs, and the simulated Rrs without the presence of SPIM, is removed. This trough is caused by the absorption of organic material.

To obtain the Rrs of SPM/SPIM alone, the Rrs values determined for SPM=0/SPIM=0 were subtracted from the total Rrs values. This was done using both the simulated total Rrs and radiometer Rrs values. The resultant Rrs values for SPIM are greater than those for SPM. This is theoretically due to the higher absorption of SPM due to the chlorophyll component.

Variation between the numerous spectra curves depicting Rrs in relation to either SPM or SPIM is typically the greatest in the 550-650nm range, which includes the green `and red portion of the EMS. The red portion of the EMS is the most sensitive of the visible portion to suspended sediment, and the least affected by organic material containing chlorophyll (Zhao, 2009).

Comparison of the computed total Rrs and *in situ* Rrs spectra curves validate the theory of OACs and their combined influence on the total reflectance observed by either the satellite or *in situ* radiometer. The computed Rrs spectra curves successfully approximate the majority of the observed spectra curves. Additionally, all computed Rrs

spectra curves match the standard reflectance spectra for clear and algae-laden waters depicted in Figure 5.3. A semi-analytical model utilizing the inherent optical properties investigated in this simulation was attempted, but failed to produce significant results.

CHAPTER VI

CONCLUSION

6.1 Retrieval Algorithms

It was hypothesized that remote sensing reflectance (Rrs) may be used to estimate SPM and SPIM concentrations in the Weeks Bay estuary in Alabama. Previously developed bio-optical algorithms were evaluated using the field collected SPM, SPIM, and Rrs values. None of the previously developed algorithms resulted in significant R^2 or RMSE (%) values. Once the previously developed algorithms were modified to include coefficients specific to the Weeks Bay data, only the modified SPM/SPIM algorithms produced significant relationships. All but one of the models previously developed SPIM algorithms with modified coefficients produced RMSE values of under 30%. R^2 values ranged from 0.1563 to 0.5173. The best fit SPIM algorithm, taken from Kong et al. (2015a), produced an R^2 of 0.5173 with an RMSE of 13.67% (1.74 mg/L) and a strong Pearson correlation coefficient of 0.90.

In order to find an improved model with a higher R^2 and lower RMSE (%), a series of reflectance parameters were related to SPM concentrations with regression techniques. The 29 tested reflectance parameters included single bands, band ratios, band combinations, natural logs of bands, and combinations of the previously listed. Through the analysis of these additional reflectance parameters, an algorithm utilizing the variable (Band 3 – Band 5)/ (Band 3 + Band 5) with a strong Pearson correlation coefficient

(R=0.80), low RMSE (17.65%), and moderate R^2 (R^2=0.4744) was found for determining SPM concentrations using Rrs. Through additional analysis of the reflectance parameters, numerous SPIM retrieval algorithms were found with a strong Person correlation coefficient (R>0.8), low RMSE (RMSE<20%), higher R^2 (R^2>0.19), and significant p-value (p<0.05). A nonlinear cubic algorithm utilizing the reflectance parameter Ln(Band 4)/Ln(Band 3) presents the lowest RMSE (12.50%), highest R^2 (R^2=0.6504), and a strong Pearson correlation coefficient. Additionally, a significant linear algorithm utilizing the reflectance parameter Band 4/Band 3 (RMSE= 17.48%, R^2=0.2619, R=0.83) may be used to determine SPIM concentrations using Rrs. These algorithms support the initial hypothesis that Rrs values may be used to estimate SPM and SPIM concentrations in Weeks Bay.

Weeks Bay is optically complex with varying proportions of inorganic and organic particulate matter, as well as variations in particle size, shape, and source, making the development of a SPM retrieval algorithm more difficult than a SPIM retrieval algorithm. A larger dataset may be needed to develop a stronger model for the retrieval of SPM in Weeks Bay.

6.2 Research Limitations and Future Research

This study faced a number of limitations that result in a number of possible future research studies. This study was unable to validate the proposed models through the application of the algorithms to Landsat-8 imagery of Weeks Bay. Once future research has validated the application of these algorithms to Landsat-8 imagery, future studies may download and atmospherically correct Landsat-8 imagery to obtain the Rrs values necessary to apply the proposed models. By applying the proposed models to Landsat-8

imagery, future research may monitor suspended sediment concentrations on a synoptic scale in Weeks Bay. Researchers may create sediment concentration maps for both future and historic Landsat-8 imagery, allowing for a number of questions on sediment transfer to be investigated.

A primary limitation of this study was the limited size of the data set. *In situ* samples were collected on four separate sampling trips, with an average of only 12 sample sites per trip. This greatly limited the number of sample sites able to be utilized in this study. Out of those four sampling trips, only one trip was able to occur on a clear sky day. Additional field sampling would allow for a better representation of SPM concentrations in order to further improve the SPM retrieval algorithm. It may be beneficial for additional sampling to range evenly over each season, in order to account for seasonal meteorological differences. Future research may investigate the influence of meteorological influences such as precipitation, wind speed, and wind direction.

Future research may also further investigate modeling SPM concentrations based on the IOPs of the water body by creating a semi-analytical model that utilizes the breakdown of the optically active components. Due to the evident magnitude differences between the simulated and *in situ* Rrs values, it may be necessary to fine tune the processes used to estimate these OACs. Each OAC presents an additional potential source of error in the development of a semi-analytical model.

6.3 Importance

Excessive concentrations of suspended sediments and organic matter serves as a contaminant for estuarine ecosystems. SPM concentrations may be used as a proxy for other contaminants that adhere and are transported along with suspended sediments such

as insecticides, phosphorus, toxic metals, and pathogens. As an estuary, Weeks Bay creates critical habitats for a variety of wildlife including species of fish, mammals, amphibians, reptile, and birds. As a suburb of Mobile, Alabama, the watershed surrounding Weeks Bay is one of the fastest growing regions of Alabama due to increased suburbanization. Because of the increase in urban land cover, it is important to monitor the effects that this development is having on surface runoff, and the accumulation of sediments and other pollutants in Weeks Bay. The development of an SPM and SPIM retrieval algorithm will allow for the future monitoring of suspended sediment within the bay, as well as the ability to analyze historic changes since increased development began. Future research may download Landsat-8 imagery, both present and historical, and apply the model(s) presented in this thesis to obtain estimations on the SPM/SPIM concentrations present in Weeks Bay during the Landsat-8 overpass.

REFERENCES

Amos, C. L., & Alfoeldi, T. T. (1979). The Determination of Suspended Sediment Concentration in a Macrotidal System Using Landsat Data. Journal of Sedimentary Research, 49(1), 159–173. http://doi.org/10.1306/212F76DF-2B24-11D7-8648000102C1865D

Baldwin County EDA. (2017). Baldwin County Economic Development Alliance (EDA). Retrieved February 7, 2017, from http://baldwineda.com/data/demographics/

Basnyat, P., Teeter, L. D., Flynn, K. M., & Lockaby, B. G. (1999). Relationships between landscape characteristics and nonpoint source pollutio2 inputs to coastal estuaries. Environmental Management, 23(4), 539–549. http://doi.org/10.1007/s002679900208

Bhavya, P.S., Kumar, Sanjeev, Gupta, G.V.M., Suharma, K.V., Sudheesh, V., Dhanya, K. R. (2016). Carbon isotopic composition of suspended particulate matter and dissolved inorganic carbon in the. Current Science, 110(8), 1539–1543. http://doi.org/10.18520/cs/v110/i8/1536-1539

Binding, C. E., Bowers, D. G., & Mitchelson-Jacob, E. G. (2005). Estimating suspended sediment concentrations from ocean colour measurements in moderately turbid waters; The impact of variable particle scattering properties. Remote Sensing of Environment, 94(3), 373–383. http://doi.org/10.1016/j.rse.2004.11.002

Booth, J. G., Miller, R. L., Mckee, B. A., & Leathers, R. A. (2000). Wind-induced bottom sediment resuspension in a microtidal coastal environment. Continental Shelf Research, 20, 785–806.

Bowers, D. G., & Binding, C. E. (2006). The optical properties of mineral suspended particles: A review and synthesis. Estuarine, Coastal and Shelf Science, 67(1-2), 219–230. http://doi.org/10.1016/j.ecss.2005.11.010

Cartwright, J. H. (2002). Identifying Potential Sedimentation Sources Through a Remote Sensing and GIS Analysis of Land Use/Land Cover for the Weeks Bay Watershed. Mississippi State University.

Chalov, S., Jarsjo, J., Kasimov, N. S., Romanchenko, A., Pietron, J., Thorslund, J., & Promakhova, E. V. (2015). Spatio-temporal variation of sediment transport in the Selenga. Environmental Earth Science, 73, 663–680. http://doi.org/10.1007/s12665-014-3106-z

Chapman, M., Lembo, A., & Monroe, C. (2014). An Introduction to Statistical Problem Solving in Geography (3rd ed.). Long Grove, Illinois: Waveland Press, Inc.

Chen, S., Huang, W., Chen, W., & Chen, X. (2011). An enhanced MODIS remote sensing model for detecting rainfall effects on sediment plume in the coastal waters of Apalachicola Bay. Marine Environmental Research, 72(5), 265–72. http://doi.org/10.1016/j.marenvres.2011.09.014

Coll, M., Schmidt, A., Romanuk, T., & Lotze, H. K. (2011). Food-Web Structure of Seagrass Communities across Different Spatial Scales and Human Impacts. PLoS ONE, 6(7). http://doi.org/10.1371/journal.pone.0022591

D'Sa, E. J. D., Miller, R. L., & Mckee, B. A. (2007). Suspended particulate matter dynamics in coastal waters from ocean color : Application to the northern Gulf of Mexico. Geophysical Research Letters, 34(December), 1–6. http://doi.org/10.1029/2007GL031192

Dash, P., Walker, N. D., Mishra, D. R., Hu, C., Pinckney, J. L., & D'Sa, E. J. (2011). Estimation of cyanobacterial pigments in a freshwater lake using OCM satellite data. Remote Sensing of Environment, 115(12), 3409–3423. http://doi.org/10.1016/j.rse.2011.08.004

Devi, G. K., Ganasri, B. P., & Dwarakish, G. S. (2015). Applications of Remote Sensing in Satellite Oceanography: A Review. Aquatic Procedia, 4, 579–584. http://doi.org/10.1016/j.aqpro.2015.02.075

Doxaran, D., Cherukuru, N., & Lavender, S. J. (2006). Apparent and inherent optical properties of turbid estuarine waters : measurements, empirical quantification relationships, and modeling. Applied Optics, 45(10), 2310–2324.

Doxaran, D., Froidefond, J., Lavender, S., & Castaing, P. (2002). Spectral signature of highly turbid waters Application with SPOT data to quantify suspended particulate matter concentrations. Remote Sensing of Environment, 81, 149–161.

EPA. (2000). Stressor Identification Guidance Document. Washington, DC.

Espinoza Villar, R., Martinez, J. M., Guyot, J. L., Fraizy, P., Armijos, E., Crave, A., Lavado, W. (2012). The integration of field measurements and satellite observations to determine river solid loads in poorly monitored basins. Journal of Hydrology, 444-445, 221–228. http://doi.org/10.1016/j.jhydrol.2012.04.024

Estes, M. G., Al-Hamdan, M. Z., Ellis, J. T., Judd, C., Woodruff, D., Thom, R. M., Herder, T. (2015). A modeling system to assess land cover land use change effects on SAV habitat in the Mobile Bay Estuary. Journal of the American Water Resources Association, 51(2), 513–536. http://doi.org/10.1111/jawr.12263

Forstall, R. L. (1995). Alabama Population of Counties by Decennial Census: 1900-1990. Retrieved from http://www.census.gov/population/cencounts/al190090.txt

Franz, B. A., Bailey, S. W., & Kuring, N. (2015). Ocean color measurements with the Operational Land Imager on Landsat-8 : Implementation and evaluation in SeaDAS Ocean color measurements with the Operational Land Imager on Landsat-8 : implementation and evaluation in SeaDAS, (March). http://doi.org/10.1117/1.JRS.9.096070

Frost, J. (2014). Why Are There No P Values for the Variables in Nonlinear Regression? Retrieved January 8, 2017, from http://blog.minitab.com/blog/adventures-in-statistics-2/why-are-there-no-p-values-for-the-variables-in-nonlinear-regression

Frost, J. (2016). Understanding Analysis of Variance (ANOVA) and the F-test. Retrieved from http://blog.minitab.com/blog/adventures-in-statistics-2/understanding-analysis-of-variance-anova-and-the-f-test

Gernez, P., Lafon, V., Lerouxel, A., Curti, C., Lubac, B., Cerisier, S., & Barillé, L. (2015). Toward Sentinel-2 High Resolution Remote Sensing of Suspended Particulate Matter in Very Turbid Waters: SPOT4 (Take5) Experiment in the Loire and Gironde Estuaries. Remote Sensing, 7(8), 9507–9528. http://doi.org/10.3390/rs70809507

Gohin, F. (2011). Annual Cycles of chlorophyll-a, non-algal suspended particulate matter, and turbidity observed from space and in-situ in coastal waters. Ocean Science, 7(5), 705–732.

Gregg, T., Prahl, F. G., & Simoneit, B. R. T. (2015). Suspended particulate matter transport of polycyclic aromatic hydrocarbons in the lower Columbia River and its estuary. Limnology and Oceanography, 60, 1935–1949. http://doi.org/10.1002/lno.10144

Han, B., Loisel, H., Vantrepotte, V., Mériaux, X., Bryère, P., Ouillon, S., Zhu, J. (2016). Development of a Semi-Analytical Algorithm for the Retrieval of Suspended Particulate Matter from Remote Sensing over Clear to Very Turbid Waters. Remote Sensing, 8(211), 1–23. http://doi.org/10.3390/rs8030211

Han, Z., Jin, Y. -Q. Q., & Yun, C. -X. X. (2006). Suspended sediment concentrations in the Yangtze River estuary retrieved from the CMODIS data. International Journal of Remote Sensing, 27(19), 4329–4336. http://doi.org/10.1080/01431160600658164

Hill, M. S. (1997). Understanding Environmental Pollution. Cambridge, UK: Cambridge University Press.

Horváth, H., Kovács, A. W., Riddick, C., & Présing, M. (2013). Extraction methods for phycocyanin determination in freshwater filamentous cyanobacteria and their application in a shallow lake Extraction methods for phycocyanin determination in freshwater fi lamentous cyanobacteria and their application in a shallow l. European Journal of Phycology, 48(3), 278–286. http://doi.org/10.1080/09670262.2013.821525

Hu, C., Chen, Z., Clayton, T. D., Swarzenski, P., Brock, J. C., & Muller-Karger, F. E. (2004). Assessment of estuarine water-quality indicators using MODIS medium-resolution bands: Initial results from Tampa Bay, FL. Remote Sensing of Environment, 93(3), 423–441. http://doi.org/10.1016/j.rse.2004.08.007

Jenson, J. R. (2006). Remote Sensing of the Environment: An Earth Resource Perspective (2nd ed.). Upper Saddle River, NJ: Prentice Hall.

Kaba, E., Philpot, W. D., & Steenhuis, T. (2014). Evaluating suitability of MODIS-terra images for reproducing historic sediment concentrations in water bodies: Lake Tana, Ethiopia. International Journal of Applied Earth Observation and Geoinformation, 26(1), 286–297. http://doi.org/10.1016/j.jag.2013.08.001

Kaufman, Y. J., & Davis, C. O. (2003). Remote sensing of suspended sediments and shallow coastal waters. IEEE Transactions on Geoscience and Remote Sensing, 41(3), 559–566. http://doi.org/10.1109/TGRS.2003.810227

Kennett, J. (1982). Marine Geology. Englewood Cliffs, NJ: Prentice-Hall.

Ko, B. C., Kim, H. H., & Nam, J. Y. (2015). Classification of Potential Water Bodies Using Landsat 8 OLI and a Combination of Two Boosted Random Forest Classifiers. Sensors, 15(6), 13763–13777. http://doi.org/10.3390/s150613763

Kentucky Water Watch. (n.d.). Total Suspended Solids and water quality. Retrieved from http://ky.gov/nrepc/water/ramp/rmtss.htm

Kong, J., Sun, X. M., Wong, D. W., Chen, Y., Yang, J., Yan, Y., & Wang, L. X. (2015). A semi-analytical model for remote sensing retrieval of suspended sediment concentration in the Gulf of Bohai, China. Remote Sensing, 7(5), 5373–5397. http://doi.org/10.3390/rs70505373

Kong, J., Sun, X., Wang, W., Du, D., Chen, Y., & Yang, J. (2015). An optimal model for estimating suspended sediment concentration from Landsat TM images in the Caofeidian coastal waters. International Journal of Remote Sensing, 36(19-20), 5257–5272. http://doi.org/10.1080/01431161.2015.1043159

Kumar, S., Finlay, J. C., & Sterner, R. W. (2011). Isotopic composition of nitrogen in suspended particulate matter of Lake Superior : implications for nutrient cycling and organic matter transformation. Biochemistry, 103, 1–14. http://doi.org/10.1007/s10533-010-9441-6

Kutser, T., Pierson, D. C., Kallio, K. Y., Reinart, A., & Sobek, S. (2005). Mapping lake CDOM by satellite remote sensing. Remote Sensing of Environment, 94(4), 535–540. http://doi.org/10.1016/j.rse.2004.11.009

Lee, Z. P., Carder, K. L., Peacock, T. G., Davis, C. O., & Mueller, J. L. (1996). Method to derive ocean absorption coefficients from remote-sensing reflectance. Applied Optics, 35(3), 453–462.

Lellis-Dibble, K. a., McGlynn, K. E., & Bigford, T. E. (2008). Estuarine fish and shellfish species in U.S. commercial and recreational fisheries : economic value as an incentive to protect and restore. Habitat.

Liu, X., & Wang, M. (2014). River runoff effect on the suspended sediment property in the upper Chesapeake Bay using MODIS observations and ROMS simulations. Journal of Geophysical Research: Oceans, 119, 8646–8661. http://doi.org/10.1002/2014JC010081

Lobo, F. L., Costa, M. P. F., & Novo, E. M. L. M. (2015). Time-series analysis of Landsat-MSS/TM/OLI images over Amazonian waters impacted by gold mining activities. Remote Sensing of Environment, 157, 170–184. http://doi.org/10.1016/j.rse.2014.04.030

Lodhi, M. A., Rundquist, D. C., Han, L., & Kuzila, M. S. (1998). Estimation of suspended sediment concentration in water using integrated surface reflectance. Geocarto International. http://doi.org/10.1080/10106049809354637

Ma, Y., Qin, Y., Zheng, B., & Zhang, L. (2015). Seasonal variation of enrichment, accumulation and sources of heavy metals in suspended particulate matter and surface sediments in the Daliao river and Daliao river estuary, Northeast China. Environmental Earth Science, 73, 5107–5117. http://doi.org/10.1007/s12665-015-4325-7

Merritt, D. (2016). Estimation of suspended particulate matter concentration in the Mississippi Sound using MODIS imagery. Mississippi State University.

Mertes, L., Smith, M. O., & Adams, J. B. (1993). Estimating Suspended Sediment Concentrations in Surface Waters of the Amazon River Wetlands from Landsat Images. Remote Sensing of Environment, (43), 281–301.

Miller, R. L., & McKee, B. A. (2004). Using MODIS Terra 250 m imagery to map concentrations of total suspended matter in coastal waters. Remote Sensing of Environment, 93(1-2), 259–266. http://doi.org/10.1016/j.rse.2004.07.012

Miller-Way, T., Dardeau, M., & Crozier, G. (1996). Weeks Bay National Estuarine Research Reserve: An estuarine profile and bibliography (Vol. Dauphin Is).

Min, J. E., Ryu, J. H., Lee, S., & Son, S. H. (2012). Monitoring of suspended sediment variation using Landsat and MODIS in the Saemangeum coastal area of Korea. Marine Pollution Bulletin, 64(2), 382–390. http://doi.org/10.1016/j.marpolbul.2011.10.025

Mobley, C. (2010). Overview of Optical Oceanography. Retrieved from http://www.oceanopticsbook.info/view/overview_of_optical_oceanography/introduction

Morel, A., & Prieur, L. (1977). Analysis of variations in ocean color. Limnology and Oceanography, 22(4), 709–722.

Mueller, J. L., Clark, K., Kuwahara, S., Lazon, G., Brown, W., Fargion, S., Lykke, R. (2003). Ocean optics protocols for satellite ocean color sensor validation, revision 4, Volume VI: Special topics in ocean protocols and appendices. NASA Technical Memorandum, 6(211621), 1–124.

National Oceanographic Data Center (NODC). (2017). Water Temperature Table of All Coastal Regions. Retrieved from https://www.nodc.noaa.gov/dsdt/cwtg/all_meanT.html

Needles, L. A., Lester, S. E., Ambrose, R., Andren, A., Beyeler, M., Connor, M. S., Wendt, D. E. (2013). Managing Bay and Estuarine Ecosystems for Multiple Services. Estuaries and Coasts, 38, 1–14. http://doi.org/10.1007/s12237-013-9602-7

Nieke, B., Rueter, R., Heuermann, R., Wang, H., Babin, M., Therriault, J. C. (1997). Light absorption and fluorescence properties of chromophoric dissolved organic matter (CDOM), in the St. Lawrence Estuary (Case 2 waters). Pergamon, 17(3), 235–252.

NOAA. Coastal Zone Management Act of 1972, as amended through the Energy Policy Act of 2005 (2005).

NOAA National Estuarine Research Reserve System (NERRS). System-wide Monitoring Program. Data accessed from the NOAA NERRS Centralized Data Management Office website: http://www.nerrsdata.org/; accessed 12 December 2016.

NOAA. (2008). Monitoring Estuaries. Retrieved from http://oceanservice.noaa.gov/education/kits/estuaries/estuaries10_monitoring.html

NOAA, & Alabama Department of Conservation and National Resources. (2007). Weeks Bay National Estuarine Research Reserve Management Plan.

Ohrel, R. L., & Register, K. (2006). Volunteer Estuary Monitoring: A Methods Manual.

Orth, R. J., Carruthers, T. J. B., Dennison, W. C., Duarte, C. M., Fourqurean, J. W., Heck, K. L., Olyarnik, S. (2006). A global crisis for seagrass ecosystems. Bioscience, 56(12), 987–996.

Pavelsky, T. M., & Smith, L. C. (2009). Remote sensing of suspended sediment concentration, flow velocity, and lake recharge in the Peace-Athabasca Delta, Canada. Water Resources Research, 45(11), 1–16. http://doi.org/10.1029/2008WR007424

Potter, B. (n.d.). Estuaries. Retrieved from https://www.niwa.co.nz/education-and-training/schools/students/estuaries

Qu, L. (2014). Remote Sensing Suspended Sediment Concentration in the Yellow River. Doctoral Dissertations., Paper 383.

Reynolds, R. A., & Mitchell, B. G. (2001). A chlorophyll-dependent semi-analytical reflectance model derived from field measurements of absorption and backscattering coefficients within the Southern Ocean. Journal of Geophysical Research, 106, 7125–7138.

Ritchie, J. C., & Cooper, C. M. (2001). Remote sensing techniques for determining water quality: Applications to TMDLS. TMDL Science Issues Conference, 367–375.

Roberts, F., & Roberts, D. (2017). Correlation Coefficient. Retrieved from https://mathbits.com/MathBits/TISection/Statistics2/correlation.htm

Roesler, Collin, Perry, M. J. (1995). *In situ* phytoplankton absorption, flouresence emission, and particulate backscattering spectra determined from reflectance. Journal of Geophysical Research, 100, 13,279–13,294.

Schroeder, W., & Wiseman, W. (1986). Low-frequency shelf-estuarine exchange processes in Mobile Bay and other estuarine systems on the northern Gulf of Mexico. In Estuarine Variability (p. 367).

Smith, R. C., & Baker, K. S. (1981). Optical properties of the clearest natural waters (200-800 nm). Applied Optics, 20(2), 177–184.

State by State. (n.d.). USA Today, n.d., Middle Search Plus, EBSCOhost, viewed 30 October 2016.

Tassan, S. (1994). Local algorithms using SeaWiFS data for the retrieval of phytoplankton, pigments, suspended sediment, and yellow substance in coastal waters, 33(12), 2369–2378.

Thomason, J. C. (2008). An Assessment of Suspended Sediment in Weeks Bay Reserve, Baldwin County, Alabama, Using Geospatial Modeling and Field Sampling Methods. Mississippi State University.

U.S. Census Bureau. (2000). DP-1 - Profile of General Demographic Characteristics: 2000.

U.S. Census Bureau. (2010). DP-1 - Profile of General Population and Housing Characteristics: 2010.

USGS. (2015). Landsat — Earth Observation Satellites Landsat Missions : Imaging the Earth Since 1972.

USGS. (2016). Using the USGS Landsat 8 Product. Retrieved November 1, 2016, from https://landsat.usgs.gov/using-usgs-landsat-8-product

Vazyulya, S., Khrapko, A., Kopelevich, O., Burenkov, V., Eremina, T., & Isaev, A. (2014). Regional algorithms for the estimation of chlorophyll and suspended matter concentration in the Gulf of Finland from MODIS-Aqua satellite data. Oceanologia, 56(4), 737–756. http://doi.org/10.5697/oc.56-4.737

Walker, N. D., & Rouse, Jr., L. J. (1993). Satellite Assessment of Mississippi River Discharge Plume Variability. OCS study MMS 93-0044, 50.

Wang, J. J., Lu, X. X., Liew, S. C., & Zhou, Y. (2009). Retrieval of suspended sediment concentrations in large turbid rivers using Landsat ETM+: An example from the Yangtze River, China. Earth Surface Processes and Landforms, 34(8), 1082–1092. http://doi.org/10.1002/esp.1795

Zhang, L. (2005). Use of Landsat-7 & MODIS Data in Measuring Suspended Sediment Concentration in Old Woman Creek. Ohio State University.

Zhang, M., Dong, Q., Cui, T., Xue, C., & Zhang, S. (2014). Suspended sediment monitoring and assessment for Yellow River estuary from Landsat TM and ETM+ imagery. Remote Sensing of Environment, 146, 136–147. http://doi.org/10.1016/j.rse.2013.09.033

Zhao, H. (2009). The Study of Sediment Dynamics in a Shallow Estuary Using Integrated Numerical Modeling and Satellite Remote Sensing. Louisiana State University.

Zhao, H., Chen, Q., Walker, N. D., Zheng, Q., & MacIntyre, H. L. (2011). A study of sediment transport in a shallow estuary using MODIS imagery and particle tracking simulation. International Journal of Remote Sensing, 32(21), 6653–6671. http://doi.org/10.1080/01431161.2010.512938

Zheng, Z., Li, Y., Guo, Y., Xu, Y., Liu, G., & Du, C. (2015). Landsat-based long-term monitoring of total suspended matter concentration pattern change in the wet season for Dongting Lake, China. Remote Sensing, 7(10), 13975–13999. http://doi.org/10.3390/rs71013975